Diverse Mechanisms Impair Thalamic Circuit Function in a Dravet Syndrome Mouse Model

Carleigh Studtmann

Dissertation submitted to the faculty of the Virginia Polytechnic Institute and State University in partial fulfillment of the requirements for the degree of

Doctor of Philosophy
In
Translational Biology, Medicine, and Health

Sharon A. Swanger, Chair
Konark Mukherjee
Michelle Olsen
Steven Poelzing
Mark Witcher

February 10, 2022
Roanoke, Virginia

Keywords: Dravet syndrome, corticothalamic, somatosensory

Diverse Mechanisms Impair Thalamic Circuit Function
in a Dravet Syndrome Mouse Model

Carleigh Studtmann

ABSTRACT

Dravet syndrome (DS) is an infantile epileptic encephalopathy that is caused by loss-of-function mutations in the *SCN1A* gene, which encodes the voltage-gated sodium channel, $Na_V1.1$. Haploinsufficiency of $Na_V1.1$ in DS patients leads to imbalanced excitability across brain circuits, resulting in a broad phenotypic profile including drug-resistant convulsive and non-convulsive (absence) seizures, cognitive impairment, ataxia, and sleep disruption. Dysfunction in the somatosensory corticothalamic (CT) circuit underlies several DS phenotypes including absence seizures and sleep disturbances. Yet, the precise mechanisms underlying somatosensory CT circuit dysfunction in DS remain unclear. Here, we sought to identify the cellular and synaptic mechanisms underlying somatosensory CT circuit dysfunction in a haploinsufficiency DS mouse model. This work reveals that $Na_V1.1$ haploinsufficiency leads to cell-type-specific changes in the excitability of reticular thalamic (nRT), ventral posterolateral (VPL), and ventral posteromedial (VPM) neurons. Further, we identified alterations in both glutamatergic and GABAergic synaptic connectivity within the somatosensory CT circuit in DS mice. These findings introduce glutamatergic neuron dysfunction and synaptic alterations as novel disease mechanisms underlying thalamic circuit dysfunction in DS, providing new targets for therapeutic intervention. In addition, we reveal that VPL and VPM neurons exhibit distinct firing properties in a healthy CT circuit, suggesting they differentially contribute to circuit-wide function in health and dysfunction in disease.

Diverse Mechanisms Impair Thalamic Circuit Function
in a Dravet Syndrome Mouse Model

Carleigh Studtmann

GENERAL AUDIENCE ABSTRACT

The brain is composed of biological circuits made up of excitatory and inhibitory neurons, which are connected through synapses. Proper balance between excitatory and inhibitory activity in these circuits is essential for maintaining healthy brain function. Dravet syndrome (DS) is an infantile-onset epilepsy caused by mutations in the *SCN1A* gene, which encodes the voltage-gated sodium channel, $Na_v1.1$. Loss of this protein in the brain leads to an imbalance of excitation and inhibition across a variety of brain circuits, resulting in drug-resistant seizures and cognitive, motor, and learning deficits. Disrupted excitability in the somatosensory corticothalamic (CT) circuit specifically leads to non-convulsive seizures and sleep disruption in DS. However, the mechanisms underlying this circuit's dysfunction remain unclear. Revealing these mechanisms is critical for identifying therapeutic targets by which we can correct circuit function. In this work, we used a mouse model of DS to reveal changes in the excitability of three distinct cell populations of the somatosensory CT circuit. Importantly, changes were exhibited in both excitatory and inhibitory thalamic neuron populations. We further identified impairments in the synapses, both excitatory and inhibitory, connecting the somatosensory CT circuit. These cell-type-specific changes in excitability and synaptic connectivity provide novel targets for therapeutic intervention in DS.

Acknowledgements

My sincerest gratitude to my advisor and mentor, Dr. Sharon Swanger. You have taught me much, not only about science but also about life. Your perseverance and resiliency in the midst of great challenges over the last several years have been an example to me. Thank you for being a role model to me. I will carry the lessons I have learned from you with me throughout my life. More than anything, I appreciate your patience with me as I developed both as a scientist and a person. It has been an honor to learn from you and work with you.

Thank you also to all the members of my committee- Dr. Steven Poelzing, Dr. Konark Mukherjee, Dr. Michelle Olsen, and Dr. Mark Witcher for your expertise, interest in my work, and dedication to my best interest and education.

I would also like to express my sincere gratitude to my TBMH cohort. Your support and friendship carried me through this program, particularly in our first year together. Thank you for having my back and encouraging me.

To my family and my husband, David, thank you for your unconditional love and support through this process. Your day-to-day encouragement has sustained me over the last four years. Thank you for taking a sincere interest in my work and loving me unconditionally as I evolved as a person during graduate school. Thank you especially to my dad, George, who instilled in me both my love of science and my work ethic through his own example. I have dedicated this work to you. Without your example and guidance, I would not be here.

Table of Contents

List of Figures and Tables

Chapter 1

Chapter 2

Chapter 3

List of abbreviations

nRT, reticular nucleus of the thalamus

CT, corticothalamic

VB, ventrobasal

S1, primary somatosensory cortex

S2, secondary somatosensory cortex

VPL, ventral posterolateral thalamic nucleus

VPM, ventral posteromedial thalamic nucleus

DRG, dorsal root ganglion

TC, thalamocortical

HCN, hyperpolarization-activated cyclic nucleotide-gated channel

POm, posteromedial thalamic nucleus

DS, Dravet syndrome

AIS, axon initial segment

PV, parvalbumin

SOM, somatostatin

SWD, spike-and-wave discharge

IPSC, inhibitory postsynaptic current

EPSC, excitatory postsynaptic current

vGlut1, vesicular glutamate transporter 1

vGlut2, vesicular glutamate transporter 2

vGAT, vesicular GABA transporter

RMP, resting membrane potential

aCSF, artificial cerebral spinal fluid

CACC, calcium-activated chloride channel

Ano2, anoctamin 2

Chapter 1

General Introduction

1.1 The Corticothalamic Network

The thalamus is a centrally-located structure in the mammalian brain that is composed of two portions - the dorsal and ventral thalamus (Sherman and Guillery, 2006). The dorsal thalamus contains many clusters of glutamatergic neurons, or relay nuclei, which receive specific types of incoming information and project to the cerebral cortex (Sherman and Guillery, 2006). The ventral thalamus consists primarily of the reticular nucleus of the thalamus (nRT), a group of GABAergic neurons that provide the primary inhibition to dorsal thalamic relay nuclei (Sherman and Guillery, 2006). The thalamus has historically been considered a central relay station of the brain, conveying sensory and motor information from the periphery to the cortex, where integration and conscious perception of that information occurs (Sherman and Guillery, 2006). However, more recent work has expanded the role of the thalamus in brain function to include more complex integratory processes (Briggs and Usrey, 2008; Sherman, 2007). These higher-order processes are thought to arise in part from the broad bidirectional connections between the cortex and thalamus, termed the corticothalamic (CT) network.

The CT network consists of reciprocal loops connecting thalamic relay nuclei to their corresponding cortical regions. The thalamic relay nuclei in the CT network can be divided into two functional categories based on their inputs. The nuclei which receive most of the ascending sensory input are called first order thalamic nuclei, and they play an important role in bottom-up propagation of subcortical sensory information to the cortex (Sherman and Guillery, 2006). Specifically, these nuclei serve as a last bottleneck, filtering

incoming sensory signals as they are sent to the corresponding cortical region. These nuclei also receive reciprocal cortical input, which allows for top-down cortical modulation of the incoming sensory signals. Together, the bottom-up and top-down processing of sensory information at first order thalamic nuclei is proposed to contribute to the selective attention of incoming sensory signals (Gomez-Ramirez et al., 2016). The CT network also contains higher order thalamic nuclei, which receive very little ascending sensory input but instead receive their primary input from the cortex (Sherman, 2007). Higher order nuclei project more broadly to multiple cortical regions, as well as subcortical regions. Though the precise contribution of higher order nuclei to network-wide function remains unclear, they are thought to be important for cortico-thalamo-cortical processing and may be important for diverse higher order cognitive functions (Sherman, 2007).

Dysfunction within the CT network is implicated in a number of neurological and psychiatric illnesses including Alzheimer's disease, schizophrenia, and epilepsy (Alexandra Krol, 2018; Avram et al., 2018; Hazra et al., 2016; Holmes et al., 2010). The thalamus thus offers potential therapeutic targets across a diversity of pathologies (Jeanne T. Paz, 2013). However, a fundamental understanding of the cellular, molecular, and synaptic properties underlying CT network function is critical to determining how network function becomes pathological in such disease states. The functional properties of many cell populations across the thalamus have yet to be fully elucidated.

1.2 The Somatosensory Corticothalamic Circuit

The somatosensory corticothalamic (CT) circuit is part of the CT network that transmits somatosensory information from the periphery to the somatosensory cortex (O'Reilly et al., 2021). Aside from relaying diverse sensory information, the circuit is

involved in the generation of oscillations such as slow waves and sleep spindles, which are critical for NREM sleep (O'Reilly *et al.*, 2021).

1.2.1 Somatosensory Pathways

Somatosensory information includes tactile, temperature, nociceptive, and proprioceptive information (Squire et al., 2013). These various sensory modalities are conferred by specific types of receptors in the skin including free nerve endings, muscle spindles, hair follicles, Meissner corpuscles, Pacinian corpuscles, and Ruffini corpuscles, among others (Delmas et al., 2011). There are several different pathways from the periphery to the somatosensory cortex, depending on the location of the receptor and the type of encoded somatosensory information (O'Reilly *et al.*, 2021).

The first order thalamic nucleus of the somatosensory CT circuit is the ventrobasal (VB) thalamic nucleus, which receives ascending somatosensory information from the periphery and projects to the primary somatosensory (S1) cortex. The VB nucleus is composed of two distinct subnuclei- the ventral posterolateral (VPL) and ventral posteromedial (VPM) nuclei, which receive somatosensory information from the body and the head, respectively (O'Reilly *et al.*, 2021).

Somatosensory information arising from the body is transmitted to the VPL thalamus via three primary pathways, all of which begin at peripheral sensory receptors, which are processes of pseudo-unipolar neurons whose cell bodies reside in the dorsal root ganglion (DRG; **Figure 1**; O'Reilly *et al.*, 2021). Somatosensory input from both the lower and upper body is transmitted to the VPL via the *dorsal column medial lemniscus pathway*. DRG neurons carrying information from sensory receptors in the lower and upper body synapse at the gracile or cuneate nucleus of the medulla, respectively. The pathway

decussates at the medial lemniscus before arriving at the VPL thalamus, where it projects to the primary somatosensory cortex (S1). The *spinocervical tract* is an additional pathway that transmits somatosensory information such as pressure from the body to the cortex through the VPL. DRG neurons carrying information from peripheral receptors synapse onto dorsal horn neurons. The pathway then ascends to the lateral cervical nucleus of the medulla before decussating at the medial lemniscus and arriving at the VPL, where it projects to S1. Nociceptive information from the body is transmitted to the VPL through the *spinothalamic tract.* In this pathway, DRG neurons carrying information from nociceptors in the periphery synapse in the dorsal horn of the spinal cord. This pathway decussates at the same level of the spinal cord before ascending to the VPL, where it projects to S1.

Somatosensory information arising from the head is transmitted to the VPM thalamus via two pathways that are distinct from those providing input to the VPL (**Figure 1**) (O'Reilly *et al.*, 2021). Somatosensory information from the face and head is transmitted to the VPM via the *trigeminal lemniscus pathway.* Trigeminal ganglion neurons carrying information from peripheral receptors synapse at the trigeminal nucleus of the pons. This pathway decussates at the level of the trigeminal lemniscus before arriving at the VPM, where it projects to the S1 cortex. Nociceptive information from the head is transmitted to the VPM via the *extralemniscal trigeminal pathway*. Trigeminal ganglion neurons carrying information from nociceptors synapse at the spinal nucleus of V in the medulla. This pathway ascends and decussates prior to arriving at the VPM, where it projects to the S1 cortex.

The VPL and VPM thus receive and transmit a broad range of somatosensory information from across the body and head to the primary somatosensory cortex. Pathological function within the somatosensory CT circuit can adversely affect the sensation and perception of a variety of modalities including touch discrimination, pain sensitivity, temperature detection, and proprioception. Because the VPL and VPM receive and transmit somatosensory information from distinct regions, dysfunction in the two nuclei could contribute differently to disease states. Indeed, there is evidence that the two nuclei respond with different compensatory mechanisms in a spinal cord injury mouse model (Hains et al., 2005). Historically, however, the two nuclei have mostly been studied as one VB complex in disease models (David et al., 2018; Hall and Lifshiftz, 2010; Hazra *et al.*, 2016; Jeanne T. Paz, 2013; Paz et al., 2011; Princivalle et al., 2003; Ritter-Makinson et al., 2019; Ulrike B.S. Hedrich, 2014). Thus, it remains to be investigated how these two nuclei may distinctly contribute to pathological somatosensory processing in disease states.

1.2.2. Core Somatosensory Corticothalamic Circuit

The core somatosensory CT circuit consists of the VPL and VPM thalamic nuclei, the nRT, and the S1 cortex (O'Reilly *et al.*, 2021). In the mouse brain, the VPL and VPM contain glutamatergic neurons that receive ascending somatosensory input from the periphery and project axons, termed thalamocortical (TC) fibers, to layer four S1 cortical neurons (**Figure 2**). Layer six cortical glutamatergic neurons provide reciprocal feedback through corticothalamic (CT) fibers to the VPL and VPM (O'Reilly *et al.*, 2021). Both TC and CT axons send collateral axons to the GABAergic nRT, which forms a shell around and provides the primary inhibitory input to the VPL and VPM.

Balanced synaptic connectivity between TC and CT glutamatergic projections and nRT GABAergic input to the VPL and VPM is essential for proper somatosensory CT circuit output (Shane R. Crandall, 2015; Temereanca S, 2004). TC projections to the S1 cortex are essential for somatosensory informational processing, and CT input back to VPL and VPM neurons modulates the ascending somatosensory input. CT projections far outnumber TC projections, allowing the cortex to dynamically shape sensory input (Deschenes et al., 1998; O'Reilly *et al.*, 2021). For example, activation of CT neurons can tune the receptive field or direction selectivity of VPM neurons, as well as enhance individual neuron output (Briggs and Usrey, 2008; Li and Ebner, 2007).

The GABAergic nRT serves as an additional modulator of VPL and VPM neuron output, gating the information flow from the VPL/VPM to the cortex. The CT and TC inputs to the nRT lead to feedforward and feedback inhibition of VPL and VPM neurons, respectively. Importantly, CT-nRT synapses are stronger than CT-VPL/VPM inputs, leading to consistent, robust feedforward inhibition of VPL and VPM neurons (Warren et al., 1994). The concurrent monosynaptic CT-VPL/VPM activation and disynaptic CT-nRT-VPL/VPM inhibition leads to an important frequency-dependent feature of VPL and VPM neuron output (O'Reilly *et al.*, 2021). For example, low frequency CT input leads to feedforward nRT-VPL/VPM inhibition, while higher frequency CT input results in excitation of VPL/VPM neurons (Shane R. Crandall, 2015). This intricate balance of excitation and inhibition is not only necessary for proper somatosensory informational processing, but it also plays a critical role in circuit-wide rhythmogenesis.

Feedforward and feedback nRT-VPL/VPM inhibition leads to 7-14 Hz intra-thalamic oscillations termed sleep spindles, which are necessary for the early stages of

NREM sleep (Murata and Colonnese, 2019). These oscillations are generated when hyperpolarized nRT neurons respond to depolarizing input in a burst firing mode, resulting in robust feedforward inhibition of VPL and VPM neurons. When hyperpolarized VPL or VPM neurons receive depolarizing input, they respond in their own burst firing mode, thereby re-activating nRT neurons (Fogerson and Huguenard, 2016). The resulting feedback cycle between rebound bursts in the nRT and VPL/VPM underlie sleep spindles (Fogerson and Huguenard, 2016; Huguenard and Prince, 1994; Kim et al., 2012; Warren *et al.*, 1994). The transition into a rebound burst firing mode is an essential property of VPL, VPM, and nRT neurons and their contribution to intra-thalamic oscillations.

1.2.3 Firing Modes of Thalamic Neurons

Thalamic neurons have unique functional properties compared to many other neuron populations in the brain, which allow for their diverse contribution to circuit function. Both thalamic relay neurons and nRT neurons exhibit two distinct firing modes- a depolarization-induced tonic firing mode and a hyperpolarization-induced rebound burst firing mode (Llinas and Steriade, 2006; Sherman, 2001). The mode of firing in nRT, VPL, and VPM neurons depends on the activation state of voltage-gated T-type Ca^{2+} channels expressed in dendrites. These T-type Ca^{2+} channels are inactivated at depolarized membrane potentials and de-inactivated with sustained hyperpolarized membrane potentials (Llinas and Steriade, 2006). Thus, when thalamic neurons at a depolarized membrane potential receive depolarizing input, T-type Ca^{2+} channels remain inactivated and canonical action potential channels including voltage-gated sodium and potassium channels are activated, resulting in tonic firing (**Figure 3**). However, when thalamic neurons at a sufficiently hyperpolarized membrane potential receive depolarizing input,

de-inactivated T-type Ca^{2+} channels become activated and respond with a low-threshold spike. This spike is sufficient to activate voltage-gated sodium and potassium channels, resulting in the rapid firing of multiple action potentials on top of the low-threshold spike, termed rebound bursts (Llinas and Steriade, 2006). There are multiple T-type Ca^{2+} channel isoforms expressed in the thalamus, with $Ca_V3.1$ predominantly expressed in VPL/VPM neurons and $Ca_V3.2$ and $Ca_V3.3$ expressed in nRT neurons (Astori et al., 2011; Talley et al., 1999). In addition to T-type Ca^{2+} channels, both VPL/VPM and nRT neurons express hyperpolarization-activated cation channels (HCN), which also contribute to their hyperpolarization-induced rebound bursting. Isoforms HCN2 and HCN4 are expressed in the nRT and VPL/VPM of mice, with HCN2 more highly expressed in the nRT than the VPL/VPM (Abbas et al., 2006). While both cell populations demonstrate burst firing, this channel diversity may underlie distinct burst firing properties including burst threshold or duration.

These two distinct firing modes encode information differently. Tonic firing can relay incoming input with high fidelity, even at high frequencies, while burst firing is nonlinear in nature, responding to input in an all-or-nothing manner (McCormick and Feeser, 1990; Sherman, 2001). During alert states, the nRT and VPL/VPM fire predominantly in a tonic mode, which is thought to underlie general somatosensory informational processing, including the propagation and gating of peripheral sensory information to the cortex (Jones, 2002). The canonical understanding is rebound bursting primarily contributes to intra-thalamic oscillations (Steriade et al., 1987). As previously described, oscillations in the somatosensory thalamus occur when hyperpolarized nRT and VPL/VPM neurons receive depolarizing input, resulting in a cycle of rebound bursts

between the two regions (Fogerson and Huguenard, 2016). Thus, thalamic tonic and burst firing underlie distinct types of informational processing, and the transition between the two firing modes is essential for proper circuit-wide function.

In addition to receiving distinct sensory information, recent evidence suggests that the VPL and VPM may play distinct roles in circuit-wide oscillations based on their unique connectivity with the nRT (Clemente Perez et al., 2017). Some studies investigate the regions individually, but most investigate the VB, including the VPL and VPM as one population (Abbas *et al.*, 2006; Astori *et al.*, 2011; Cheong et al., 2011; Ha et al., 2016; Huguenard and Prince, 1994; Jacobsen et al., 2001; Talley *et al.*, 1999; Warren *et al.*, 1994; Zobeiri et al., 2019). The cellular mechanisms underlying their resting potential, tonic firing, and burst firing have not been systematically investigated and compared (Chiaia et al., 1991; Landisman and Connors, 2007). It remains unknown whether VPL and VPM neurons express distinct membrane channels such as T-type Ca^{2+} or HCN channel isoforms (Abbas *et al.*, 2006; Astori *et al.*, 2011; McKay et al., 2006; Talley *et al.*, 1999). A comprehensive comparison of the cellular properties of VPL and VPM neurons is necessary to understand how they may differentially contribute to circuit-wide rhythmogenesis.

1.2.4 Higher Order Somatosensory CT Nucleus

The somatosensory CT circuit encompasses more than the core circuit discussed above, including a higher order nucleus termed the posterior medial nucleus (POm) of the thalamus. The connectivity of the POm is distinct from and more extensive than the VPL and VPM nuclei (**Figure 4**). While the POm receives a small amount of ascending sensory information, its primary input is from layer five cortical neurons (Mo et al., 2017; O'Reilly

et al., 2021; Sherman and Guillery, 2006). In addition to the nRT, the POm also recieves inhibitory input from the zona incerta and the anterior pretectal nucleus, two subthalamic regions with broad connectivity in the brain (O'Reilly *et al.*, 2021). The POm projects to layers one and five of the S1 cortex, in addition to the secondary somatosensory (S2), motor, auditory, entorhinal, and insular cortices (Ohno et al., 2012). POm collaterals also project to the nRT and the striatum (Ohno *et al.*, 2012). While the precise function of the POm within the broader circuit remains unknown, there is evidence that it may regulate information flow between the S1 and S2 cortices (Castejon et al., 2016) or be involved in higher order decision processes (El-Boustani et al., 2020). In general, higher order thalamic nuclei are thought to be integral for cortico-thalamo-cortical processing, and thus may be involved in integrating information across modalities (Sherman and Guillery, 2006).

1.2.5 Somatosensory Corticothalamic Circuit Summary

The somatosensory CT circuit is responsible for processing a variety of sensory modalities from both the body and head, as well as generating oscillations that are critical to proper sleep. These diverse functions are enabled by the intricate synaptic balance of excitation and inhibition in the circuit, as well as the two distinct firing modes exhibited by thalamic neurons. Due to its multifunctionality, pathological function in the somatosensory CT circuit is implicated in diverse diseases from chronic pain to autism, schizophrenia, and epilepsy (Baran et al., 2019; Khan et al., 2016; Paz *et al.*, 2011). Specifically, somatosensory CT circuit dysfunction is present in models of Dravet Syndrome (DS), a debilitating infantile epilepsy with few effective treatments (Kalume et al., 2015; Ritter-Makinson *et al.*, 2019). A more thorough understanding of the distinct

cellular properties underlying nRT, VPL, and VPM function could offer cell-type-specific therapies for a variety of diseases, including DS.

1.3 Dravet Syndrome

Dravet syndrome (DS), also known as severe myoclonic epilepsy in infancy, is an infantile epileptic encephalopathy that is caused in seventy to eighty percent of cases by mutations in the *SCN1A* gene, which encodes the voltage-gated sodium channel $Na_v1.1$ (Dravet, 2011). DS is considered a rare genetic disorder, affecting an estimated 1 in 20,000 to 1 in 40,000 children (Bayat et al., 2015; Brunklaus et al., 2012; Hurst, 1990). The disease is characterized by a highly variable phenotype profile including infantile-onset febrile seizures followed by the development of multiple intractable seizure types (Dravet, 2011). As the child ages, progressive developmental delay occurs and can include ataxia, sleep disruption, learning and cognitive impairments, behavioral disorders, and autistic features (Dravet, 2011). DS is also characterized by a high rate of premature death (estimated twenty percent) due to both status epilepticus and sudden unexpected death in epilepsy (SUDEP) (Shmuely et al., 2016). Despite the availability of many anti-epileptic drugs, most DS patients' seizure burden remains unmanaged, even when multiple anti-epileptic drugs are employed (Catarino et al., 2011; Rumiko Takayama, 2014). Due to the debilitating nature of the disease across the lifespan, novel therapeutics are needed to reduce seizure burden and correct other phenotypes of the disease

1.3.1 Etiology

Scn1a mutations underlie a spectrum of developmental epileptic encephalopathies, and DS is among the most severe (Mulley et al., 2005). The *Scn1a* gene encodes the alpha subunit of the voltage-gated sodium channel, $Na_v1.1$, which is expressed in the central and

peripheral nervous system, as well as the heart (Escayg and Goldin, 2010). There are over 500 mutations associated with DS and about half are truncation mutations, leading to haploinsufficiency of the protein (Marini et al., 2011). In the human brain, $Na_V1.1$ expression increases after birth and replaces $Na_V1.3$ expression by about six months of age (Cheah et al., 2013). This switch between $Na_V1.1$ and $Na_V1.3$ expression occurs at about postnatal day 14 in mice (Cheah *et al.*, 2013). In both cases, the rise of $Na_V1.1$ expression in the central nervous system coincides with symptom onset in DS including generalized and often febrile seizures (Cheah *et al.*, 2013).

In the central nervous system, $Na_V1.1$ is expressed predominantly, though not exclusively, at the axon initial segment (AIS) of specific inhibitory neuron populations (Ikuo Ogiwara, 2007). In addition, the protein is expressed in both small and large diameter sensory neurons in the dorsal root ganglion and in select glutamatergic populations, including VPL and VPM thalamic neurons (Ho and O'Leary, 2011; Ikuo Ogiwara, 2013). However, investigations regarding the cellular mechanisms underlying DS have largely focused on affected inhibitory neuron populations.

Mutations in the *Scn1a* gene lead to impaired action potential firing in inhibitory neuron populations across the brain in models of DS. $Na_V1.1$ reportedly can be expressed at the axon initial segment, the nodes of Ranvier, and the soma depending on the cell type, and it is critical for the generation and propagation of action potentials (Catterall et al., 2010; Duflocq et al., 2008; Westenbroek et al., 1989). $Na_V1.1$ is expressed at the AIS of fast-spiking, parvalbumin (PV)-expressing cortical interneurons, which exhibit impairment in the amplitude and number of spikes fired in response to depolarization in a loss-of-function DS mouse model (Ikuo Ogiwara, 2007). The excitability of both somatostatin

(SOM)-expressing inhibitory Martinotti cortical cells and Purkinje cerebellar neurons are also reduced in haploinsufficiency models of DS (Chao Tai, 2014; Franck Kalume, 2007). Altered burst and tonic firing has been exhibited by inhibitory nRT neurons in several DS mouse models including a truncation mutation and point mutation model (Kalume *et al.*, 2015; Ritter-Makinson *et al.*, 2019; Ulrike B.S. Hedrich, 2014). Hippocampal CA1 horizontal stratum-oriens inhibitory neurons exhibit impaired excitability in a point mutation DS model (Yael Almog, 2021), as well as a truncation mutation model (Mistry et al., 2014).

Thus, the canonical understanding of DS is as a disease of inhibitory neuron dysfunction, whereby reduced excitability in inhibitory populations leads to hyperexcitability within particular brain circuits, resulting in both seizures and other phenotypes of the disease (Catterall, 2016). Of importance, there is recent evidence that CA1 pyramidal neurons of the hippocampus, an excitatory neuron population, exhibit altered intrinsic excitability prior to and after seizure onset in a DS model (Yael Almog, 2021). In addition, there are other excitatory neuron populations that express $Na_V1.1$ at high levels, but their excitability has remained largely uninvestigated due to the focus on inhibitory neuron impairment (Ikuo Ogiwara, 2013). It is important to understand the contribution of excitatory neuron populations to DS disease mechanisms, as they may open the door to new therapeutic approaches.

1.3.2 Symptomology and Treatment

The symptomology of DS is progressive in nature, beginning with febrile convulsive seizures in the first year of life (Dravet, 2011). In the first few years of life, the patient's seizure burden increases and includes a variety of seizure types such as focal,

generalized, myoclonic, and absence seizures (Dravet, 2011). A hallmark of DS symptomology is the drug-resistant nature of nearly all seizure types experienced by patients. It is estimated that over 90% of DS patients continue to experience generalized tonic-clonic seizures into adulthood, with less than 10% experiencing seizure remission (Rumiko Takayama, 2014). Historically, first-line treatments for DS patients have included drugs that augment the levels or function of GABA in the brain, such as benzodiazepines, in order to offset the hyperexcitability leading to seizures (J. Helen Cross, 2019). These drugs are not effective for many patients in reducing seizure burden, and they lead to adverse side effects such as severe drowsiness (Catterall, 2016). There are recommended second and third-line treatments that do not act through GABA modulation, including the ketogenic diet and ethosuximide, which is effective in reducing absence seizures in some patients (J. Helen Cross, 2019). A number of recent drugs have been approved for use in DS patients including fenfluramine, which augments serotonin levels; cannabidiol, the first cannabis-derived FDA-approved drug; and stiripentol, which has multiple mechanisms of action including GABA enhancement (Ceulemans et al., 2012; Devinsky et al., 2018; J. Helen Cross, 2019). Though most DS patients are treated with multiple of these approved anti-epileptic drugs, one or more seizure types typically remain unmanaged even into adulthood.

As the patient ages, a variety of other phenotypes emerge including ataxia, cognitive impairments, attention deficits, autistic features, and sleep disruption (Francesca Darra, 2019; J.J.L. Berkvens, 2015; Jill Rodda, 2012; Laura Canafoglia, 2017; Ragona, 2011). These phenotypes may arise, in part, from consistent epileptic activity within brain circuits during development (Catarino *et al.*, 2011). DS is also characterized by a highly

variable phenotypic profile between patients, a characteristic that may be the result of genetic modifiers (Meisler et al., 2010). While treatments are sometimes given to try and manage these phenotypes, they are largely progressive in nature and remain uncontrolled in most patients throughout adulthood (Catarino *et al.*, 2011). Because patients generally exhibit motor, cognitive, behavioral, and sleep impairments, the quality of life for most patients is low and the burden for full-time caregivers is high (Dravet, 2011).

The known mechanisms of DS suggest that the diverse non-seizure phenotypes arise from the dysregulation of particular circuits in the brain. For example, reduced excitability in Purkinje neurons of the cerebellum is thought to lead to dysregulation of cerebellar circuit activity which underlies ataxia and motor impairments in the disease (Franck Kalume, 2007). Cognitive impairments and autistic features, as well as seizure generation, have been linked to hyperexcitability in the cortex due to dysfunction in multiple inhibitory neuron populations (Chao Tai, 2014; Ikuo Ogiwara, 2007; Moran Rubinstein, 2015; Stacey C. Dutton, 2013; Ulrike B.S. Hedrich, 2014). Further, imbalance in hippocampal circuit function is proposed to underlie learning and memory deficits in the disease (Alex Bender, 2016; Frank H Yu, 2006; Stacey C. Dutton, 2013; Ulrike B.S. Hedrich, 2014). The involvement of specific neuron populations within particular circuits suggests that attempting to correct such phenotypes through global modulation of excitation or inhibition is unlikely to succeed. Rather, specifically targeting impaired neuronal populations within affected circuits may be a more efficacious therapeutic approach.

1.3.3 Somatosensory Corticothalamic Circuit Dysfunction in Dravet Syndrome

Importantly, pathological activity in the thalamus is thought to underlie absence seizures and sleep impairments in DS (Kalume *et al.*, 2015; Ritter-Makinson *et al.*, 2019). There is evidence of altered thalamic activity in some DS patients (Jan Moehring, 2013), and case studies indicate that thalamic deep brain stimulation can relieve seizures in some patients (Annika Luttjohann, 2013; Danielle M. Andrade, 2010). Further, it is well-established that absence seizures, a prominent phenotype of the disease, arise in the corticothalamic network (Huguenard, 2019). Absence seizures are marked by characteristic 3-4 Hz spike and wave discharges (SWD) present in EEGs, including a sharp spike that purportedly reflects highly synchronized neuronal spiking in the thalamus and cortex and a slow wave indicating recovery from spiking (Huguenard, 2019). Early studies into absence seizures provided evidence that both cortical and thalamic neurons are required for SWD generation (Gloor et al., 1990). The current model of absence seizure generation involves cortical neurons providing enhanced, high-frequency input to the thalamus, leading to strong burst firing in nRT cells, which results in inhibition of VPL/VPM neurons via $GABA_B$ receptors preferentially. Hyperpolarized VPL/VPM neurons respond in a bursting mode, and the resulting synchrony of firing in the nRT, VPL/VPM, and cortex underlies slower (3-4 Hz) oscillations than occur in sleep spindles (6-14 Hz) (Huguenard, 2019; Jacobsen *et al.*, 2001). However, the precise cellular and synaptic mechanisms through which loss of $Na_V1.1$ leads to absence seizure generation in DS have yet to be fully elucidated.

One recent study in a haploinsufficiency DS mouse model revealed that a compensatory reduction in the calcium-activated potassium current in nRT neurons leads to prolonged bursting in these cells, which may contribute to absence seizure generation

(Ritter-Makinson *et al.*, 2019). DS mice in this study recapitulated absence seizures observed in humans, exhibiting poly-spike-and-wave components, which were phase-locked to high-frequency nRT and VPL/VPM bursts (Ritter-Makinson *et al.*, 2019). Absence seizures are a common and debilitating symptom of DS and are behaviorally characterized by brief gaps in consciousness (Dravet, 2011). These types of seizures seem to be more common in DS in childhood, but even brief hypersynchronous activity over critical periods of brain development could lead to altered brain circuit formation and refinement resulting in persistent circuit dysfunction (Catarino *et al.*, 2011; Tsuda et al., 2013).

There is evidence that somatosensory CT circuit dysregulation also contributes to sleep impairments in DS (Kalume *et al.*, 2015). As previously described, 6-14 Hz sleep spindles are generated in the somatosensory CT circuit and occur during NREM sleep (Fogerson and Huguenard, 2016; Murata and Colonnese, 2019). There is evidence to suggest these spindles are involved in cortical plasticity and memory consolidation. At least 75% of DS patients report sleep disturbances including most commonly difficulty initiating and remaining asleep (Shane H Licheni, 2017). Some patients reported trying a variety of medications to aid in sleep, yet most continued to experience impaired sleep even while using medication (Shane H Licheni, 2017). While sleep spindles have not been assessed in human DS patients, there is evidence of reduced sleep spindles in a DS mouse model with $Na_V1.1$ haploinsufficiency (Kalume *et al.*, 2015). In addition, DS mice exhibited interictal spikes during NREM sleep, as well as reduced delta power and increased brief wakes. These findings were associated with reduced whole-cell Na_V current and impaired hyperpolarization-induced rebound bursting in nRT neurons (Kalume *et al.*,

2015). Bursting in nRT neurons is necessary for intra-thalamic oscillations which underlie sleep spindles, as previously described.

1.3.4 Mechanisms Underlying Somatosensory Circuit Dysfunction

Though the evidence of dysfunction in the somatosensory CT circuit in DS is clear, the precise cellular and synaptic mechanisms underlying the dysfunction remain unknown. In the somatosensory cortex, reduction in the excitability of both PV-expressing and somatostatin-expressing inhibitory neurons has been reported, without alterations in glutamatergic pyramidal neurons (Chao Tai, 2014; Morgana Favero, 2018). This presumably leads to hyperexcitability within the somatosensory cortex and augmented layer 6 CT output to the thalamus. Several different DS mouse models exhibit altered nRT neuronal excitability, yet there are contradictory reports regarding the direction of such altered excitability. Both a *Scn1a*-haploinsufficient and the $Na_V1.1$-R1648H DS mouse model exhibited hypo-excitability of nRT neurons, including reduced depolarization-induced tonic firing and hyperpolarization-induced rebound bursting (Franck Kalume, 2015; Ulrike B.S. Hedrich, 2014). In contrast, the $Na_V1.1$-R1407X DS mouse model exhibited hyperexcitability of PV-expressing nRT neurons including prolonged rebound bursts and enhanced depolarization-induced tonic firing (Ritter-Makinson *et al.*, 2019). These discrepancies could be partially explained by variability in the specific model or age range studied. There is evidence of distinct changes in cell excitability across different stages of the disease in the cortex and hippocampus, but there have been no longitudinal investigations of thalamic excitability in DS (Morgana Favero, 2018; Yael Almog, 2021). It is important to understand how nRT neurons are dysregulated in the disease in order to illuminate how they contribute to circuit-wide dysfunction. In addition, identifying the

specific mechanisms underlying altered nRT excitability could provide novel therapeutic targets to correct their function.

There have been no reports of altered excitability in VPL or VPM neurons in DS models. Yet, both VPL and VPM neurons express $Na_V1.1$ at high levels, so haploinsufficiency of $Na_V1.1$ in DS could lead to altered neuron function (Ikuo Ogiwara, 2013). This is of particular interest, as many other excitatory neuron populations do not express $Na_V1.1$ and are reported not to have altered excitability in DS. We hypothesized that haploinsufficiency of $Na_V1.1$ in DS leads to altered excitability of VPL and VPM neurons, which contributes to altered circuit-wide function. Altered glutamatergic neuron function in the VPL or VPM could provide novel opportunities for therapeutic intervention, which has not yet been investigated.

There have also been no reports of altered synaptic connectivity in the somatosensory CT circuit in DS. The $Na_V1.1$-R1648H mouse model exhibited reduced spontaneous inhibitory postsynaptic currents (IPSCs) in VPL/VPM neurons, but this was attributed to reduced nRT firing and thus less inhibitory input to the VPL/VPM (Ulrike B.S. Hedrich, 2014). Though no synaptic-level changes have yet been reported, epileptic activity occurring in the thalamus across infancy could alter activity-dependent synaptic formation and refinement during critical periods of circuit development. Indeed, synaptic connectivity between the nRT and VPL/VPM is still being heavily refined in rodents at postnatal day 14, which is the onset of seizures in most DS models (Murata and Colonnese, 2019). Thus, we hypothesized that disrupted neuronal excitability leads to somatosensory circuit dysfunction through activity-dependent synaptic alterations.

Importantly, there is evidence in other brain regions of transient changes in cellular excitability as the disease progresses. For example, somatosensory cortical PV-expressing interneurons exhibit reduced excitability for a transient period between postnatal days 18 and 21 before being rescued by postnatal day 55 (Morgana Favero, 2018). If a transient window of altered excitability exists in these cell populations, persistent synaptic alterations may be responsible for long-term circuit dysfunction and associated disease phenotypes. Revealing such synaptic-level alterations could offer novel therapeutic options to correct circuit function even after cell excitability may return to normal.

If altered intrinsic excitability does indeed give rise to impaired synaptic connectivity in DS, then both mechanisms may contribute to circuit-wide dysfunction leading to two primary strategies for correcting circuit function. Firstly, intrinsic excitability could be rescued by attempting to increase $Na_V1.1$ levels through genetic therapeutic approaches. There is recent work testing the feasibility of antisense oligonucleotides to augment *Scn1a* levels and reduce seizure burden in a DS mouse model (Zhou Han, 2020). The goal of this approach would be to reduce epileptic activity throughout life, including during development, when it may prevent impaired activity-dependent synaptic formation. However, this approach is time-sensitive and would likely require intervention prior to critical periods of circuit development to successfully prevent altered synaptic development. Secondly, the synaptic alterations could be targeted using a wide array of available synaptic modulators. Importantly, there are a variety of synaptic-level targets in the thalamus such as glutamatergic receptors. A broad range of AMPA, NMDA, and metabotropic glutamate receptor subtypes are expressed in the nRT and VPL/VPM, and increasing subtype-specific modulators are being developed, allowing for

synaptic-level intervention (Bashkim Kadriu, 2021; Caleigh M. Azumaya, 2017; Mariacristina Mazzitelli, 2018; N Hovelso, 2012). However, the precise cellular and synaptic mechanisms underlying somatosensory CT circuit dysfunction in DS must be elucidated in order to identify the appropriate therapeutic approach to correct circuit function.

1.4 Hypothesis and Objectives

Accumulating evidence has revealed the importance of the thalamus in brain-wide integratory processing, yet there remain many unexplored facets of thalamic function. Specifically, cellular heterogeneity within thalamic nuclei and the role of distinct cell types in healthy and diseased circuit function remain largely uninvestigated. The core somatosensory thalamus consists of three distinct cell types including GABAergic nRT and glutamatergic VPL and VPM neurons, all of which highly express $Na_V1.1$. Though the VPL and VPM constitute unique thalamic nuclei, their cellular properties in a healthy context have not been investigated. In addition, changes in the excitability of these two nuclei have not been individually studied in the context of DS. Thus, the first objective of this work was to identify how the excitability of nRT, VPL, and VPM neurons may be disrupted in a haploinsufficiency model of DS. We hypothesized that haploinsufficiency of $Na_V1.1$ in DS leads altered excitability in all three neuron populations, which may contribute distinctly to circuit-wide pathological activity.

Because epileptic activity occurs across critical periods of somatosensory thalamic circuit development in DS, we further hypothesized that altered cellular excitability leads to long-term changes in circuit function through activity-dependent synaptic alterations. Though the VPL and VPM receive distinct ascending somatosensory information and form

distinct connectivity with the nRT, alterations in their synaptic connectivity have not been uniquely studied in DS. Thus, another objective of this work was to identify changes in GABAergic and glutamatergic synaptic input to the nRT, VPL, and VPM in a DS mouse model. Identifying existing changes in synaptic connectivity would provide novel opportunities for therapeutic intervention in the circuit.

In addition, we aimed to characterize the cellular properties of VPL and VPM neuronal populations in a non-diseased circuit, as a direct comparison of their functional properties has not been reported. A systematic investigation of the cellular properties of these two cell populations will open the door to understand how they may uniquely contribute to circuit states in both health and disease. Based on our findings in the DS model, we hypothesized that intrinsic firing properties of VPL and VPM neuron would differ in a healthy circuit.

Herein, we present evidence of distinctly altered excitability in GABAergic nRT and glutamatergic VPL and VPM neurons in a DS mouse model. In addition, we identified alterations in synaptic input to both the nRT and VPL. We further revealed distinct properties of VPL and VPM neuronal function in a healthy circuit including enhanced depolarization-induced tonic firing in VPL neurons with no change in rebound burst strength. This work expands current models of thalamic dysfunction in DS to include altered glutamatergic neuron excitability, as well as synapse dysfunction. In addition, it lays the foundation for investigations into the distinct contribution of VPL and VPM nuclei to the many diseases of somatosensory circuit dysfunction.

References

Abbas, S.Y., Ying, S.-W., and Goldstein, P.A. (2006). Compartmental distribution of hyperpoarization-activated cyclic-nucleotide-gated channel 2 and hyperpolarization-activated-activated cyclic-nucleotide-gated channel 4 in thalamic reticular and thalamocortical relay neurons. Neuroscience *141*, 1811-1825.

Alex Bender, B.L., Pierre-Pascal Lenck-Santini (2016). Cognitive Deficits Associated with Nav1.1 Alterations: Involvement of Neuronal Firing Dynamics and Oscillations. PLOS One *11*.

Alexandra Krol, R.W., Michael Halassa, Guoping Feng (2018). Thalamic Reticular Dysfunction as a Circuit Endophenotype in Neurodevelopmental Disorders. Neuron *98*, 282-295.

Annika Luttjohann, G.v.L. (2013). Thalamic stimulation in absence epilepsy. Epilepsy Research *106*, 136-145.

Astori, S., Wmmer, R.D., Prosser, H.M., Corti, C., Corsi, M., Liaudet, N., Volterra, A., Franken, P., Adelman, J.P., and Luthi, A. (2011). The Cav3.3 calcium channel is the major sleep spindle pacemaker in thalamus. PNAS *108*, 13823-13828.

Avram, M., Brandl, F., Bauml, J., and Sorg, C. (2018). Cortico-thalamic hypo- and hyperconnectivity extend consistently to basal ganglia in schizophrenia. Neuropsychopharmacology *43*, 2239-2248.

Baran, B., Karahanoglu, F.I., Myloas, D., Demanuele, C., Vangel, M., Stickgold, R., Anticevic, A., and Manoach, D.S. (2019). Increased Thalamocortical Connectivity in Schizophrenia Correlates with Sleep Spindle Deficits: Evidence for a Common Pathophysiology. Biology Psychiatry: Cognitve Neuroscience and Neuroimaging *4*, 706-714.

Bashkim Kadriu, L.M., Jenessa N. Johnston, Lisa E. Kalynchuk, Hector J. Caruncho, Maurizio Popoli, Carlos A. Zarate Jr. (2021). Positive AMPA receptor modulation in the treatment of neuropsychiatric disorders: A long and winding road. Drug Discovery Today.

Bayat, A., Hjalgrim, H., and Moller, R. (2015). The incidence of Scn1a-related Dravet syndrome in Denmark is 1:22,000: a population-based study from 2004 to 2009. Epilepsia *56*, 36-39.

Briggs, F., and Usrey, W.M. (2008). Emerging views of corticothalamic function. Current Opinion in Neurobiology *18*, 403-407.

Brunklaus, A., Ellis, R., Reavey, E., Forbes, G.H., and Zuberi, S.M. (2012). Prognostic, clinical, and demographic features in Scn1a mutation-postitive Dravet syndrome. Brain *135*, 2329-2336.

Caleigh M. Azumaya, E.L.D., Paige N. Vinson, Shaun Stauffer, Gary Sulikowski, C. David Weaver, Terunaga Nakagawa (2017). Screening for AMPA receptor auxiliary subunit specific modulators. PLOS One.

Castejon, C., Barros-Zulaica, N., and Nunez, A. (2016). Control of Somatosensory Cortical Processing by Thalamic Posterior Medial Nucleus: A New Role of Thalamus in Cortical Processing. PLOS One *11*.

Catarino, C.B., Liu, J.Y.W., Liagkouras, I., Gibbons, V.S., Labrum, R.W., Ellis, R., Woodward, C., Mary B. Davis, S., Cross, H., and Richard E. Appleton, S.C.Y., Jacinta M. McMahon, Susannah T. Bellows, Thomas S. JAcques, Sameer M. Zuberi, Matthias J. Koepp, Lillian Martinian, Ingrid E. Scheffer, Maria Thom, Sanjay M. Sisodiya (2011). Dravet syndrome as epileptic encephalopathy: evidence from long-term course and neuropathology. Brain *134*, 2982-3010.

Catterall, W.A. (2016). Dravet Syndrome: A Sodium Channel Interneuronopathy. In Ion Channels in Health and Disease, G.S. Pitt, ed. (Academic Press).

Catterall, W.A., Kalume, F., and Oakley, J.C. (2010). Nav1.1 channels and epilepsy. The Journal of Physiology *588*, 1849-1859.

Ceulemans, B., Boel, M., Leyssens, K., Rossem, C.V., Neels, P., Jorens, P.G., and Lagae, L. (2012). Successful use of fenfluramine as an add-on treatment for Dravet syndrome. Epilepsia *53*, 1131-1139.

Chao Tai, Y.A., Ruth Westenbroek, Todd Scheuer, William Catterall (2014). Impaired excitability of somatostatin- and parvalbumin-expressing cortical interneurons in a mouse model of Dravet syndrome. PNAS, E3139-E3148.

Cheah, C.S., Westenbroek, R.E., Roden, W.H., Kalume, F., Oakley, J.C., Jensen, L.A., and Catterall, W.A. (2013). Correlations in timing of sodium channel expression, epilepsy, and sudden death in Dravet syndrome. Channels *7*, 468-472.

Cheong, E., Kim, C., Choi, B.J., Sun, M., and Shin, H.-S. (2011). Thalamic ryanodine receptors are involved in controlling the tonic firing of thalamocortical neurons and inflammatory pain signal processing. Journal of Neuroscience *31*, 1213-1218.

Chiaia, N.L., Rhoades, R.W., Fish, S.E., and Killackey, H.P. (1991). Thalamic Processing of Vibrissal Information in the Rat: II. Morphological and Functional Properties of Medial Ventral Posterior Nucleus and Posterior Nucleus Neurons. The Journal of Comparative Neurology *314*, 217-236.

Clemente Perez, A., Ritter-Makinson, S., Higashikubo, B., Brovarney, S., Cho, F.S., Urry, A., Holden, S.S., Wimer, M., Dávid, C., Fenno, L.E., et al. (2017). Distinct thalamic reticular cell types differentially modulate normal and pathological cortical rhythms. Cell Reports *19*, 2130-2142.

Danielle M. Andrade, C.H., Andres M. Lozano, Richard A. Wennberg (2010). Dravet syndrome and deep brain stimulation: Seizure control after 10 years of treatment. Epilepsia *51*, 1314-1316.

David, F., C¸arc¸ak, N., Furdan, S., Onat, F., Gould, T., Me´sza´ros, A.d.m., Giovanni, G.D., Hernandez, V.M., Chan, C.S., Lo″rincz, M.L., and Crunelli, V. (2018). Suppression of

Hyperpolarization-Activated Cyclic Nucleotide-Gated Channel Function in Thalamocortical Neurons Prevents Genetically Determined and Pharmacologically Induced Absence Seizures. Journal of Neuroscience *38*, 6615-6627.

Delmas, P., Hao, J., and Rodat-Despoix, L. (2011). Molecular mechanisms of mechanotransduction in mammalian sensory neurons. Nature Reviews Neuroscience *12*, 139-153.

Deschenes, M., Vienante, P., and Zhang, Z.-W. (1998). The organization of corticothalamic projections: reciprocity versus parity. Brain Research Reviews *28*, 286-308.

Devinsky, O., Nabbout, R., Miller, I., Laux, L., Zolnowska, M., Wright, S., and Roberts, C. (2018). Long-term cannabidiol treatment in patients with Dravet syndrome: An open-label extention trial. Epilepsia *60*, 294-302.

Dravet, C. (2011). The core Dravet syndrome phenotype. Epilepsia *52* (*2*), 3-9.

Duflocq, A., Bras, B.L., Bullier, E., Couraud, F., and Davenne, M. (2008). Nav1.1 is predominantly expressed in nodes of Ranvier and axon initial segments. Molecular and Cellular Neuroscience *39*, 180-192.

El-Boustani, S., Sermet, B.S., Foustoukos, G., Oram, T.B., Yizhar, O., and Petersen, C.C.H. (2020). Anatomically and functionally distinct thalamocortical inputs to primary and secondary mouse whisker somatosensory cortices. Nature Communications *11*.

Escayg, A., and Goldin, A.L. (2010). Sodium channel Scn1a and epilepsy: mutations and mechanisms. Epilepsia *51*, 1650-1658.

Fogerson, P.M., and Huguenard, J.R. (2016). Tapping the brakes: cellular and synaptic mechanisms that regulate thalamic oscillations. Neuron *92*, 687-704.

Francesca Darra, D.B., Charlotte Dravet, Mara Patrini, Francesca Offredi, Daniela Chieffo, Elena Piazza, Elena Fontana, Giorgia Olivieri, Ida Turrini, Bernardo Bernardina, Tiziana Granata, Francesca Ragona (2019). Dravet syndrome: Early electroclinical findings and long-term outcome in adolescents and adults. Epilepsia *60*, S49-S58.

Franck Kalume, F.H.Y., Ruth E. Westenbroek, Todd Scheuer, William Catterall (2007). Reduced Sodium Current in Purkinje Neurons from Nav1.1 Mutant Mice: Implications for Ataxia in Severe Myoclonic Epilepsy in Infancy. Neurobiology of Disease *27*, 11065-11074.

Franck Kalume, J.C.O., Ruth E. Westenbroek, Jennifer Gile, Horacio O. de la Iglesia, Todd Scheuer, William A. Catterall (2015). Sleep Impairment and Reduced Interneuron Excitability in a Mouse Model of Dravet Syndrome. Neurobiology of Disease *77*, 141-154.

Frank H Yu, M.M., Ruth E. Westenbroek, Carol A. Robbins, Franck Kalume, Kimberly A. Burton, William J. Spain, G. STanley McKnight, Todd Scheuer, Willliam A. Catterall (2006). Reduced

sodium current in GABAergic interneurons in a mouse model of severe myoclonic epilepsy in infancy. Nature Neuroscience *9*, 1142-1149.

Gloor, P., Avoli, M., and Kostopoulos, G. (1990). Thalamo-cortical relationships in generalized epilepsy with bilaterally synchronous spike-and-wave discharge. Generalized Epilepsy: Neurobiological Approaches, 190-202.

Gomez-Ramirez, M., Hysaj, K., and Niebur, E. (2016). Neural mechanisms of selective attention in the somatosensory system. Journal of Neurophysiology *116*, 1218-1231.

Ha, G.E., Lee, J., Kwak, H., Song, K., Kwon, J., Jung, S.-Y., Hong, J., Chang, G.-E., Hwang, E.M., Shin, H.-S., et al. (2016). The Ca^{2+}-activated chloride channel anoctamin-2 mediates spike-frequency adaptation and regulates sensory transmission in thalamocortical neurons. Nature Communications *7*.

Hains, B.C., Saab, C.Y., and Waxman, S.G. (2005). Changes in electrophysiological properties and sodium channel Nav1.3 expression in thalamic neurons after spinal cord injury. Brain *128*, 2359-2371.

Hall, K.D., and Lifshiftz, J. (2010). Diffuse traumatic brain injury initially attenuates and later expands activation of the rat somatosensory whisker circuit concomitant with neuroplastic responses. Brain Research *1323*, 161-173.

Hazra, A., Corbett, B.F., You, J.C., Aschmies, S., Zhao, L., Li, K., Lepore, A.C., Marsh, E.D., and Chin, J. (2016). Corticothalamic network dysfucntion and behavioral deficits in a mouse model of Alzheimer's disease. Neurobiology of Aging *44*, 96-107.

Ho, C., and O'Leary, M.E. (2011). Single-cell analysis of sodium channel expression in dorsal root ganglion neurons. Mol Cell Neuroscience *46*, 159-166.

Holmes, M.D., Quiring, J., and Tucker, D.M. (2010). Evidence that juvenile myoclonic epilepsy is a disorder of frontotemporal corticothalamic networks. NeuroImage *49*, 80-93.

Huguenard, J. (2019). Current Controversy: Spikes, Bursts, and Synchrony in Generalized Absence Epilepsy: Unresolved Questions Regarding Thalamocortical Synchrony in Absence Epilepsy. Epilepsy Currents *19*.

Huguenard, J., and Prince, D. (1994). Intrathalamic rhythmicity studied in vitro: nominal T-current modulation causes robust antioscillatory effects. Journal of Neuroscience *14*, 5485-5502.

Hurst, D.L. (1990). Epidemiology of severe myoclonic epilepsy of infancy. Epilepsia *31*, 397-400.

Ikuo Ogiwara, H.M., Noriyuki Morita, Emi Mazaki, Ikuyo Inoue, Tamaki Takeuchi, Shigeyoshi Itohara, Yuchio Yanagawa, Kunihiko Obata, Teiichi Furuichi, Takao K. Hensch, Kazuhiro Yamakawa (2007). Nav1.1 Localizes to Axons of Parvalbumin-Positive Inhibitory Interneurons: A

Circuit Basis for Epileptic Seizures in Mice Carrying an Scn1a Gene Mutation. Neurobiology of Disease *27*, 5903-5914.

Ikuo Ogiwara, T.I., Hiroyuki Miyamoto, Ryohei Iwata, Tetsushi Yamagata, Emi Mazaki, Yuchio Yanagawa, Nobuaki Tamamaki, Takao K. Hensch, Shigeyoshi Itohara, Kazuhiro Yamakawa (2013). Nav1.1 haploinsufficiency in excitatory neurons ameliorates seizure-associated sudden death in a mouse model of Dravet Syndrome. Human Molecular Genetics *22*, 4784-4804.

J. Helen Cross, R.H.C., Rima Nabbout, Federico Vigevano, Renzo Guerrini, Lieven Lagae (2019). Dravet syndrome: Treatment options and management of prolonged seizures. Epilepsia *60*, S39-S48.

J.J.L. Berkvens, I.V., M.J.M.B Veendrick-Meeks, F.M. Snoeijen-Schouwenaars, H.J. Schelhaas, M.H. Willemsen, I.Y. Tan, A.P. Aldenkamp (2015). Autism and behavior in adult patients with Dravet syndrome (DS). Epilepsy & Behavior *47*, 11-16.

Jacobsen, R.B., Ulrich, D., and Huguenard, J.R. (2001). GABAb and NMDA Receptors Contribute to Spindle-Like Oscillations in Rat Thalamus In Vitro. Journal of Neurophysiology *86*.

Jan Moehring, S.v.P., Friederike Moeller, Ingo Helbig, Stephan Wolff, Olav Jansen, Hiltrud Muhle, Rainer Boor, Ulrich Stephani, Michael Siniatchkin (2013). Variability of EEG-fMRI findings in patients with SCN1A-positive Dravet Syndrome. Epilepsia *54*, 918-926.

Jeanne T. Paz, T.J.D., Eric S. Frechette, Bruno Delord, Isabel Parada, Kathy Peng, Karl Deisseroth, John R. Huguenard (2013). Closed-loop optogenetic control of thalamus as a new tool to interrupt seizures after cortical injury. Nat Neurosci *16*, 64-70.

Jill Rodda, I.S., Jacinta McMahon, Samuel Berkovic, H. Kerr Graham (2012). Progressive Gait Deterioration in Adolescents with Dravet Syndrome. Arch Neurol *69*, 873-878.

Jones, E.G. (2002). Thalamic organization and function after Cajal. Prog Brain Res *136*, 333-357.

Kalume, F., Oakley, J.C., Westenbroek, R.E., Gile, J., de la Iglesia, H.O., Scheuer, T., and Catterall, W.A. (2015). Sleep impairment and reduced interneuron excitability in a mouse model of Dravet Syndrome. Neurobiology of Disease *77*, 141-154.

Khan, S., Hashmi, J.A., Mamashli, F., Bharadwaj, F., Bharadwaj, H.M., Ganesan, S., Michmizos, K.P., Kitzbichler, M.G., Zatino, M., Garel, K.-L.A., et al. (2016). Altered Onset Response Dynamics in Somatosensory Processing in Autism Spectrum Disorder. Frontiers in Neuroscience *10*.

Kim, A., Latchoumane, C., Lee, S., Kim, G.B., Cheong, E., Augustine, G.J., and Shin, H.S. (2012). Optogenetically induced sleep spindle rhythms alter sleep architectrues in mice. PNAS *109*, 20673-20678.

Landisman, C.E., and Connors, B.W. (2007). VPM and PoM Nuclei of the Rat Somatosensory Thalamus: Intrinsic Neuronal Properties and Corticothalamic Feedback. Cerebral Cortex *17*, 2853-2865.

Laura Canafoglia, F.R., Ferruccio Panzica, Elena Piazza, Elena Freri, Simona Binelli, Vidmer Scaioli, Guiliano Avanzini, Tiziana Granata, Silvana Franceschetti (2017). Movement-activated cortical myoclonus in Dravet syndrome. Epilepsy Research *130*, 47-52.

Li, L., and Ebner, F.F. (2007). Cortical modulation of spatial and angular tuning maps in the rat thalamus. Journal of Neuroscience *27*, 167-179.

Llinas, R.R., and Steriade, M. (2006). Bursting of thalamic neurons and states of vigilance. Journal of Neurophysiology *95*, 3297-3308.

Mariacristina Mazzitelli, E.P., Sabatino Maione, and Volker Neugebauer (2018). Group II Metabotropic Glutamate Receptors: Role in Pain Mechanisms and Pain Modulation. Frontiers in Molecular Neuroscience *11*.

Marini, C., Scheffer, I.E., Nabbout, R., Suls, A., Jonghe, P.D., Zara, F., and Guerrini, R. (2011). The genetics of Dravet syndrome. Epilepsia *52* (*2*), 24-29.

McCormick, D., and Feeser, H. (1990). Functional implications of burst firing and single spike activity in lateral geniculate relay neurons. Neuroscience *39*, 103-113.

McKay, B.E., McRory, J.E., Molineux, M.L., Hamid, J., Snutch, T.P., Zamponi, G.W., and Turner, R.W. (2006). Cav3 T-type calcium channel isoforms differentially distribute to somatic and dendritic compartments in rat central neurons. European Journal of Neuroscience *24*, 2581-2594.

Meisler, M.H., O'Brien, J.E., and Sharkey, L.M. (2010). Sodium channel gene family: epilepsy mutations, gene interactions and modifier effects. Journal of Physiology *599*, 1841-1848.

Mistry, A.M., Thompson, C.H., Miller, A.R., Vanoye, C.G., George Jr, A.L., and Kearney, J.A. (2014). Strain- and age- dependent hippocampal neuron sodium currents correlate with epilepsy severity in Dravet syndrome mice. Neurobiology of Disease *65*, 1-11.

Mo, C., Petrof, I., Viaene, A., and Sherman, S. (2017). Synaptic properties of the lemniscal and paralemniscal pathways to the mouse somatosensory thalamus. PNAS *114*, E6212-E6221.

Moran Rubinstein, S.H., Chao Tai, Ruth Westenbroek, Avery Hunker, Todd Scheuer, and William Catterall (2015). Dissecting the phenotypes of Dravet Syndrome by gene deletion. Brain *138*, 2219-2233.

Morgana Favero, N.P.S., Emily Lopez, Jennifer A. Kearney, Ethan M. Goldberg (2018). A Transient Developmental Window of Fast-Spiking Interneuron Dysfunction in a Mouse Model of Dravet Syndrome. Neurobiology of Disease *38*, 7912-7927.

Mulley, J.C., Scheffer, I.E., Petrou, S., Dibbens, L.M., Berkovic, S.F., and Harkin, L.A. (2005). Scn1a mutations and epilepsy. Human Mutations *25*, 535-542.

Murata, Y., and Colonnese, M.T. (2019). Thalamic inhibitory circuits and network activity development. Brain Research *1706*, 13-23.

N Hovelso, F.S., L. P. Montezinho, P. S. Pinheiro, K. F. Herrik, and A. Mork (2012). Therapeutic Potential of Metabotropic Glutamate Receptor Modulators. Curr Neuropharmacol *10*, 12-48.

O'Reilly, C., Iavarone, E., Yi, J., and Hill, S.L. (2021). Rodent somatosensory thalamocortical circuitry: Neurons, synapses, and connectivity. Neuroscience & Behavioral Reviews *126*, 213-235.

Ohno, S., Kuramoto, E., Furuta, T., Hioki, H., Tanaka, Y.R., Fujiyama, F., Sonomura, T., Uemura, M., Sugiyama, K., and Kaneko, T. (2012). A morphological analysis of thalamocortical axon fibers of rat posterior thalamic nuclei: a single neuron tracing study with viral vectors. Cerebral Cortex *22*, 2840-2857.

Paz, J.T., Bryant, A.S., Peng, K., Fenno, L., Yizhar, O., Franklel, W.N., Deisseroth, K., and Huguenard, J.R. (2011). A new mode of corticothalamic transmission revealed in the Gria4-/- model of absence epilepsy. Nat Neurosci *14*, 1167-1173.

Princivalle, A.P., Richards, D.A., Duncan, J.S., Spreafico, R., and Bowery, N.G. (2003). Modification of $GABA_{B1}$ and $GABA_{B2}$ receptor subunits in the somatosensory cerebral cortex and thalamus of rats with absence seizures (GAERS). Epilepsy Research *55*, 39-51.

Ragona, F. (2011). Cognitive development in children with Dravet syndrome. Epilepsia *52* (*2*), 39-43.

Ritter-Makinson, S., Clemente-Perez, A., Higashikubo, B., Cho, F., Holden, S., Bennett, E., Chkaidze, A., Rooda, O.E., Cornet, M.-C., Hoebeek, F., et al. (2019). Augmented Reticular Thalamic Bursting and Seizures in Scn1a-Dravet Syndrome. Cell Reports *26*, 54-64.

Rumiko Takayama, T.F., Hideo Shigematsu, Katsumi Imai, Yukitoshi Takahashi, Kazuhiro Yamakawa, Yushi Inoue (2014). Long-term course of Dravet syndrome: A study from an epilepsy center in Japan. Epilepsia *55*, 528-538.

Shane H Licheni, J.M.M., Amy L Schneider, Margot J Davey, Ingrid E Scheffer (2017). Sleep problems in Dravet syndrome: a modifiable comorbidity. Developmental Medicine & Child Neurology *60*.

Shane R. Crandall, S.C., Barry Connors (2015). A Corticothalamic Switch: Controlling the Thalamus with Dynamic Switches. Neuron *86*, 768-782.

Sherman, S.M. (2001). Tonic and burst firing: dual modes of thalamocortical relay. Trends in Neuroscience *24*, 122-126.

Sherman, S.M. (2007). The Thalamus is More than Just a Relay. Curr Opin Neurobiol *17*, 417-422.

Sherman, S.M., and Guillery, R.W. (2006). Exploring the Thalamus and Its Role in Cortical Function (The Massachusetts Institute of Technology Press).

Shmuely, S., Sisodiya, S.M., Gunning, W.B., Sander, J.W., and Thijs, R.D. (2016). Mortality in Dravet syndrome: A review. Epilepsy & Behavior *64*, 69-74.

Squire, L.R., Berg, D., Bloom, F.E., du Lac, S., Ghosh, A., and Spitzer, N.C. (2013). Chapter 24: The Somatosensory System. In Fundamental Neuroscience, (Elsevier).

Stacey C. Dutton, C.D.M., Ligia A. Papale, Anupama Shankar, Bindu Balakrishnan, Kazu Nakazawa, Andrew Escayg (2013). Preferential inactivation of Scn1a in parvalbumin interneurons increases seizure susceptibility. Neurobiology of Disease *0*, 211-220.

Steriade, M., Domich, L., Oakson, G., and Deschenes, M. (1987). The deafferented reticular thalamic nucleus generates spindle rhythmicity. Journal of Neurophysiology *57*, 260-273.

Talley, E.M., Cribbs, L.L., Lee, J.H., Daud, A., Perez-Reyes, E., and Bayliss, D.A. (1999). Differential distribution of three members of a gene family encoding low voltage-activated (T-type) calcium currents. J Neuroscience *19*, 1895-1911.

Temereanca S, S.D. (2004). Functional topography of corticothalamic feedback enhances thalamic spatial response tuning in the somatosensory whisker/barrel system. Neuron *41*, 639-651.

Tsuda, Y., Oguni, H., Sakauchi, M., and Osawa, M. (2013). An electroclinical study of absence seizures in Dravet syndrome. Epilpsy Research *103*, 88-96.

Ulrike B.S. Hedrich, C.L., Daniel Kirschenbaum, Martin Pofahl, Jennifer Lavigne, Yuanyuan Liu, Stephan Theiss, Johannes Slotta, Andrew Escayg, Marcel Dihne, Heinz Beck, Massimo Mantegazza, Holger Lerche (2014). Impaired Action Potential Initiation in GABAergic Interneurons Caused Hyperexcitable Networks in an Epileptic Mouse Model Carrying a Human Nav1.1 Mutation. Journal of Neuroscience *34*, 14874-14889.

Warren, R.A., Agmon, A., and Jones, E.G. (1994). Oscillatory synaptic interactions between ventroposterior and reticular neurons in mouse thalamus in vitro. Journal of Neurophysiology *72*.

Westenbroek, R., DK, M., and Catterall, W. (1989). Differential subcellular localization of the RI and RII Na^+ channel subtypes in central neurons. Neuron *3*, 695-704.

Yael Almog, S.F., Marina Brusel, Anat Mavashov, Karen Anderson, Moran Rubinstein (2021). Developmental alterations in firing properties of hippocampal CA1 inhibitory and excitatory neurons in a mouse model of Dravet syndrome. Neurobiology of Disease *148*.

Zhou Han, C.C., Anne Christiansen, Sophina Ji, Qian Lin, Charles Anumonwo, Chante Liu, Steven C Leiser, Meena, Isabel Aznarez, Gene Liau, Lori L Isom (2020). Antisense oligonucleotides increase Scn1a expression and reduce seizures and SUDEP incidence in a mouse model of Dravet syndrome. Sci Transl Med *12*.

Zobeiri, M., Chaudhary, R., Blaich, A., Rottmann, M., Herrmann, S., Meuth, P., Bista, P., Kanyshkova, T., Lüttjohann, A., Narayanan, V., et al. (2019). The Hyperpolarization-Activated HCN4 Channel is Important for Proper Maintenance of Oscillatory Activity in the Thalamocortical System. Cerebral Cortex *29*, 2291-2304.

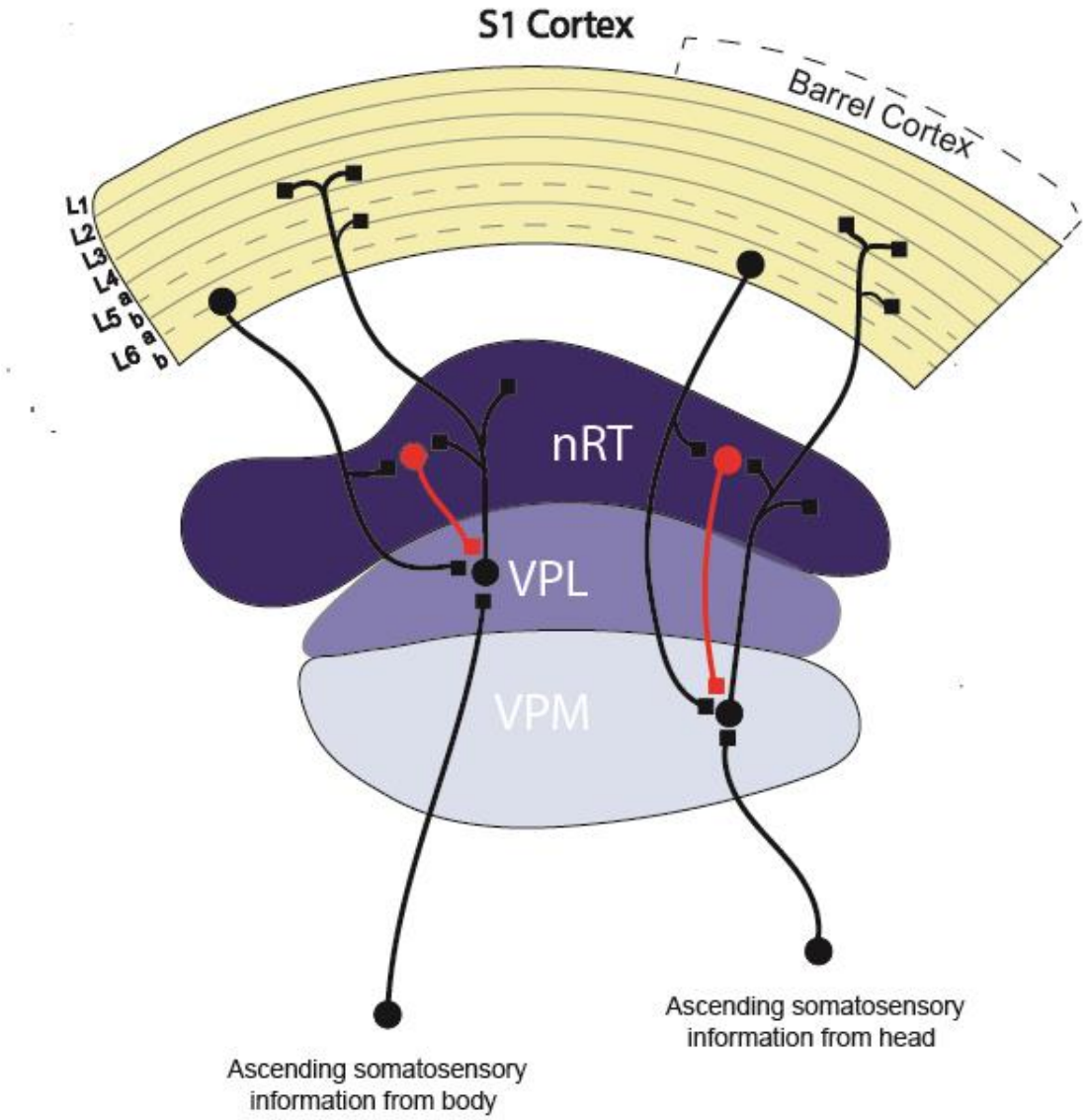

Figure 1. The Core Somatosensory Corticothalamic Circuit
The core somatosensory CT circuit includes the VPL and VPM thalamic nuclei, which receive ascending somatosensory input from the body and head, respectively. The VPL and VPM project to the primary somatosensory cortex (S1), which returns reciprocal feedback. Both cortical neurons and VPL/VPM neurons send collaterals to the inhibitory nRT, which provides the primary inhibitory input to the VPL and VPM.

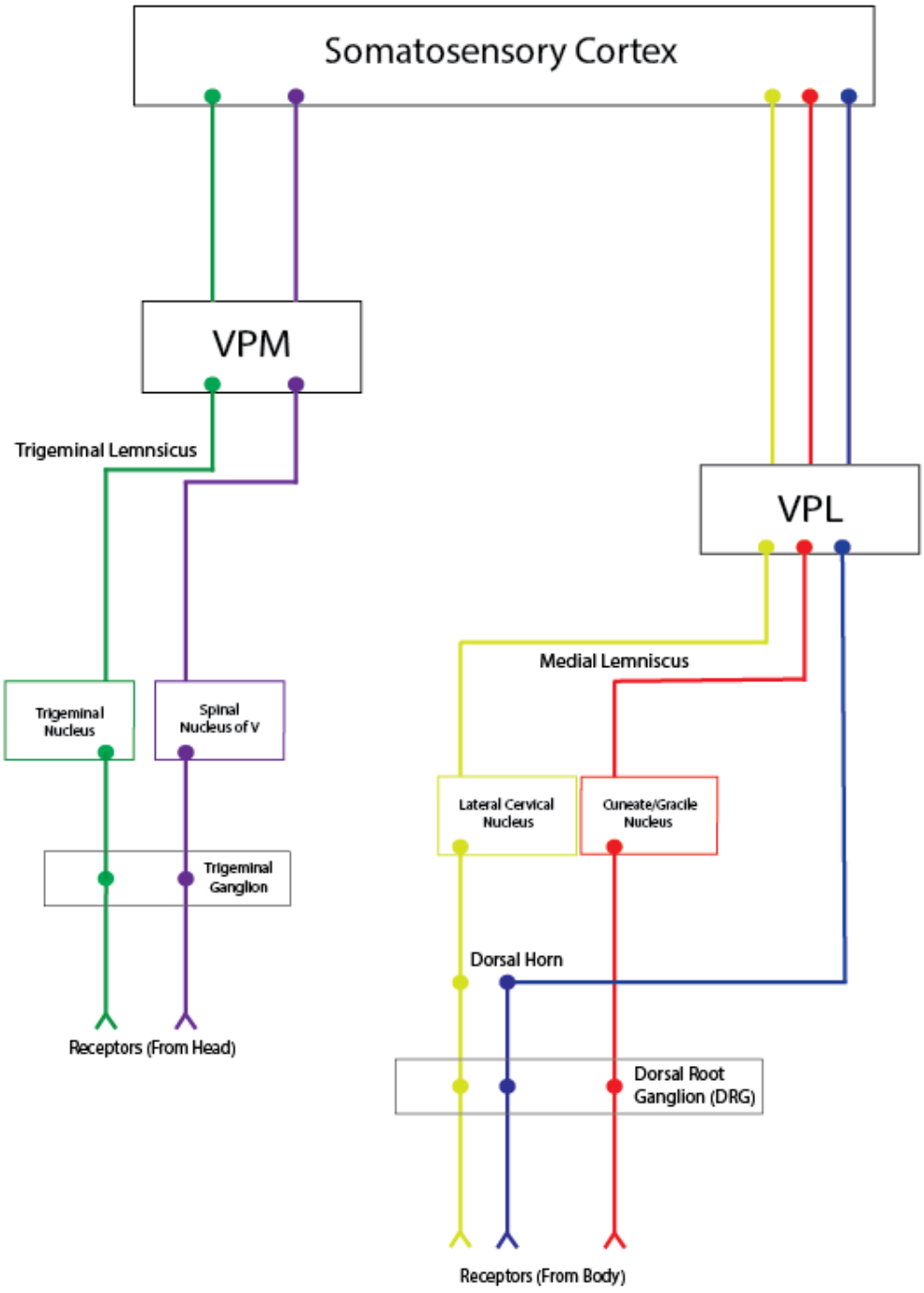

Figure 2. Somatosensory Pathways
The *dorsal column medial lemniscus pathway* (red) carries somatosensory information from the body to the VPL thalamus. The *spinothalamic tract* (blue) carries nociceptive information from the body to the VPL thalamus. The *spinocervical tract* (yellow) also carries nociceptive information from the body to the VPL thalamus. The *trigeminal lemniscus pathway* (green) carries somatosensory information from the head to the VPM thalamus. The *extralemnsical trigmeninal pathway* (purple) carries nociceptive information from the head to the VPM thalamus. Adapted from O'Reilly *et al.*, 2015.

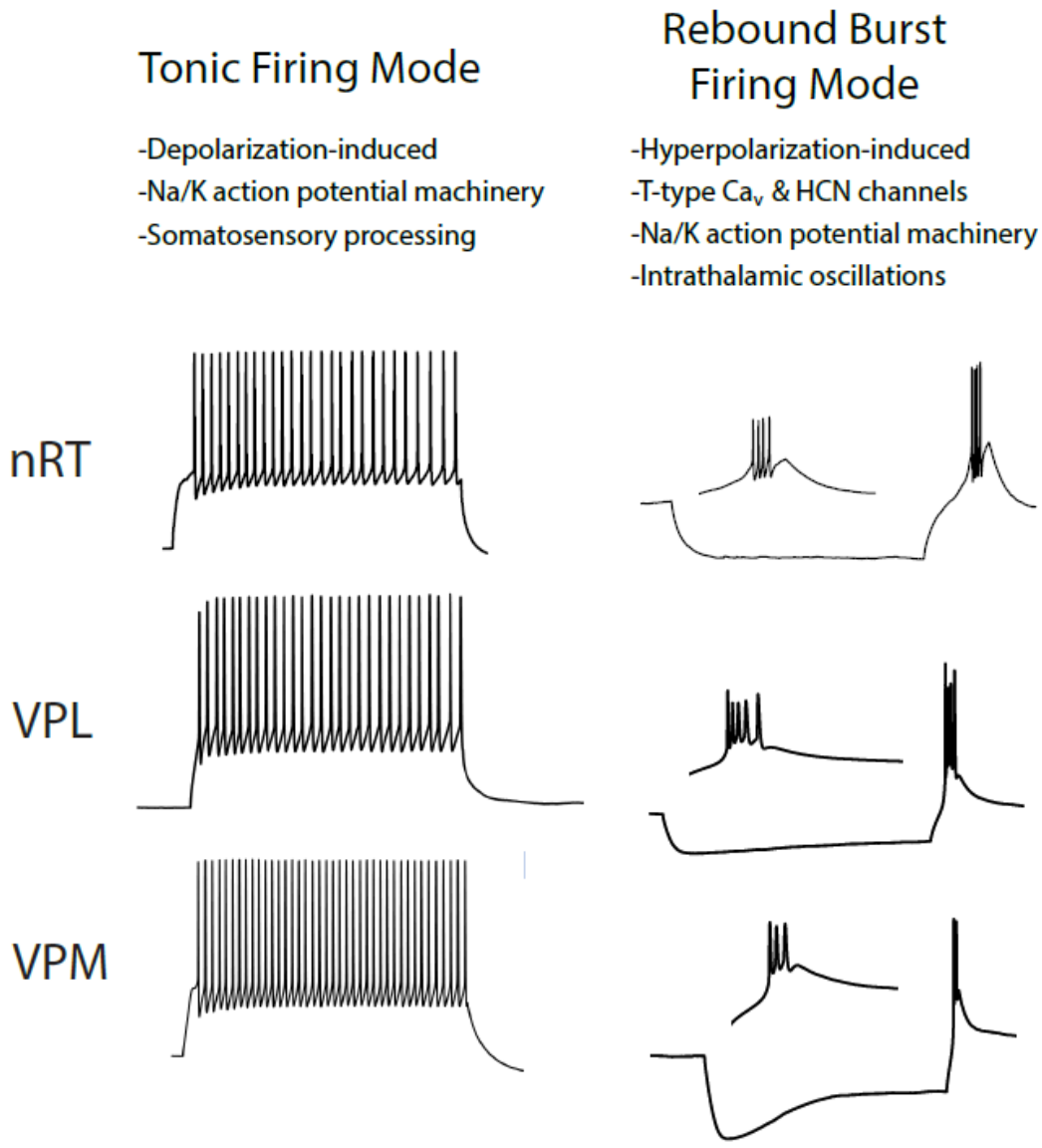

Figure 3. Two Firing Modes of Thalamic Neurons
Thalamic neurons, including nRT, VPL, and VPM neurons, display two unique firing modes. The tonic firing mode is depolarization-induced and is thought to underlie general somatosensory informational processing. The hyperpolarization-induced rebound burst mode underlies intra-thalamic oscillations.

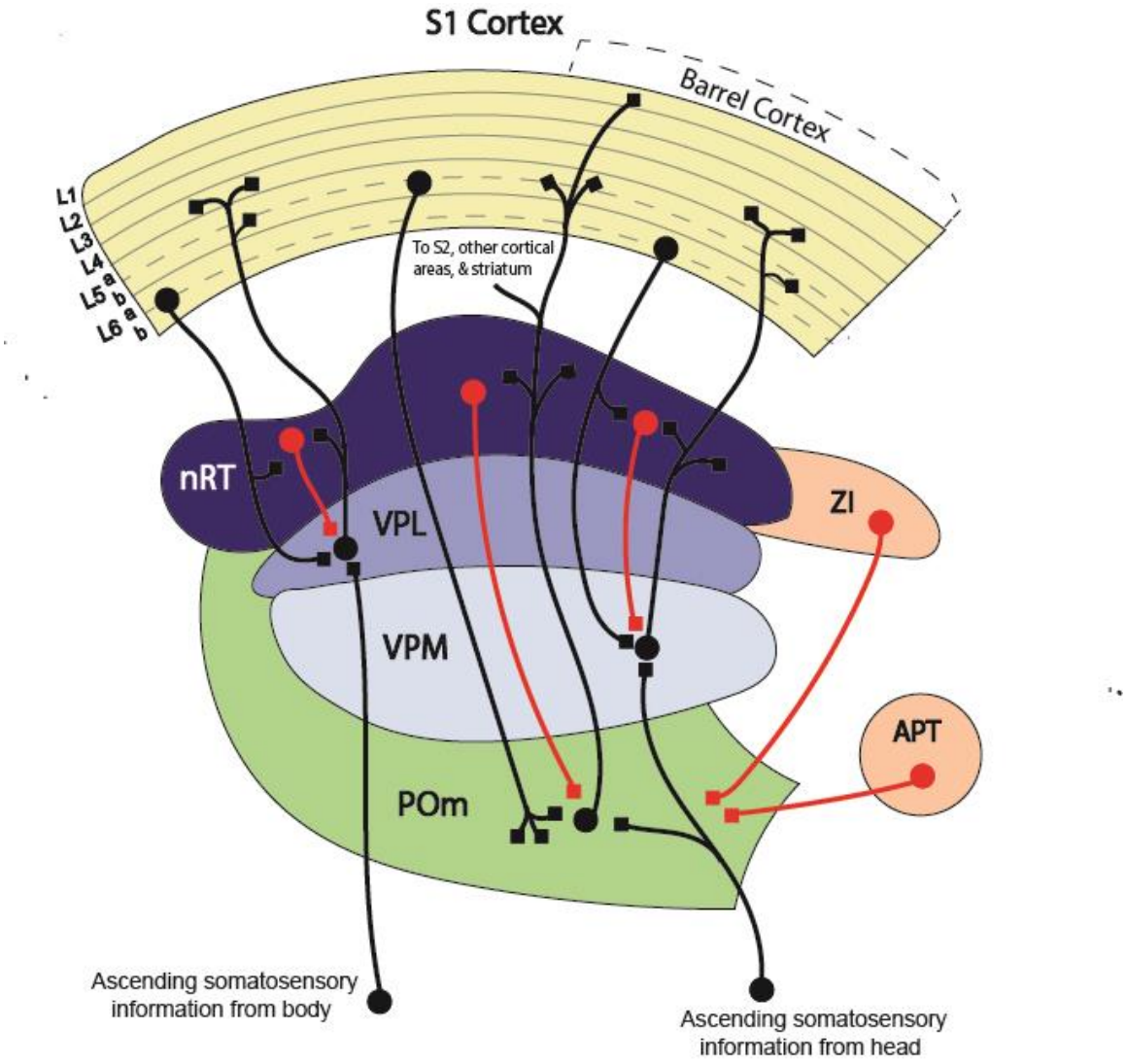

Figure 4. Complete Somatosensory CT Circuit Including the POm Nucleus
The full somatosensory corticothalamic circuit includes the posterior medial nucleus (POm), a higher order thalamic nucleus. The POm recieves inhibitory input from areas outside the nRT including the zona incerta (ZI) and anterior pretectal nucleus (APT). The nucleus projects to a variety of cortical areas including the primary and secondary somatosensory cortices. Adapted from O'Reilly *et al.*, 2015

Chapter 2

$Na_V1.1$ haploinsufficiency impairs glutamatergic and GABAergic neuron function in the thalamus

Carleigh Studtmann[ab], Marek Ladislav[a], Mackenzie A. Topolski[a], Mona Safari[ab], and Sharon A. Swanger[acd]

[a]Center for Neurobiology Research, Fralin Biomedical Research Institute at VTC, Virginia Tech, Roanoke, VA, USA.

[b]Graduate Program in Translational Biology, Medicine, and Health, Virginia Tech, Blacksburg, VA, USA.

[c]Department of Biomedical Sciences and Pathobiology, Virginia-Maryland College of Veterinary Medicine, Virginia Tech, Blacksburg, VA, USA.

[d]Department of Internal Medicine, Virginia Tech Carilion School of Medicine, Roanoke, VA, USA.

Corresponding Author:

Sharon A. Swanger

Fralin Biomedical Research Institute at VTC

Virginia Tech

2 Riverside Circle

Roanoke, VA 24016

Abstract

Thalamocortical network dysfunction contributes to seizures and sleep deficits in Dravet syndrome (DS), an infantile epileptic encephalopathy, but the underlying molecular and cellular mechanisms remain elusive. DS is primarily caused by mutations in the *SCN1A* gene encoding the voltage-gated sodium channel $Na_V1.1$, which is highly expressed in GABAergic reticular thalamus (nRT) neurons as well as glutamatergic thalamocortical neurons. We hypothesized that $Na_V1.1$ haploinsufficiency alters somatosensory corticothalamic circuit function through both intrinsic and synaptic mechanisms in nRT and thalamocortical neurons. Using *Scn1a* heterozygous mice of both sexes aged P25-P30, we discovered reduced excitability of nRT neurons and thalamocortical neurons in the ventral posterolateral (VPL) thalamus, while thalamocortical ventral posteromedial (VPM) neurons exhibited enhanced excitability. $Na_V1.1$ haploinsufficiency enhanced GABAergic synaptic input and reduced glutamatergic input to VPL neurons, but not VPM neurons. In addition, glutamatergic input to nRT neurons was reduced in *Scn1a* heterozygous mice. These findings introduce alterations in glutamatergic synapse function and aberrant glutamatergic neuron excitability in the thalamus as disease mechanisms in DS, which has been widely considered a disease of GABAergic neurons. This work reveals additional complexity that expands current models of thalamic dysfunction in DS and identifies new components of corticothalamic circuitry as potential therapeutic targets.

Keywords

Dravet syndrome, Nav1.1, *SCN1A*, somatosensory thalamus, reticular thalamus, thalamocortical neuron, glutamatergic, GABAergic, synaptic transmission, excitability

Abbreviations

DS: Dravet syndrome, nRT: reticular nucleus of the thalamus, VPM: ventral posteromedial nucleus, VPL: ventral posterolateral nucleus, VB: ventrobasal complex, CT: corticothalamic, TC: thalamocortical, VGLUT1: vesicular glutamate transporter 1, VGLUT2: vesicular glutamate transporter 2, VGAT: vesicular GABA transporter

Introduction

Dravet syndrome (DS) is an infantile epileptic encephalopathy most often caused by mutations in the *SCN1A* gene, which encodes the alpha subunit of the $Na_V1.1$ voltage-gated sodium channel (Claes et al., 2001; Dravet, 2011). DS is characterized by intractable convulsive and non-convulsive (absence) seizures in infancy as well as progressive symptomology including ataxia, intellectual disability, attention deficits, autistic features, sleep disruptions, and a high risk of sudden death (Berkvens et al., 2015; Darra et al., 2019; Dravet, 2011; Licheni et al., 2018; Ragona, 2011; Rodda et al., 2012; Takayama et al., 2014). $Na_V1.1$ is expressed in the axon initial segment as well as distal axons of primarily, but not exclusively, GABAergic neuron populations (Favero et al., 2018; Hedrich et al., 2014; Ogiwara et al., 2007). More than half of DS mutations lead to haploinsufficiency of $Na_V1.1$, which disrupts the excitatory/inhibitory balance across a variety of brain circuits in DS models (Bender et al., 2016; Kalume et al., 2007; Ogiwara *et al.*, 2007; Ritter-Makinson et al., 2019; Tai et al., 2014). The multifaceted DS phenotype likely arises from dysfunction of specific cell-types within these brain circuits (Bender et al., 2013; Han et al., 2012; Hedrich *et al.*, 2014; Kalume et al., 2015; Kalume *et al.*, 2007; Ogiwara *et al.*, 2007; Ritter-Makinson *et al.*, 2019; Rubinstein et al., 2015a; Tai *et al.*, 2014), which may contribute to the limited efficacy of pharmacological tools targeting brain-wide excitation or inhibition in DS (Chiron, 2011; Cross et al., 2019; Gataullina and Dulac, 2017; Takayama *et al.*, 2014). Therefore, elucidating the precise cellular and molecular mechanisms underlying dysfunction in particular circuits may provide more specific therapeutic targets to ameliorate DS symptoms.

The somatosensory corticothalamic (CT) circuit controls somatic information flow

between the periphery and the cerebral cortex, and it is involved in attention, pain processing, and sleep (Beenhakker and Huguenard, 2009; Wolff and Vann, 2019; Zikopoulos and Barbas, 2006). This circuit generates oscillatory sleep spindles that are critical for NREM sleep (Fernandez and Luthi, 2020), and under pathological conditions these oscillations can become hypersynchronous, leading to absence seizures (Cheong and Shin, 2013; Lee et al., 2004; McCafferty et al., 2018). Altered thalamic activity is evident in some DS patients (Moehring et al., 2013), and DS mouse models exhibit somatosensory CT circuit dysfunction including reduced sleep spindles, hypersynchronous oscillations, and absence seizures (Hedrich *et al.*, 2014; Kalume *et al.*, 2015; Ritter-Makinson *et al.*, 2019). However, the molecular and cellular mechanisms underlying thalamic dysfunction in DS are not well understood.

The core somatosensory CT circuit comprises layer VI somatosensory cortical neurons, the ventrobasal (VB) thalamus, and the reticular nucleus of the thalamus (nRT). The VB thalamus includes two glutamatergic thalamocortical neuron populations - the ventral posterolateral (VPL) and ventral posteromedial (VPM) thalamus. Both VPL and VPM neurons receive somatic and nociceptive information from the periphery; however, VPL neurons receive input from the body via the medial lemniscus and spinothalamic tract, whereas VPM neurons receive input from the head via the trigeminothalamic tract. The VPL and VPM transmit this distinct information to the somatosensory cortex, which provides reciprocal glutamatergic feedback to the thalamus (Ab Aziz and Ahmad, 2006; Brecht and Sakmann, 2002; Lenz, 1992). These corticothalamic and thalamocortical projections send axon collaterals to the GABAergic nRT, which provides the primary inhibitory input to the VPL and VPM (**Figure 1A**). Neurons in the nRT, VPL, and VPM

have two firing modes critical for somatosensory CT circuit function: a tonic firing mode involved in somatosensory processing, and a burst firing mode underlying intra-thalamic oscillations (Sherman, 2001; Steriade and Llinas, 1988). GABAergic nRT neurons as well as glutamatergic VPL and VPM neurons express $Na_V1.1$ at high levels (Ogiwara et al., 2013; Papale et al., 2013). Interestingly, many glutamatergic neuron populations do not highly express $Na_V1.1$, so its expression in VPL and VPM neurons may uniquely contribute to disease pathophysiology and provide distinctive therapeutic targets (Ogiwara *et al.*, 2013).

Given the delicate balance of excitation and inhibition in the somatosensory CT circuit, changes in either intrinsic excitability or synaptic connectivity could significantly alter thalamocortical network function in DS (Shane R. Crandall, 2015; Temereanca S, 2004). To effectively target thalamic dysfunction, it is critical to understand precisely how the circuitry is dysregulated. We hypothesized that $Na_V1.1$ haploinsufficiency alters somatosensory CT circuit function through both intrinsic and synaptic mechanisms in GABAergic nRT and glutamatergic thalamocortical neurons. Herein, we report cell-type-specific alterations to neuronal excitability and synapse function in nRT and thalamocortical neurons. These findings expand current models of somatosensory thalamic dysfunction in DS by introducing impaired thalamocortical neuron excitability and thalamic synapse dysfunction as novel disease mechanisms.

Materials and Methods

Mouse model

Mouse studies were performed according to protocols approved by the Institutional Animal Care and Use Committee at Virginia Polytechnic Institute and State University and

in accordance with the National Institutes of Health guidelines. *Scn1a*^{tm1Kea} mice (037107-JAX), which are on a 129S6/SvEvTac background, were purchased from the Mutant Mouse Resource and Research Center (Miller et al., 2014). The *Scn1a*^{tm1Kea} colony was maintained by crossing heterozygous 129S6/SvEvTac-*Scn1a*$^{tm1Kea/WT}$ mice with wild type 129S6/SvEvTac mice. Experimental mice were F1 hybrids generated by crossing heterozygous 129S6/SvEvTac-*Scn1a*$^{tm1Kea/WT}$ mice with C57BL/6J mice (000664, JAX). Genotyping was performed by Transnetyx using real-time PCR. Mice were housed in a 12 hour light/dark cycle with *ad libitum* access to food and water. Age-matched WT and *Scn1a*$^{+/-}$ littermates of both sexes aged P25-P30 were used for all experiments.

Fluorescence in situ hybridization

For mRNA detection, mice were euthanized by isoflurane overdose and brains were rapidly dissected and flash frozen in OCT. Brains were cryosectioned (20 μm), fixed with 4% paraformaldehyde (PFA), and RNAscope (ACDBio) multiplex fluorescent in situ hybridization (FISH) was performed according to the manufacturer's instructions with probes against *Scn1a*, *Gad1, and Slc17a6* (VGLUT2*).* Tiled 20X images of coronal brain sections were acquired with CellSens software and an Olympus IX83 widefield fluorescence microscope equipped with a Hamamatsu Orca Flash IV camera, X-Cite Xylis LED, and DAPI, FITC, TRITC, and Cy5 filter sets. 20X images of the thalamus were also acquired with a Zeiss 700 laser-scanning confocal and Zen Black software using 405, 488, 561, and 633 lasers. The images were processed for presentation using ImageJ software.

Western blotting

Mice were euthanized by isoflurane overdose and transcardially perfused with ice-cold 1X PBS. Brains were dissected and coronal slices (1 mm) were made using a brain

matrix. Tissue punches from the VB thalamus and nRT were snap frozen in liquid nitrogen. Tissue was sonicated in buffer containing (in mM) 65 Tris base, 150 NaCl, 1 EDTA, 50 NaH_2PO_4, 10 $Na_4P_2O_7$, 1 Na_3VO_4, 50 NaF, 1% Triton X-100, and 0.5% deoxycholic salt. Samples were centrifuged at 13,500 x *g* for 15 minutes at 4°C, denatured using Laemmli sample buffer with 200 mM dithiothreitol, and heated at 95°C. Equal amounts of protein were run on Mini-PROTEAN TGX stain-free gels, which were activated using UV light exposure to covalently bind fluorophores to protein. Protein was transferred to polyvinylidene difluoride (PVDF) membranes, and fluorescence imaging on a ChemiDoc MP System was used to image total protein content. Membranes were probed with anti-$Na_V1.1$ antibodies (1:1000; NeuroMab; Antibodies Inc. 75-023) and goat anti-mouse HRP-conjugated secondary antibodies (1:10,000; Jackson Immunoresearch 115-035-146), and then visualized using Pico Plus substrate (ThermoFisher) and a ChemiDoc MP System. Bands were quantified using Image Lab, and band intensity was normalized to total protein levels.

Immunohistochemistry and microscopy

$Na_V1.1$ immunohistochemistry was performed as previously described (Alshammari et al., 2016). Briefly, mice were euthanized by isoflurane overdose and transcardially perfused with 1X PBS followed by ice-cold 1% PFA and 0.5% methanol in 1X PBS. Brains were post-fixed in 1% PFA and 0.5% methanol in 1X PBS for 24 hr, transferred to 30% sucrose in 1X PBS for 48 hr, and then flash frozen in OCT. Cryosections (20 μm) were slide-mounted, treated with 100% acetone at -20°C for 7 min, blocked with FAB fragments and 10% normal donkey serum (NDS), and then immunostained with mouse anti-$Na_V1.1$ (1:200; NeuroMab; Antibodies Inc., 75-023) and Alexa 488-conjugated

anti-mouse IgG1 secondary antibodies (ThermoFisher). Images were acquired with a Zeiss 700 laser-scanning confocal, 20X objective, 488 argon laser, and Zen Black software.

For synaptic marker immunostainings, mice were transcardially perfused with 1X PBS followed by 4% PFA in 1X PBS, and the brains were post-fixed in 4% PFA for 24 hr, cryoprotected in 30% sucrose in 1X PBS, and flash frozen in OCT. Cryosections (20 μm) were treated with 0.8% sodium borohydride in 1X Tris-buffered saline (TBS) at room temperature, and then 0.01M sodium citrate buffer, pH 6.0, at 100°C for 10 min. Sections were permeabilized with 0.5% Triton X-100 in 1X TBS, pH 7.4, and immunostained with antibodies against: VGLUT1 (1:100; Synaptic Systems; 135-511), VGLUT2 (1:200; Synaptic Systems; 135-402), VGAT (1:200; Synaptic Systems; 131-103), and gephyrin (1:200; Synaptic Systems; 147-011). Sections were incubated with Alexa 555-conjugated anti-mouse IgG1 and Alexa 488-conjugated anti-rabbit secondary antibodies (ThermoFisher), as appropriate. Images were acquired with a Zeiss 700 laser-scanning confocal, a 100X objective, and 488 or 533 lasers. Three random fields were imaged from the left and right nRT, VPL, and VPM in two sections for a total of 9 – 12 images per mouse.

Image Analysis

Images were assigned numerical identifiers and analysis was performed blind to genotype. The *Synapse Counter* plugin from ImageJ was used to analyze the number and size of VGAT/gephyrin, VGLUT1, and VGLUT2 puncta. Synapse size restrictions in *Synapse Counter* were set as follows: VGAT in all regions (20-1000 px^2), gephyrin in all regions (10-400 px^2), VGLUT1 in all regions (10-400 px^2), VGLUT2 in nRT (70-1200 px^2), and VGLUT2 in VPL and VPM (60-3000 px^2). Data from each synapse marker were

averaged for all images from one mouse. The area occupied by cell bodies and white matter tracks were automatically detected in VGLUT1 images using ImageJ, and the number of synapses was corrected for this area. Images were processed for presentation in ImageJ, and WT and DS images within each figure are displayed with equivalent intensity settings.

Electrophysiology

Mice were deeply anesthetized with an overdose of inhaled isoflurane and transcardially perfused with ice-cold sucrose-based artificial cerebrospinal fluid (aCSF) containing (in mM) 230 sucrose, 24 $NaHCO_3$, 10 glucose, 3 KCl, 10 $MgSO_4$, 1.25 NaH_2PO_4, and 0.5 $CaCl_2$ saturated with 95% O_2 / 5% CO_2. The brain was removed and glued to a vibratome stage (Leica VT1200S), and horizontal 300 μm slices were cut in an ice-cold sucrose-aCSF bath. Slices were incubated in a NaCl-based aCSF containing (in mM) 130 NaCl, 24 $NaHCO_3$, 10 glucose, 3 KCl, 4 $MgSO_4$, 1.25 NaH_2PO_4, and 1 $CaCl_2$ saturated with 95% O_2 / 5% CO_2 at 32°C for 30 min. The slices were then equilibrated to room temperature (RT) for 30 minutes and maintained at room temperature until used for recordings up to 8 hr later. One cell was recorded per slice, and no more than two cells in any dataset are from the same mouse.

Recordings were made using a Multiclamp 700B amplifier (Molecular Devices), sampled at 20 kHz (Digidata 1550B, Molecular Devices), and low-pass filtered at 10 kHz using Axon pClamp 11 software (Molecular Devices). The extracellular recording solution contained (in mM) 130 NaCl, 24 $NaHCO_3$, 10 glucose, 3 KCl, 1 $MgSO_4$, 1.25 NaH_2PO_4, and 2 $CaCl_2$ saturated with 95% O_2 / 5% CO_2, and was maintained at 32°C for all recordings. For whole-cell current-clamp recordings, borosilicate glass recording electrodes (4-5 MΩ) were filled with (in mM) 130 K-gluconate, 4 KCl, 2 NaCl, 10 HEPES,

0.2 EGTA, 4 ATP-Mg, 0.3 GTP-Tris, 14 phosphocreatine-K, and 0.1% biocytin, pH 7.3. Pipette capacitance neutralization and bridge balance were enabled during current-clamp recordings for capacitance and series resistance compensation. Membrane potential values were corrected for the liquid junction potential after the recording (15 mV). To analyze intrinsic membrane properties, voltage responses were elicited by 200 ms hyperpolarizing current injections between 20 – 100 pA (20 pA steps). Depolarization-induced spike firing was elicited by 500 ms depolarizing current injections between 10 – 400 pA (10 pA steps). Hyperpolarization-induced rebound bursting was elicited by 500 ms hyperpolarizing current injections between 50 – 200 pA (50 pA steps). All current-clamp experiments were conducted from the natural resting membrane potential (RMP) of the cell, and three trials were completed for each current injection experiment.

For whole-cell voltage-clamp recordings, borosilicate glass recording electrodes (4-5 MΩ) were filled with (in mM) 120 $CsMeSO_3$, 15 CsCl, 8 NaCl, 10 tetraethylammonium chloride, 10 HEPES, 1 EGTA, 3 Mg-ATP, 0.3 Na-GTP, 1.5 $MgCl_2$, 1 QX-314, and 0.1% biocytin, pH 7.3. After a ten minute equilibration period, mEPSCs and mIPSCs were recorded in the presence of 1 μM TTX in two minute epochs at a holding potential of -70 mV and 0 mV, respectively. Holding commands were adjusted for the 10 mV liquid junction potential during the recordings. Series resistance and cell capacitance were monitored throughout the experiment, but were not compensated, and cells were excluded if either parameter changed >20%.

Biocytin labeling in acute brain slices

The cell location was confirmed after electrophysiology recordings by biocytin labeling (**Figure S1**). Briefly, brain slices were fixed with 4% PFA in 1X PBS, pH 7.4,

overnight at 4°C, washed in 1X PBS, and then stored at -20°C in cryoprotectant solution containing 0.87 M sucrose, 5.37 M ethylene glycol, and 10 g/L polyvinyl-pyrrolidone-40 in 0.1 M phosphate buffer, pH 7.4. For biocytin labeling, slices were blocked with 10% NDS in 1X PBS with 0.25% Triton X-100, and then incubated with 1.0 µg/ml DyLight 594-conjugated streptavidin (Jackson Immunoresearch) in blocking solution overnight at RT. Slices were stained with DAPI for 1 hr at RT and placed on a glass slide with a coverslip and DABCO mounting media (Sigma Aldrich). 10X images were acquired on an Olympus IX83 microscope with a Hamamatsu Orca Flash 4.0 camera, X-Cite Xylis LED, and DAPI and TRITC filter sets using CellSens software.

Electrophysiology data analysis

Recordings were assigned numerical identifiers and analysis was performed blind to genotype. All current-clamp recordings were analyzed in Clampfit 11 (Molecular Devices). RMP was measured from current-clamp recordings two minutes following breakthrough of the cell membrane. Input resistance (R_{in}) was determined from the amplitude of voltage responses to 200 ms hyperpolarizing current injections, the time constant (τ_m) was determined by a mono-exponential fit of the voltage response, and cell capacitance was calculated by $C_m = \tau_m/R_{in}$. The Clampfit 11 threshold detection module was used to quantify the number of spikes, spike frequency, and latency to the first spike in response to 500 ms depolarizing current injections or upon removal of 500 ms hyperpolarizing current injections. Rheobase was defined as the smallest depolarizing current injection that elicited an action potential. Values were averaged across three runs for all current injection experiments.

The shape of single action potentials was analyzed using the Action Potential Search module in ClampFit 11. The baseline was manually set, and single action potentials at or near rheobase were analyzed for amplitude, half width, rise and decay time, after-hyperpolarization amplitude, and threshold. Spike frequency adaptation was evaluated by measuring spike frequency across depolarizing current injections for VPL and VPM neurons. Some VPL and VPM neurons had a prolonged inter-event interval between the first two spikes following depolarization; therefore, the frequency of the first three spikes following current injection were averaged in VPL and VPM neurons and were compared to the frequency of the last two spikes. The ratio of these frequencies (last two spikes/first three spikes) is reported as the adaptation ratio. Because many DS nRT neurons fired very few spikes in response to depolarization, only the frequency of the first three spikes following depolarization was assessed. The frequencies from multiple runs in the same cell were averaged.

For mIPSC and mEPSC analysis, recordings of 4 – 6 minutes were analyzed to determine inter-event interval, amplitude, and decay kinetics using MiniAnalysis software (Synaptosoft). Data were digitally filtered at 1 kHz. Automated detection identified events with amplitude ≥ 7 pA (~5 x RMS noise), and then events ≥ 5 pA were manually detected and automated detection accuracy was assessed. The reported numbers of mEPSCs per cell were normalized to the total recording time for each cell. The decay time at 37% of the peak was determined for each mEPSC in MiniAnalysis. To group mEPSCs as Type 1 (fast) or Type 2 (slow), the decay times for all mEPSCs were plotted as a frequency distribution for each cell independently, and then distributions were tested for bimodality by Hardigan's dip test in Matlab. All distributions were multimodal ($p < 0.05$). The bimodal distribution

was separated at the decay time (x-value) corresponding to the minimum frequency (y-value) between the two modes. To determine this minimum y-value, each distribution was interpolated using the Akima spline method (GraphPad Prism 9), and the first derivative of the spline was plotted to determine the x-intercept between the two modes, which is the decay time corresponding to the minimum frequency. This value was determined for each cell independently. All events with decay times faster than this cutoff value were Type 1 and those with slower decay times were Type 2.

The reported amplitude and inter-event interval values for each cell are averages of the amplitude and inter-event interval measured for each Type 1 mEPSC, Type 2 mEPSC, or mIPSC recorded from the cell. The average mEPSC and mIPSC decay times for each cell were determined from ensemble averages of all Type 1 mEPSCs, Type 2 mEPSCs, or mIPSCs recorded from each cell. The 10-90% peak to baseline decay times of the ensemble averages were fitted using the following double-exponential function:

$$Response = Amp_{FAST}exp(-time/\tau_{FAST}) + Amp_{SLOW}exp(-time/\tau_{SLOW})$$

Equation 1

Where τ_{FAST} is the fast deactivation time constant, τ_{SLOW} is the slow deactivation time constant, Amp_{FAST} is the current amplitude of the fast deactivation component, and Amp_{SLOW} is the current amplitude of the slow deactivation component. The weighted decay time constant (τ_W) was calculated by:

$$\tau_W = [Amp_{FAST}/(Amp_{FAST} + Amp_{SLOW})]\tau_{FAST} + [Amp_{SLOW}/(Amp_{FAST} + Amp_{SLOW})]\tau_{SLOW}$$

Equation 2

Statistical analysis

A priori power analyses were performed in GPower 3.1 to estimate required samples sizes given appropriate statistical tests with $\alpha = 0.05$, power $(1 - \beta) = 0.8$, and a moderate effect size or effect sizes based on pilot data. Statistical analyses were performed in GraphPad (Prism). All datasets were tested for normality with the Shapiro-Wilk test and equal variances using an F test (two independent groups) or the Brown-Forsythe test (three or more groups). Normal datasets with equal variances were analyzed by unpaired t-test or ANOVA with corrections for multiple comparisons. Non-normal datasets were analyzed with the Mann-Whitney U test (two independent groups) or Kruskal-Wallis test (three or more groups). Repeated measures datasets were analyzed by two-way repeated measures ANOVA, and a mixed-effects analysis was used when any data points were missing. The specific tests used and associated test statistics are reported in the respective figure legend or table. All group data are plotted as mean ± s.e.m. in the figures, and numerical data reported in the text are mean ± s.e.m., unless otherwise stated.

Results

Scn1a mRNA and $Na_V1.1$ protein expression in GABAergic and glutamatergic neurons in the thalamus

To evaluate how thalamic neuron function is impaired in DS, we utilized the F1 hybrid 129S-*Scn1a*$^{+/-}$ x C57Bl/6J mouse model at age P25-P30, hereafter referred to as DS mice. Given extensive strain differences in DS mouse model phenotypes, we first examined *Scn1a* mRNA and $Na_V1.1$ protein levels to confirm high expression in GABAergic nRT and glutamatergic VPL and VPM neurons in wild type F1:129S-*Scn1a*$^{+/+}$ x C57Bl/6J (WT) mice at P25-P30. Indeed, multiplex FISH revealed abundant *Scn1a* mRNA expression in

Gad1-positive GABAergic nRT neurons as well as glutamatergic VPL and VPM neurons detected by *Slc17a6* mRNA, which encodes VGLUT2 (**Figure 1B,C**). $Na_V1.1$ protein was detected in the nRT, VPL, and VPM by immunohistochemistry (**Figure 1D**). In addition, western blotting of VPL/VPM and nRT tissue punches showed reduced $Na_V1.1$ protein levels in DS mice relative to WT littermates, confirming haploinsufficiency in the thalamus of this DS model (VPL/VPM: 59.4 ± 2.6% of WT; nRT: 53.8 ± 1.1% of WT; **Figure 1E,F**).

GABAergic nRT neuron excitability is impaired in DS mice

Previous studies have reported opposing effects on nRT neuron excitability in different DS mouse models as well as age-dependent changes in GABAergic neuron excitability in the cortex (Favero *et al.*, 2018; Hedrich *et al.*, 2014; Kalume *et al.*, 2015; Ritter-Makinson *et al.*, 2019; Tai *et al.*, 2014). To determine how nRT neuron excitability was affected in this DS mouse model, we examined intrinsic membrane properties, depolarization-induced spike firing, and hyperpolarization-induced rebound bursting of neurons at their RMP in acute brain slices.

In response to depolarizing current injections, WT nRT neurons fired action potentials tonically, as expected. A majority of nRT neurons from DS mice fired a low number of action potentials immediately following current injection, but a subpopulation fired long-latency low-threshold spikes with bursts of action potentials (6 of 16 neurons); we will hereafter refer to these two groups as "DS" neurons and "DS-burst" neurons, respectively (**Figure 2A**). We compared the intrinsic membrane properties of DS and DS-burst neurons to determine whether these might be two distinct nRT neuron populations. The DS-burst group had a significantly hyperpolarized RMP and significantly reduced input resistance (R_{in}) compared to both WT and DS neurons, while cell capacitance (C_m)

and the membrane time constant (τ) were not significantly different (**Table 1, Supplementary Figure S2A**). The input resistance, cell capacitance, and the membrane time constant were not significantly different between WT and DS neurons. These data suggest that a subpopulation of nRT neurons have a hyperpolarized RMP in DS mice, which may increase the likelihood of nRT burst firing in response to depolarizing input at rest.

Both DS and DS-burst neurons fired significantly fewer action potentials in response to depolarizing current injections compared to WT (**Figure 2B).** DS neurons had a shorter latency between current injection and the first spike, while DS-burst neurons had a longer latency due to the low-threshold spike (WT: 7.4 ± 1.2 ms, DS: 3.8 ± 0.4 ms; DS-burst: 16.6 ± 1.5 ms; **Figure 2C**). DS neurons required significantly more current to elicit an action potential compared to WT neurons (rheobase: WT: 62 ± 12 pA, DS: 119 ± 16 pA; DS-burst: 50 ± 10 pA; **Figure 2D**). However, the frequency of the first three action potentials fired by WT (164 ± 25 Hz) and DS neurons (135 ± 30 Hz) were not significantly different (unpaired t-test, $p = 0.48$). Furthermore, we found no significant difference in action potential amplitude, half width, rise or decay time, after-hyperpolarization amplitude, or threshold measured from single action potentials in WT and DS neurons (**Table S1**). These data suggest $Na_V1.1$ haploinsufficiency impairs sustained firing in the majority of nRT neurons without altering RMP, the shape of single action potentials, or the frequency at which the initial spikes are fired.

Burst firing in nRT neurons contributes to oscillatory activity between nRT and VPL/VPM neurons, and aberrant thalamic oscillations underlie sleep impairments and absence seizures in DS. Therefore, we investigated how $Na_V1.1$ haploinsufficiency

impacted rebound burst firing after removal of hyperpolarizing current injections in nRT neurons at RMP (**Figure 2E**). DS and DS-burst nRT neurons fired significantly fewer action potentials per burst than WT neurons, which is reported as the median with 95% confidence intervals [WT: 4 (2.0, 6.0), DS: 1.3 (0.5, 4.0), DS-burst: 0 (0, 3.0); **Figure 2F**], while burst latency was not altered (WT: 75 ± 7.4 ms; DS: 72 ± 7.5 ms; **Figure 2G**). Burst latency was not reported for the DS-burst group as only one of five neurons exhibited a rebound burst. These data suggest that $Na_V1.1$ haploinsufficiency impairs nRT neuron resting excitability, including alterations in both depolarization-induced spike firing and rebound burst firing following hyperpolarization, which may be due to impaired action potential generation as well as the observed hyperpolarized RMP in a subpopulation of neurons.

Aberrant excitability of glutamatergic VPL neurons in DS mice

Previous studies of the somatosensory thalamus in DS mouse models examined the VB complex, which includes both VPL and VPM neurons; however, these two cell populations have different synaptic connectivity and may have distinct intrinsic membrane properties. Therefore, we evaluated these two cell populations independently.

We determined how $Na_V1.1$ haploinsufficiency impacted the intrinsic membrane properties, depolarization-induced spike firing, and hyperpolarization-induced rebound burst firing in VPL and VPM neurons at their RMP.

VPL neurons in DS mice had a significantly hyperpolarized RMP relative to WT, while input resistance, cell capacitance, and the membrane time constant were not significantly different (**Table 1, Supplementary Figure S2B**). VPL neurons in DS mice fired significantly fewer spikes than WT mice over a range of depolarizing current

injections as detected by a significant interaction effect between genotype and current injection in the ANOVA; however, no significant differences were detected by pairwise comparisons at individual current injections (**Figure 3A,B**). Neither the rheobase (WT: 143 ± 26 pA; DS: 172 ± 50 pA) nor spike latency (WT: 9.2 ± 1.8 ms; DS: 15.8 ± 3.5 ms) were significantly affected in VPL neurons (**Figure 3C,D**). No significant differences in action potential shape, including amplitude, half width, rise or decay time, after-hyperpolarization amplitude, and threshold, were detected for DS VPL neurons compared to WT (**Table S1**).

To further examine how VPL neuron spike firing was disrupted in DS mice, we measured spike frequency at the beginning and the end of depolarizing current injections, and then calculated a spike frequency adaptation ratio. Interestingly, the frequency of the first three spikes was unchanged in DS VPL neurons (120 ± 8 Hz) compared to WT (127 ± 4 Hz), while the frequency of the last two spikes was significantly reduced (WT: 68 ± 2 Hz; DS: 36 ± 2 Hz; **Figure 3E**). As a result, the spike frequency adaptation ratio was significantly reduced in DS VPL neurons (0.28 ± 0.01) compared to WT (0.55 ± 0.01; **Figure 3F**), which indicates that spiking during sustained depolarization is impaired in DS VPL neurons. In addition, VPL neurons from DS mice fired more spikes per rebound burst upon recovery from hyperpolarization compared to WT (WT: 1.7 ± 0.4 spikes; DS: 3.6 ± 0.6 spikes; **Figure 3G,H**), while burst latency was not significantly affected (WT: 35.4 ± 5.1 ms; DS: 40.1 ± 3.7 ms; **Figure 3I**). Taken together, these data demonstrate that DS mice have reduced depolarization-induced spike firing and enhanced spike adaptation as well as enhanced hyperpolarization-induced rebound burst firing in VPL neurons, which may be due, in part, to the observed hyperpolarized RMP.

Glutamatergic VPM neurons are hyperexcitable in DS mice

VPM neurons had significantly greater input resistance in DS mice compared to WT mice, while RMP, cell capacitance, and the membrane time constant were not significantly different (**Table 1, Supplementary Figure S2C**). Given the increased input resistance, VPM neurons would be predicted to have enhanced responses to current injections in DS mice. Indeed, VPM neurons fired significantly more action potentials in DS mice than WT at corresponding depolarizing current injections (**Figure 4 A,B**). In addition, DS neurons required significantly less current to elicit an action potential (WT: 185 ± 11 pA; DS: 114 ± 21 pA; **Figure 4C**) and had a shorter spike latency (WT: 42.0 ± 8.0 ms; DS: 16.8 ± 6.5 ms; **Figure 4D**). Spike firing frequency in DS VPM neurons was significantly increased for the first three spikes (WT: 84 ± 7 Hz; DS: 137 ± 4 Hz) and the last two spikes (WT: 44 ± 3 Hz; DS: 73 ± 3 Hz) compared to WT (**Figure 4E**), but the spike frequency adaptation ratio was similar in WT (0.47 ± 0.06) and DS neurons (0.48 ± 0.07; **Figure 4F**). No significant differences were found in the shape of single action potentials including amplitude, half width, rise or decay time, after-hyperpolarization amplitude, or threshold for WT and DS mice (**Table S1**). In addition, the number of spikes per hyperpolarization-induced rebound burst (WT: 2.5 ± 0.3; DS: 3.0 ± 0.5; **Figure 4G,H**) and burst latency (WT: 20.5 ± 2.2 ms; DS: 18.1 ± 1.7 ms) were not significantly different between WT and DS mice (**Figure 4I**). Together, these data suggest that VPM neurons have enhanced tonic firing in response to depolarization in DS mice, which may be due to altered intrinsic membrane properties as indicated by the increased input resistance.

Reduced glutamatergic input to nRT neurons in DS mice

We hypothesized that altered intrinsic excitability in thalamic neurons would disrupt activity-dependent synapse development and thus exacerbate thalamocortical network dysfunction in DS. The nRT receives glutamatergic inputs from corticothalamic (CT) and thalamocortical (TC) neurons. Deficits in CT-nRT and TC-nRT connectivity would disrupt feed-forward and feedback inhibition of VPL/VPM neurons, respectively (see **Figure 1A**). Previous work revealed that nRT EPSCs can be divided into two populations based on decay kinetics, and it was postulated that CT-nRT synapses mediate the slow decaying EPSCs and TC-nRT synapses mediate the fast decaying EPSCs (Deleuze and Huguenard, 2016). Therefore, to investigate how nRT glutamatergic inputs differed between WT and DS mice, we recorded nRT mEPSCs, grouped the events based on decay times, and analyzed the two kinetically distinct mEPSC populations (**Figure 5A**). Faster decaying events are referred to here as Type 1, and slower decaying events are referred to as Type 2 (**Figure 5B,C**).

The total number of mEPSCs recorded per cell was not significantly altered in DS mice (1266 ± 180) relative to WT (1533 ± 254; unpaired t-test, $p = 0.38$), but the ratio of Type 1 to Type 2 mEPSCs was increased in DS mice relative to WT (WT: 1.3 ± 0.3; DS: 2.9 ± 0.4; **Figure 5D**). The inter-event interval was significantly increased for Type 2 events in DS mice (1.03 ± 0.18 s) relative to WT (0.58 ± 0.11 s), while the Type 1 inter-event interval was not significantly altered (WT: 0.56 ± 0.14 s; DS: 0.40 ± 0.07 s; **Figure 5E**). There was no main effect of genotype on inter-event interval suggesting that the overall frequency of nRT glutamatergic input was unchanged. Furthermore, mEPSC amplitude was unaltered in both Type 1 (WT: 13.9 ± 1.7 pA, DS: 14.9 ± 1.2 pA) and Type

2 (WT: 12.9 ± 1.3 pA, DS: 11.8 ± 0.4 pA) mEPSC populations in DS mice compared to WT (**Figure 5F**), and there was no change in the decay time for Type 1 events (WT: 2.6 ± 0.3 ms, DS: 3.6 ± 0.4) or Type 2 events (WT: 5.4 ± 0.7 ms; DS: 6.9 ± 0.9 ms; **Supplementary Figure S3**). These data suggest that DS nRT neurons have a selective decrease in the frequency of the slow decaying mEPSC population (Type 2) with no change in glutamatergic synapse strength.

To evaluate changes in nRT glutamatergic synaptic input in an input-specific manner, we immunostained brain sections from WT and DS mice for CT-specific presynaptic marker VGLUT1 and TC-specific presynaptic marker VGLUT2 (**Figure 5G**) (Graziano et al., 2008). DS mice exhibited no significant differences in either VGLUT1 puncta number (102.8 ± 7.4 % of WT) and size (101.8 ± 2.7 % of WT) or VGLUT2 puncta number (89.7 ± 14.3 % of WT) and size (97.1 ± 4.2 % of WT; **Figure 5H**). Taken together, the imaging and physiology data are consistent with reduced glutamate release at a subset of glutamatergic nRT synapses with no change in the number of CT or TC synapses onto nRT neurons.

In mice aged P25-P30 used herein, there are no GABAergic mIPSCs in nRT neurons and, therefore, we could not evaluate the frequency or strength of spontaneous GABAergic synaptic transmission. However, we did evaluate GABAergic synapse number and size by immunostaining for presynaptic marker VGAT and postsynaptic marker gephyrin in WT and DS tissue (**Supplementary Figure S4A**). We did not detect any significant differences in VGAT puncta number (102 ± 12% of WT) and size (102 ± 2% of WT), gephyrin puncta number (101 ± 18% of WT) and size (104 ± 2% of WT), or the number (100 ± 10% of WT) and size (103 ± 2% of WT) of VGAT/gephyrin colocalized

regions (**Supplementary Figure S4B**). If GABAergic synapse density is indeed unchanged in the nRT, then this finding together with the observed reduction in mEPSC frequency could indicate imbalanced excitatory and inhibitory input to the nRT in DS mice.

Synapse-specific alterations in glutamatergic input to VPL neurons

VPL and VPM neurons receive descending glutamatergic CT inputs as well as ascending glutamatergic sensory inputs through the medial lemniscus and spinothalamic tract as well as the trigeminothalamic tract, respectively. Previous studies have shown that evoked EPSCs at these two inputs have distinct kinetics, with ascending inputs having faster decay times than CT input (Castro-Alamancos, 2002; McCormick and von Krosigk, 1992; Miyata and Imoto, 2006). Therefore, we hypothesized that VPL and VPM mEPSCs could be distinguished based on decay time similarly to nRT neurons. Indeed, a frequency histogram of mEPSC decay times resulted in two distinct populations in VPL (**Figure 6A-C**) and VPM (**Figure 6G-I**) neurons. We cannot unequivocally identify these kinetically distinct populations as ascending and descending inputs to VPL/VPM neurons; therefore, we refer to faster decaying mEPSCs as Type 1 and slower decaying mEPSCs as Type 2.

In VPL neurons, the total number of mEPSCs was significantly reduced in DS mice (712 ± 86) relative to WT (1102 ± 111; $p = 0.01$). Furthermore, the ratio of Type 1 to Type 2 mEPSCs was decreased in DS mice relative to WT (WT: 0.79 ± 0.11; DS: 0.31 ± 0.03; **Figure 6D**), with no change in the decay times for Type 1 mEPSCs (WT: 5.9 ± 0.8 ms; DS: 6.2 ± 0.8 ms) or Type 2 mEPSCs (WT: 9.2 ± 0.8 ms; DS: 8.8 ± 1.0 ms; **Supplementary Figure S5A,B**). The change in relative proportions of Type 1 and Type 2 mEPSCs was driven by a significant increase in the inter-event interval for Type 1 mEPSCs (WT: 1.02 ± 0.20 s; DS: 3.95 ± 0.69 s), whereas the Type 2 mEPSC inter-event interval was not significantly affected (WT: 0.73 ± 0.12 s; DS: 1.11 ± 0.17 s; **Figure 6E**). Furthermore,

mEPSC amplitude was significantly reduced for both Type 1 (WT: 8.5 ± 0.5 pA; DS: 7.0 ± 0.2 pA) and Type 2 (WT: 9.5 ± 0.2 pA; DS: 8.0 ± 0.2 pA) events in DS VPL neurons compared to WT (**Figure 6F**). These data suggest that VPL neurons in DS mice have a global decrease in glutamatergic synapse strength, but a specific reduction in the frequency of the faster decaying mEPSC population.

Interestingly, VPM neurons in WT and DS mice had similar total numbers of mEPSCs (WT: 915 ± 138; DS: 1190 ± 128; p = 0.70), and the ratio of Type 1 and Type 2 events was not significantly different (WT: 0.2 ± 0.03; DS: 0.23 ± 0.03; **Figure 6J**). Furthermore, mEPSC decay times were similar for Type 1 (WT: 3.5 ± 0.3 ms; DS: 4.0 ± 0.5 ms) and Type 2 mEPSCs (WT: 7.0 ± 0.7 ms; DS: 8.0 ± 0.6 ms; **Supplementary Figure S5C,D**). VPM neurons in WT and DS mice also exhibited no significant differences in the inter-event interval of Type 1 (WT: 4.0 ± 1.1 s; DS: 2.6 ± 0.7 s) and Type 2 mEPSCs (WT: 0.64 ± 0.16 s; DS: 0.48 ± 0.07 s) or the amplitude of Type 1 (WT: 7.0 ± 0.3 pA; DS: 7.3 ± 0.4 pA) and Type 2 mEPSCs (WT: 8.5 ± 0.5 pA; DS: 8.9 ± 0.6 pA; **Figure 6K,L**). Taken together, the mESPC data suggest that $Na_V1.1$ haploinsufficiency may affect synapse development in VPL and VPM neurons differently leading to cell-type-specific roles for these glutamatergic neuron populations in thalamic dysfunction in DS.

To evaluate glutamatergic synapses in the VPL and VPM in an input-specific manner, we immunostained for VGLUT1 to label CT synapses and VGLUT2 to label ascending sensory synapses, and then quantified the number and size of synaptic puncta (**Figure 7A,B**). The number of VGLUT2 puncta in the VPL was decreased in DS mice relative to WT (83.7 ± 3.2% of WT), whereas the number of VGLUT1 puncta was unchanged (99.9 ± 6.7% of WT, **Figure 7C**). The size of VGLUT1 and VGLUT2 puncta

were not significantly different between WT and DS mice (VGLUT1: 96.7 ± 3.2 % of WT; VGLUT2: 107 ± 6.1 % of WT). Furthermore, the VPM in WT and DS mice had similar VGLUT1 and VGLUT2 puncta number (VGLUT1: 112.3 ± 5.9 % of WT; VGLUT2: 87.0 ± 12.7 % of WT) and size (VGLUT1: 96.2 ± 3.2 % of WT; VGLUT2: 101.5 ± 7.2 % of WT; **Figure 7D**). These imaging data are consistent with a specific reduction in the number of ascending sensory synapses in the VPL.

Inhibitory synaptic input is enhanced in VPL neurons

VPL and VPM neurons receive inhibitory input from nRT neurons, with VPL neurons receiving input from both somatostatin- and parvalbumin-positive neurons and VPM neurons receiving input from parvalbumin-positive nRT neurons (Clemente-Perez et al., 2017). We hypothesized that aberrant excitability within the somatosensory thalamic circuitry would alter inhibitory synaptic input from the nRT to VPL and VPM neurons. Therefore, we analyzed the decay time, frequency, and amplitude of mIPSCs in VPL and VPM neurons (**Figure 8A,G**). VPL neuron mIPSC decay time was significantly faster in DS mice (16.8 ± 2.4 ms) compared to WT (25.4 ± 2.1 ms; **Figure 8B**), which suggests that either postsynaptic receptor composition or the proximal-distal distribution of GABAergic inputs may be altered in DS mice. Moreover, VPL neurons exhibited reduced mIPSC inter-event interval in DS mice (0.133 ± 0.023 ms) compared to WT (0.266 ± 0.033 ms; **Figure 8C**), whereas VPL mIPSC amplitude was not significantly altered in DS mice (23.0 ± 1.1 pA) relative to WT (20.3 ± 0.6 pA; **Figure 8D**). VPM neurons in DS mice had no significant differences relative to WT in mIPSC decay time (WT: 29.8 ± 5.5 ms; DS: 35.8 ± 7.9 ms), inter-event interval (WT: 0.294 ± 0.06 s; DS: 0.269 ± 0.06 s), or amplitude (WT: 19.2 ± 0.7 pA; DS: 19.7 ± 0.6 pA; **Figure 8H-J**). These data suggest that $Na_V1.1$ haploinsufficiency enhances the frequency of GABAergic input to VPL neurons without

affecting GABAergic input to VPM neurons.

To further evaluate how GABAergic inputs were altered in DS mice, we immunolabeled VGAT and gephyrin in WT and DS thalamus and quantified the number and size of inhibitory synapses (**Figure 8E,K**). We detected no significant differences in WT and DS VPL when comparing VGAT puncta number (86 ± 7.5 % of WT), VGAT puncta size (102 ± 3.2 % of WT), gephyrin puncta number (87 ± 5.5 % of WT), or gephyrin puncta size (106 ± 3.5 % of WT; **Figure 8F**). We also quantified colocalized regions of VGAT and gephyrin puncta in the VPL and found no significant differences in the number (87 ± 5.6 % of WT) or size (106 ± 3.5 % of WT; **Figure 8F**). Similarly, we did not find any significant differences in GABAergic synapse labeling in VPM when we compared VGAT puncta number (90 ± 7.5 % of WT), VGAT puncta size (109 ± 4.2 % of WT), gephyrin puncta number (96 ± 12.4 % of WT), or gephyrin puncta size (105 ± 3.0 % of WT; **Figure 8L**). We also found no significant differences in colocalized VGAT and gephyrin puncta number (97 ± 8.6 % of WT) or size (109 ± 1.3 % of WT) in the VPM (**Figure 8L**). Taken together, the mIPSC and VGAT/gephyrin data are consistent with enhanced frequency and accelerated kinetics of GABAergic synaptic transmission in VPL neurons of DS mice, which may occur through changes in presynaptic release and/or postsynaptic receptor expression as opposed to changes in GABAergic synapse number.

Discussion

Collectively, these data provide novel insight into the mechanisms underlying somatosensory CT circuit dysfunction in a $Na_V1.1$ haploinsufficiency DS mouse model. The excitability of GABAergic nRT neurons and glutamatergic VPL and VPM neurons was disrupted in a cell-type-specific manner, including alterations in both depolarization-

induced spike firing and hyperpolarization-induced rebound burst firing in nRT and VPL neurons. Unexpectedly, VPL and VPM neurons exhibited opposing changes to depolarization-induced firing, suggesting they may differentially contribute to circuit-wide dysfunction in DS. Glutamatergic synaptic input to both the nRT and VPL was reduced, and GABAergic synaptic input to the VPL was enhanced, further contributing to an imbalance of synaptic input to the region. Together, these results indicate that synaptic- and cellular-level changes in GABAergic and glutamatergic neuron populations contribute to somatosensory thalamic dysfunction in DS.

As expected, $Na_V1.1$ haploinsufficiency resulted in altered excitability in GABAergic nRT neurons, including altered depolarization- and hyperpolarization-induced firing. Previous studies revealed reduced tonic and burst firing in *Scn1a*-haploinsufficient and $Na_V1.1$-R1648H mouse models of DS (Hedrich *et al.*, 2014; Kalume *et al.*, 2015). Consistent with these studies, we observed reductions in the number of spikes fired in response to depolarization and the number of spikes per rebound burst in nRT DS neurons. Our excitability experiments were conducted from RMP, while some previous work studied changes in tonic and burst firing while holding the cell at a constant membrane potential (Hedrich et al., 2014). Unlike these previous studies, we identified a subset of DS nRT neurons with a hyperpolarized RMP. These neurons fired low-threshold spikes with bursts of action potentials in response to depolarization, which is a unique finding compared to previous studies reporting hypoexcitability of DS nRT neurons (Hedrich et al., 2014). However, the majority of DS nRT neurons responded to depolarization with a low number of spikes immediately upon current injection, and their RMP was slightly hyperpolarized compared to WT neurons, but the difference was not statistically

significant. It is thus unlikely that this small hyperpolarization in RMP caused the dramatic reduction in spike firing in these DS nRT neurons, suggesting that there are also likely impairments in their tonic firing properties. From a circuit-level perspective, DS nRT neurons responding to depolarizing input with a reduced number of spikes or in a burst firing mode could result in profound somatosensory informational processing deficits, as both the number of spikes and mode of spiking communicate critical somatosensory information to the cerebral cortex.

Both populations of DS nRT neurons exhibited a significant reduction in the number of spikes per hyperpolarization-induced rebound burst compared to WT neurons. It is possible that the observed reduction in RMP in a subset of nRT neurons may cause their T-type calcium channels to be de-inactivated at rest and thus require depolarization, not hyperpolarization, to be activated. Therefore, the hyperpolarized RMP could contribute to reduced rebound burst spiking as well as rebound bursting in response to depolarization in this subset of DS nRT neurons. However, it is unlikely that changes in RMP underlie the reduced rebound burst firing in all DS nRT neurons, as the larger population of neurons did not display a significant change in RMP. This indicates that there are also impairments in either the T-type calcium channel low threshold-spike or sodium/potassium-dependent action potential firing; however, additional studies are required to elucidate the precise mechanism underlying reduced rebound burst firing in DS nRT neurons. Regardless of the underlying mechanisms, impaired nRT neuron burst firing could change nRT-VPL/VPM bursting patterns leading to altered intra-thalamic oscillations, which are critical for sleep spindles.

The identity of the two subsets of DS nRT neurons identified here remains unclear.

There are several recent studies characterizing functionally distinct subpopulations of nRT neurons including parvalbumin-, somatostatin-, and calbindin-expressing neurons (Clemente-Perez *et al.*, 2017; Li et al., 2020; Martinez-Garcia et al., 2020). These neuron populations are reported to have distinct distributions within the nRT and different functional properties such as rebound burst strength, intrinsic membrane properties, and tonic spike firing properties (Clemente-Perez *et al.*, 2017; Martinez-Garcia *et al.*, 2020). While the RMP and input resistance of the two DS nRT neuron populations identified here were significantly different, no other membrane properties differed between the populations. Further, because tonic and rebound burst states were not isolated in this study, it remains unknown whether these two populations have distinct intrinsic firing properties. Thus, future studies will be needed to elucidate whether these two DS nRT neuron groups represent functionally or molecularly distinct populations.

In contrast to our findings, the $Na_V1.1$-R1407X mouse model exhibited hyperexcitability of parvalbumin-positive nRT neurons including prolonged hyperpolarization-induced rebound bursts and enhanced depolarization-induced spike firing (Ritter-Makinson *et al.*, 2019). Discrepancies between models could be attributed to the specific etiology of the disease model or the background strain as DS models are known to have a high degree of strain-dependent phenotype variability (Miller *et al.*, 2014; Rubinstein et al., 2015b). The age of the mice could also cause discrepancies between studies as some cortical neuron populations exhibit a transient window of altered excitability (Favero *et al.*, 2018); however, developmental studies of thalamic dysregulation have not been reported in DS mouse models. From a therapeutic perspective, these model-specific effects indicate that successful patient treatment may largely depend

on the patient's specific genetic alteration. As truncation mutations resulting in haploinsufficiency are responsible for about half of all DS cases, the mechanisms uncovered in this study may be relevant to a large population of patients with DS.

The hyperpolarization of the RMP in both nRT and VPL neurons was an unexpected finding of this study, and how $Na_V1.1$ haploinsufficiency leads to this change remains unknown. nRT neurons exhibit a persistent sodium current, which is a slow-inactivating current that amplifies even small depolarizations in membrane potential (Landisman, 2012). Thus, it is likely that this persistent sodium current contributes to the RMP of nRT neurons, and loss of $Na_V1.1$ or compensatory changes in Na_V channel expression or function could contribute to the observed hyperpolarized RMP. Indeed, altered persistent sodium current has been proposed as a mechanism contributing to disrupted cell excitability in epilepsies caused by sodium channel mutations including DS (Stafstrom, 2007). Whether VPL and VPM neurons exhibit a persistent sodium current has not been established, though other thalamic nuclei such as the dLGN do exhibit this current in rats (Parri and Crunelli, 1998). These findings provide impetus for investigating the persistent sodium current in the VPL and VPM and whether it contributes to the observed hyperpolarized RMP. In addition, spontaneous glutamatergic input likely depolarizes the RMP of thalamic neurons, and the observed reduction in glutamatergic input could hyperpolarize nRT and VPL neuron RMP leading to altered excitability. This would provide an interesting therapeutic opportunity, as correcting the synaptic-level deficits could potentially ameliorate the hyperpolarized RMP and altered firing. Finally, altered potassium channel expression has been implicated in nRT dysfunction in other DS models (Layer et al., 2021; Ritter-Makinson *et al.*, 2019), and it is possible that $Na_V1.1$

haploinsufficiency alters potassium channel expression or function leading to the hyperpolarized RMP and altered excitability evident in nRT and VPL neurons.

Interestingly, this study also discovered opposing changes in glutamatergic VPL and VPM neuron excitability as well as distinct effects on intrinsic membrane properties. Many glutamatergic neuron populations express $Na_V1.1$ at low levels and reportedly exhibit no altered excitability in DS, but recent evidence suggests that CA1 pyramidal neuron excitability is altered and changes over the time course of the disease (Almog et al., 2021). Previous investigations have reported no alterations in the excitability of VB neurons in DS models (Hedrich *et al.*, 2014; Ritter-Makinson *et al.*, 2019). This could be due to differences in the specific DS model, the developmental time period studied, or a lack of differentiating between the VPL and VPM, the two regions comprising the VB thalamus, which could have resulted in an averaging of cell-type-specific alterations and no overall change.

The cellular properties of VPL and VPM neurons have not yet been directly compared, and thus our understanding of how $Na_V1.1$ haploinsufficiency leads to opposing changes in their excitability is limited. We speculate that different $Na_V1.1$ expression levels or subcellular localization may underlie distinct roles for $Na_V1.1$ in normal VPL and VPM neuron physiology. Alternatively, the expression of different complements of Na_V, Ca_V, or K_V channels in VPL and VPM neurons could lead to distinct compensatory mechanisms that underlie cell-type-specific alterations in the DS model. This is supported by evidence from a spinal cord injury model wherein VPL neurons exhibit increased $Na_V1.3$ expression post-injury, while VPM neurons do not (Zhao et al., 2006). Additionally, as previously stated, reduced glutamatergic input to nRT and VPL neurons, specifically, could

hyperpolarize their RMP and lead to hypoexcitability. While the specific mechanisms underlying the distinct changes in intrinsic properties are unknown, these findings suggest that the VPL and VPM may contribute differentially to circuit dysfunction and successful correction of circuit function may require cell-type-specific therapeutic targets.

An additional discovery of this study is altered synaptic connectivity in the thalamus. nRT neurons receive glutamatergic input from CT and TC neurons, and substantial evidence suggests that CT-nRT EPSCs have slower decay kinetics than TC-nRT EPSCs (Deleuze and Huguenard, 2016). VPL and VPM neurons receive glutamatergic input from CT neurons and ascending sensory afferents, and its is well-established that CT EPSCs have slower decay kinetics than sensory EPSCs (Castro-Alamancos, 2002; McCormick and von Krosigk, 1992; Miyata and Imoto, 2006). Indeed, mEPSCs recorded from nRT, VPL, and VPM neurons can be separated into two kinetically distinct populations, which we analyzed independently to assess potential synapse-specific alterations in DS mice. DS nRT neurons exhibited reduced frequency of the slow-decaying mEPSC population, which are putative CT-nRT synaptic events. Altered CT-nRT synaptic connectivity may disrupt feed-forward CT-nRT-TC inhibition, which is critical for proper CT circuit function. VPL neurons in this DS mouse model exhibited a global reduction in the amplitude of mEPSCs as well as reduced frequency of the fast-decaying population of mEPSCs, which are putative ascending sensory synaptic events. Consistent with this result, we observed a reduction in VGLUT2 synaptic puncta specifically in the VPL thalamus. VPL neurons also exhibited increased mIPSC frequency. Thus, VPL neurons receive an imbalance of synaptic input including excessive inhibition and insufficient excitation, which could contribute to dysfunctional somatosensory processing as well as altered

reciprocal VPL-nRT connectivity.

The cell-type- and input-specific nature of these synaptic alterations suggests that tuning circuit excitability may require pathway-specific therapeutic targets. The distinct changes in VPL and VPM synaptic connectivity could be due to their respective changes in excitability or their distinct sources of ascending input as the VPL and VPM receive somatosensory information from the body and head, respectively. A most intriguing finding is the putative reduction in CT-nRT input without a corresponding reduction in CT input to either VPL or VPM neurons. The CT axons that innervate nRT neurons are collaterals of those innervating VPL and VPM neurons, suggesting that a postsynaptic mechanism may disrupt synapse development in the nRT. We did not detect a corresponding change in VGLUT1 puncta in the nRT, and thus our observations are consistent with alterations in glutamate release, glutamate receptor expression, or dendritic filtering. Determining the underlying mechanism will require investigating specific glutamate receptor populations as well as studying synaptic potentials under more physiological conditions in addition to the voltage-clamp studies conducted herein.

The $Na_V1.1$-R1648H DS model previously showed reduced spontaneous IPSCs in glutamatergic thalamocortical neurons, but no changes in mIPSCs (Hedrich *et al.*, 2014). Another DS model exhibited no change in spontaneous EPSCs in nRT or VB neurons (Ritter-Makinson *et al.*, 2019). These discrepancies could be due to the specific cell populations that were studied as the previous studies examined VB neurons, which presumably included both VPL and VPM neurons. Furthermore, we discovered differential effects in two kinetically distinct mEPSC populations in nRT and VPL neurons, whereas previous studies evaluated all spontaneous EPSCs as one group, which may have obscured

synapse-specific effects. Furthermore, age-dependent changes may contribute to different findings as studies at earlier developmental time points may not reveal such synaptic-level changes (Hedrich *et al.*, 2014). Developmental studies will be important for elucidating the time course over which both intrinsic and extrinsic alterations occur.

From a clinical perspective, the dysfunction in glutamatergic synapses as well as glutamatergic VPL and VPM neurons observed here may present a unique opportunity for therapeutic intervention. Specifically, the diversity of glutamate receptor expression in the thalamus provides a wide array of therapeutic targets. Modulating glutamate receptors is becoming increasingly feasible as a variety of subtype-selective modulators for metabotropic glutamate receptors, AMPA receptors, and NMDA receptors have been developed (Azumaya et al., 2017; Hansen et al., 2018; Hovelso et al., 2012; Kadriu et al., 2021; Mazzitelli et al., 2018). For example, a recent study indicated that the GluN2A positive allosteric modulator GNE-0723 reduces low-frequency oscillations and epileptiform activity in a DS mouse model, providing evidence that NMDA receptor modulation could be a viable therapeutic option (Hanson et al., 2020). The GluN2C and GluN2D subunits of NMDA receptors have more restricted expression patterns, including relatively high expression in the thalamus, and recently developed GluN2C/2D-specific modulators could offer a means to tune thalamic function with more limited adverse effects (Acker et al., 2011; Khatri et al., 2014; Liu et al., 2019; Mullasseril et al., 2010; Swanger et al., 2018; Yi et al., 2020). Thus, the data presented here lay the foundation to explore glutamatergic synapse modulation as a possible therapeutic strategy to correct thalamic dysfunction in DS.

Altogether, this evidence indicating cell-type-specific dysfunction advances our

understanding of how GABAergic and glutamatergic neuron populations may together contribute to pathological thalamocortical network function. We posit that altered depolarization-induced spike firing may impair VPL cell output and enhance VPM cell output in response to ascending sensory information. The reduced ascending input to the VPL may further impair somatic information processing, perhaps contributing to reduced sensitivity to pain and attention deficits evident in the disease (Catarino et al., 2011; Villas et al., 2017). Burst firing in the somatosensory thalamus underlies oscillatory activity critical for thalamocortical network function, and disrupted burst firing is associated with absence seizures, sleep disorders, and chronic pain (Fogerson and Huguenard, 2016; Hains et al., 2006; Henderson et al., 2013). Intra-thalamic oscillations occur when nRT neurons at a hyperpolarized RMP receive depolarizing input from the cortex, which leads to feed-forward nRT-VPL and nRT-VPM inhibition. VPL and VPM neurons are then hyperpolarized and will burst upon recovery from hyperpolarization leading to feedback inhibition from the nRT. In this DS model, VPL neurons had a hyperpolarized RMP and fired significantly more spikes during burst firing. Some nRT neurons exhibited a hyperpolarized RMP and an increased propensity to burst in response to depolarization, which could result in augmented feed-forward inhibition of VPL and VPM neurons. Thus, together these mechanisms may result in enhanced bursting in all three cell populations that contributes to aberrant thalamic oscillations in DS (Kalume *et al.*, 2015; Ritter-Makinson *et al.*, 2019). A complete understanding of how these cellular and synaptic mechanisms contribute to circuit dysfunction will require elucidating how cells respond to excitatory drive from ascending and descending synaptic inputs.

Conclusions

In summary, this work discovered cell-type-specific dysregulation of synapses and excitability within the somatosensory thalamus in a DS mouse model. Specifically, the findings introduce altered glutamatergic neuron excitability and synapse function as disease mechanisms that may contribute to thalamocortical network dysfunction underlying aberrant sensory processing, disrupted sleep, and absence seizures. Cell-type-specific intrinsic and synaptic disease mechanisms could affect thalamic function distinctly and thus contribute to particular symptoms or developmental stages of DS. Further investigation is required to elucidate how these previously unidentified mechanisms contribute to DS symptomology across the course of the disease and whether modulating specific therapeutic targets in the glutamate system can restore thalamic function and ameliorate corresponding phenotypes.

Funding

This work was supported by the National Institutes of Health [NS105804], CURE Epilepsy, the Dravet Syndrome Foundation, and Brain Research Foundation.

Declaration of interests

None

Author contributions

Carleigh Studtmann: Validation, Formal analysis, Investigation, Writing – original draft, Visualization; *Marek Ladislav:* Methodology, Validation, Writing – review & editing, Supervision; *Mackenzie A. Topolski:* Validation, Investigation, Writing – review & editing; *Mona Safari:* Investigation, Writing – review & editing; *Sharon A. Swanger:* Conceptualization, Methodology, Validation, Formal analysis, Investigation, Resources, Writing – original draft, Visualization, Supervision, Project administration, Funding acquisition.

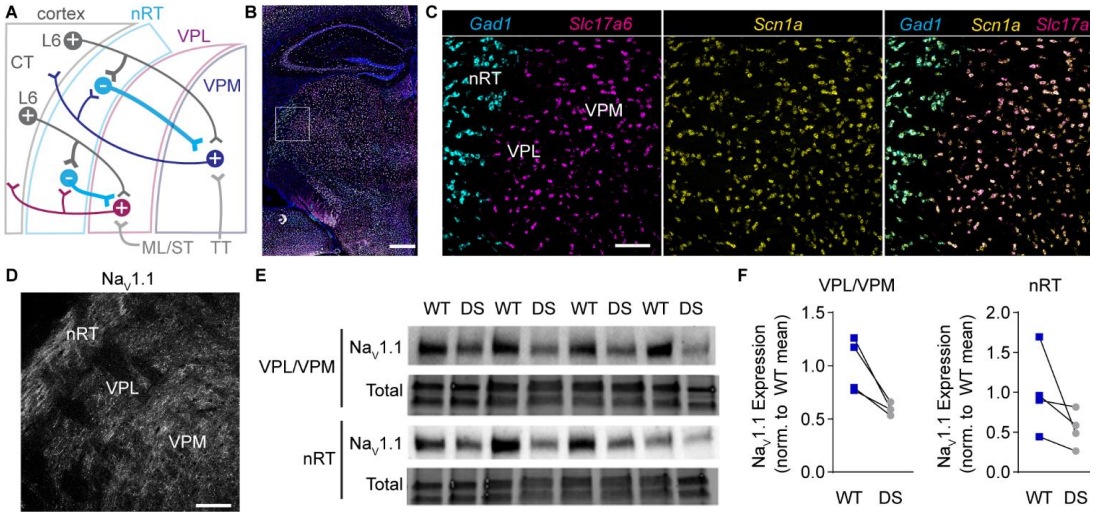

Figure 1. *Scn1a* mRNA and Na$_V$1.1 protein expression in the somatosensory thalamus. **A.** A circuit diagram illustrates somatosensory corticothalamic (CT) circuit connectivity. Layer 6 (L6) glutamatergic CT neurons innervate nRT, VPL, and VPM neurons. GABAergic nRT neurons innervate VPL and VPM neurons, which send glutamatergic projections to the cortex and collaterals to the nRT. Ascending glutamatergic sensory afferents from the medial lemniscus and spinothalamic tract (ML/ST) innervate VPL neurons and the trigeminothalamic tract (TT) innervates VPM neurons. **B.** A representative 20X tiled image of a coronal mouse brain section shows *Scn1a* (yellow), *Gad1* (cyan), and *Slc17a6* (magenta) mRNA labeled by FISH with DAPI counterstain (blue). Scale bar: 500 µm. **C.** 20X images of the boxed region in panel B show that *Gad1*+ and *Slc17a6*+ neurons express *Scn1a* mRNA. **D.** A representative 20X image shows Na$_V$1.1 immunolabeling in the nRT, VPL, and VPM. Scale bar: 100 µm (C, D)**. E.** A western blot shows Na$_V$1.1 and total protein expression in nRT and VPL/VPM tissue punches from WT and DS mice (n = 4 littermate pairs). **F.** Na$_V$1.1 protein levels were quantified by densitometry and normalized to the WT mean.

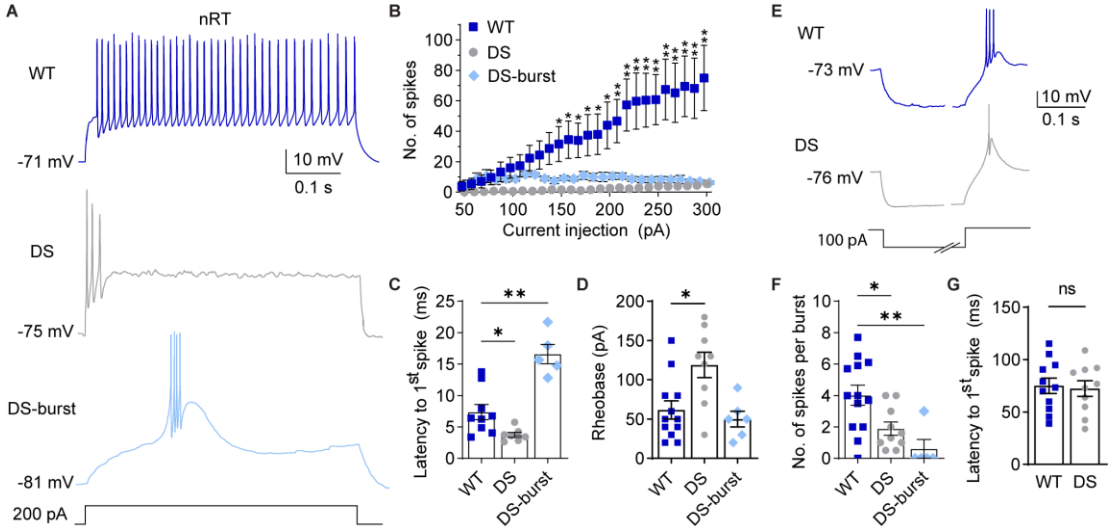

Figure 2. nRT neuron excitability is altered in DS mice. A. Representative traces show nRT neuron spike firing in response to depolarizing current injections from RMP. **B.** The number of spikes at each current injection for WT (n = 9 cells from 6 mice), DS non-burst firing cells (labeled DS, n = 8 cells from 6 mice), and DS burst firing neurons (DS-burst, n = 5 cells from 4 mice) were analyzed by mixed-effects analysis for repeated measures (Genotype: $F(2,18) = 6.431$, $p = 0.008$, Current x genotype: $F(50,440) = 6.051$, $p < 0.001$) with posthoc Dunnett's tests at each current injection. *p<0.05 for WT vs. DS, **p< 0.05 for both WT vs. DS and WT vs. DS-burst. **C**. Latency to the first spike was quantified and analyzed by one-way ANOVA: $F(2,17) = 20.38$, $p = 0.001$; posthoc Dunnett's tests, *p = 0.034, **p = 0.015. **D.** Rheobase was quantified for WT (n = 12 cells from 8 mice), DS (n = 9 cells from 7 mice), and DS-burst (n = 6 cells from 5 mice), and analyzed by one-way ANOVA: $F(2,24) = 7.016$, $p = 0.004$; posthoc Dunnett's tests, *p = 0.007, WT vs. DS-burst: p = 0.800. **E.** Representative traces show rebound burst firing upon recovery from 500 ms hyperpolarizing current injections. The time axis was broken to facilitate displaying both the hyperpolarization and spike periods. **F.** The number of spikes per burst were compared by the Kruskal-Wallis test ($H = 13.94$, $p = 0.001$), due to non-normal distribution of the data (Shapiro-Wilk test, $p < 0.001$), and posthoc Dunn's tests: *p = 0.041, **p = 0.001 (WT: n = 13 cells from 8 mice, DS: n = 10 from 8 mice, DS-burst: n = 5 from 5 mice). **G.** Latency to the first spike for WT and DS groups were compared by an unpaired t-test (p = 0.803). The symbols in all bar graphs represent individual neurons.

Table 1. Membrane properties of nRT, VPL, and VPM neurons.

	nRT			
	WT	**DS**	**DS-burst**	**ANOVA**
RMP (mV)	-68.9 ± 1.7	-71.2 ± 1.3	-81.2 ± 2.0*	F (2,18) = 13.24 p < 0.001
C_m (pF)	99.9 ± 0.9	107 ± 4	119 ± 14	F(2,18) = 1.672 p = 0.216
R_{in} (MΩ)	274 ± 35	273 ± 21	158 ± 25**	F(2,18) = 4.781 p =0.022
Tau (ms)	27.4 ± 3.6	29.2 ± 2.5	17.9 ± 2.4	F(2,18) = 3.517 p = 0.051
N	7 (6)	9 (7)	5 (5)	

	VPL			VPM		
	WT	**DS**	**p value**	**WT**	**DS**	**p value**
RMP (mV)	-74.7 ± 1.0	-78.1 ± 0.7	*0.03	-74.9 ± 0.9	-72.4 ± 1.7	0.20
C_m (pF)	223 ± 30	207 ± 28	0.69	186 ± 14	198 ± 31	0.70
R_{in} (MΩ)	123 ± 14	125 ± 15	0.91	117 ± 10	154 ± 12	*0.03
Tau (ms)	29.8 ± 6.9	25.9 ± 4.5	0.66	22.0 ± 3.1	29.8 ± 5.1	0.19
N	10 (7)	8 (6)		10 (8)	6 (5)	

Pairwise comparisons were performed using post hoc Sidak's tests; *nRT RMP: WT vs. DS-burst, $p < 0.001$, DS vs. DS-burst, $p = 0.002$, WT vs. DS, $p = 0.547$; **nRT R_{in}: WT vs. DS-burst, $p = 0.035$, DS vs. DS-burst, $p = 0.029$, WT vs. DS, $p = 0.998$. VPL and VPM parameters were compared across genotype by unpaired t-tests. N values are the number of cells followed by the number of mice in parentheses.

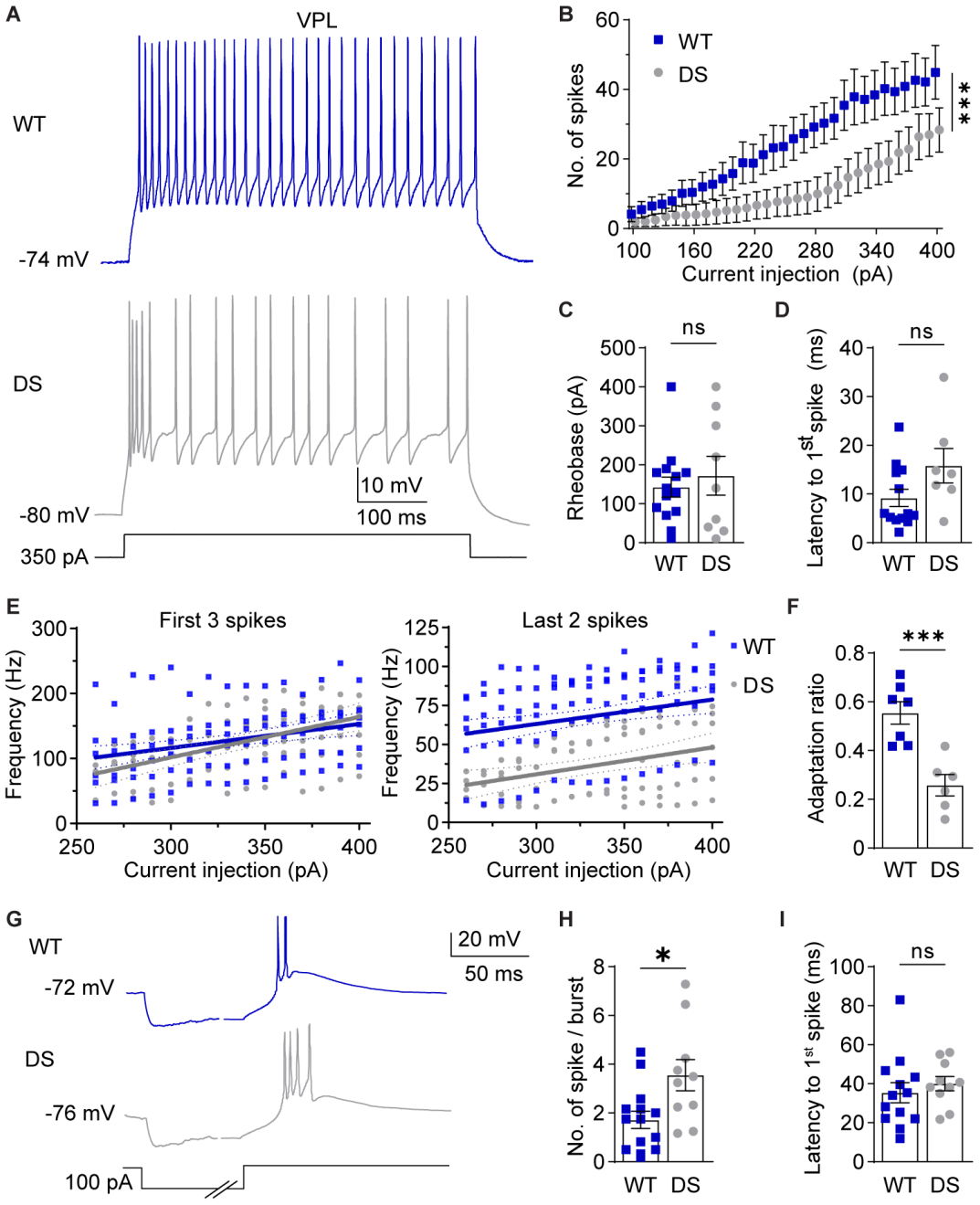

Figure 3. $Na_V1.1$ haploinsufficiency alters VPL neuron excitability.

Figure 3. $Na_V1.1$ haploinsufficiency alters VPL neuron excitability. A. Representative traces show WT and DS VPL neuron spike firing in response to depolarizing current injections at RMP. **B.** The number of spikes fired by VPL neurons across current injections were analyzed by two-way repeated measures ANOVA (WT: n = 13 cells from 7 mice; DS: n = 8 cells from 6 mice; Genotype: $F(1,19) = 3.605$; $p = 0.07$, Interaction: $F(30,570) = 2.200$; ***$p < 0.001$) and posthoc Sidak's tests at each current injection ($p > 0.05$ at each current amplitude). **C.** Rheobase was analyzed by unpaired t-test for WT (n = 14 cells from 7 mice) and DS (n = 9 cells from 6 mice) VPL neurons ($p = 0.571$). **D.** Latency was analyzed by Mann-Whitney test ($p = 0.183$) due to failed normality Shapiro-Wilk test ($p = 0.026$). **E**. The frequency of the first 3 spikes and last 2 spikes were plotted for each cell across current injections. Linear regression of WT and DS data yielded the plotted lines with 95% confidence interval (CI) bands, and fits were compared by sum of squares F tests. First 3 spikes: $F(2,176) = 1.600$, $p = 0.205$. Last 2 spikes: $F(2,161) = 42.89$, $p < 0.001$. **F**. Spike frequency adaptation ratios (last 2 spikes/first 3 spikes) were averaged across all current injections for each cell and compared by an unpaired t-test ($p < 0.001$). **G.** Representative traces show VPL neuron rebound burst firing at RMP upon recovery from hyperpolarization. The time axis was broken to facilitate displaying the hyperpolarization and spike periods. **H.** Spikes per burst (*$p = 0.01$) and (**I**) burst latency ($p = 0.49$) were compared by unpaired t-tests (WT: n = 13 cells from 7 mice; DS: n = 10 cells from 6 mice). The symbols in all bar graphs represent individual neurons.

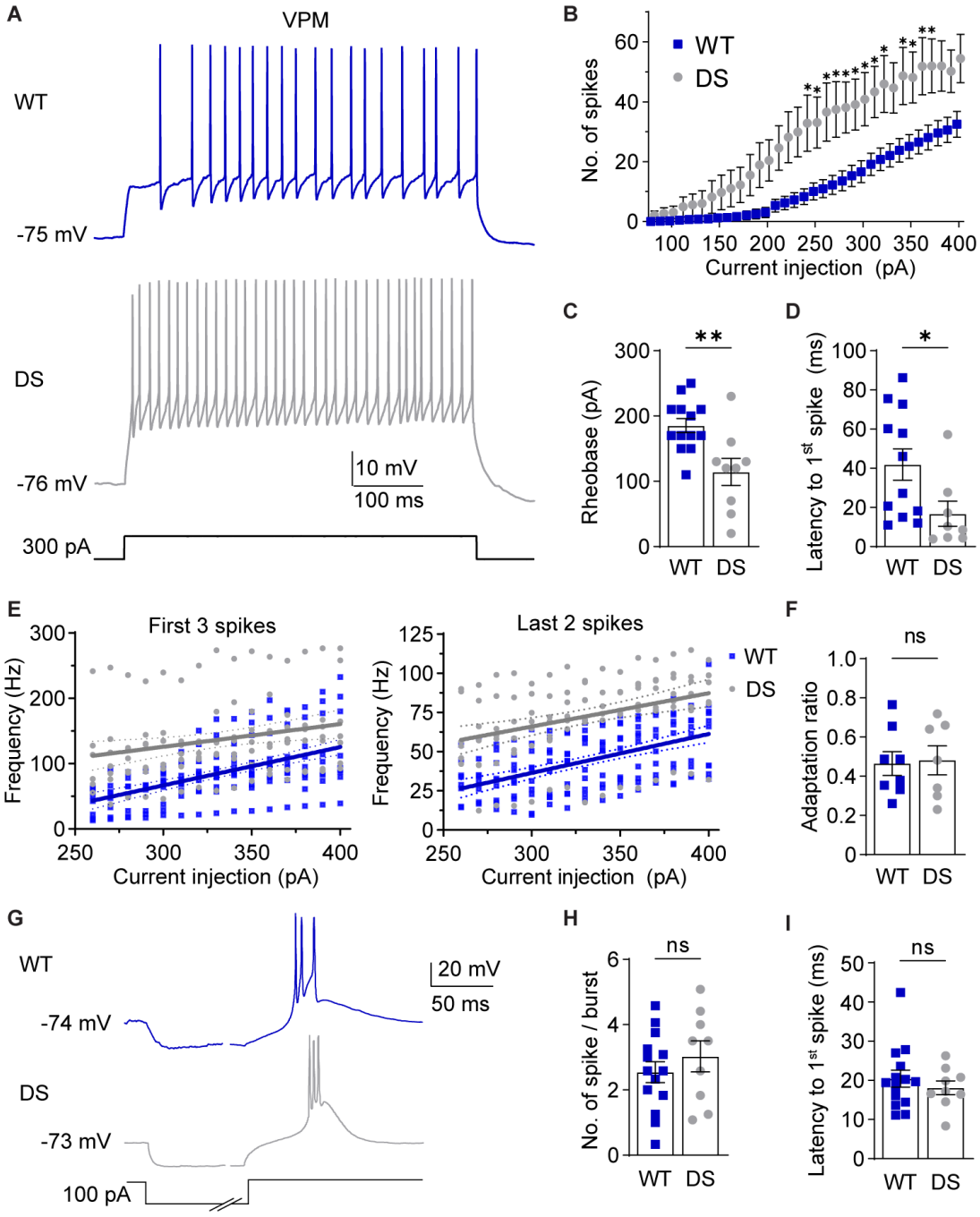

Figure 4. $Na_V1.1$ haploinsufficiency alters VPM neuron excitability.

Figure 4. $Na_V1.1$ haploinsufficiency alters VPM neuron excitability. A. Representative traces show VPM spike firing in response to depolarizing current injections from RMP. **B.** The number of spikes at each current injection were analyzed by two-way repeated measures ANOVA (WT: n = 12 cells from 8 mice; DS: n = 9 from 5 mice; Genotype: $F(1,19) = 7.992$, $p = 0.011$, Interaction: $F(32,608) = 4.677$, $p < 0.001$) with posthoc Sidak's tests at each current injection (*$p < 0.05$). **C.** Rheobase for WT (n = 13 cells from 8 mice) and DS (n = 9 cells from 5 mice) VPM neurons was analyzed by unpaired t-test (**$p = 0.004$). **D.** Spike latency for WT (n = 12 cells from 8 mice) and DS (n = 8 cells from 5 mice) VPM neurons were compared by an unpaired t-test (*$p = 0.037$). **E**. The frequency of the first 3 spikes and last 2 spikes were plotted for each cell across current injections. Linear regression of WT and DS data yielded the plotted lines with 95% CI bands, and fits were compared by sum of squares F tests. First 3 spikes: $F(2,244) = 36.50$, $p < 0.001$. Last 2 spikes: $F(2,244) = 59.13$, $p < 0.001$. **F**. Spike frequency adaptation ratios (last 2 spikes/first 3 spikes) were averaged across all current injections for each cell and compared by an unpaired t-test ($p = 0.860$). **G.** Representative traces show rebound burst firing upon recovery from hyperpolarization. **H.** Spikes per burst ($p = 0.39$) and (**I**) burst latency for VPM neurons ($p = 0.46$, WT: n = 14 cells from 8 mice, DS: n = 9 cells from 5 mice) were analyzed by unpaired t-tests. The symbols in all bar graphs represent individual neurons.

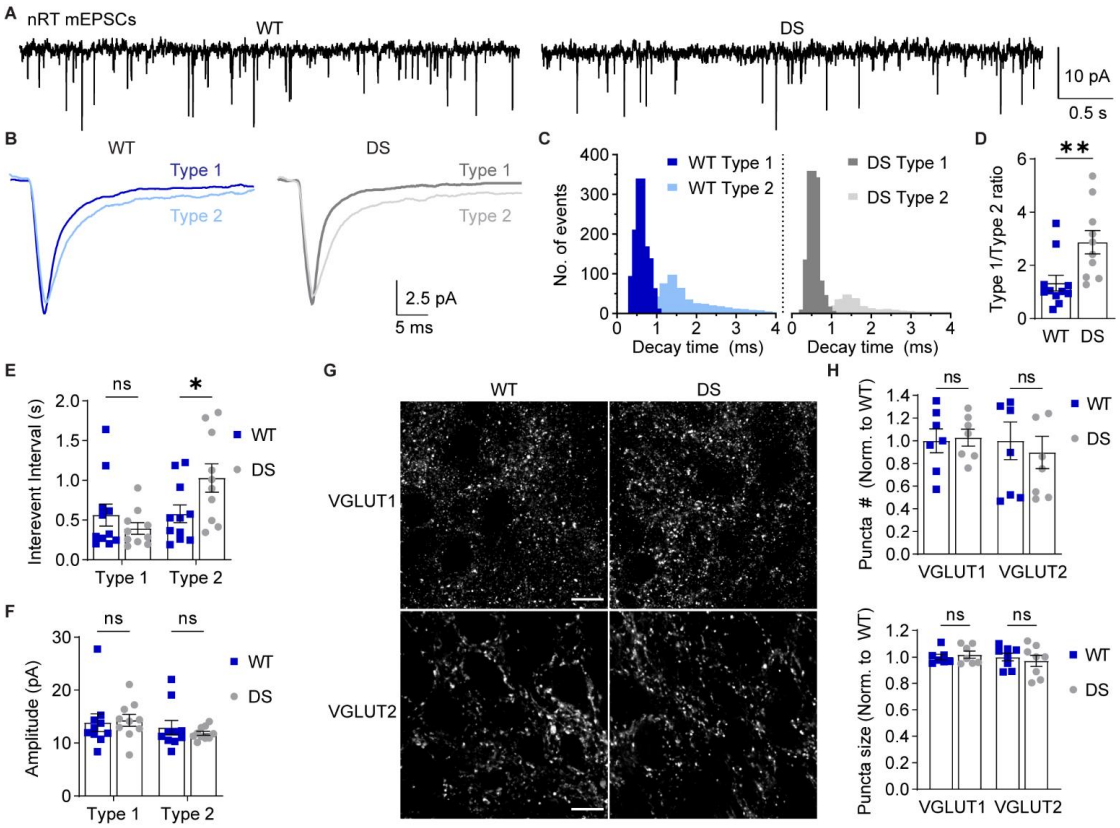

Figure 5. Selective reduction in Type 2 nRT mEPSC frequency in DS mice. A. mEPSCs were recorded from nRT neurons in acute brain slices in the presence of TTX. **B.** Representative traces show ensemble averages of WT and DS Type 1 and Type 2 mEPSCs as determined by decay time. **C.** The decay time distributions from each cell were averaged for WT and DS groups to generate the depicted histogram of the mean number of events per cell (bin size = 0.1 ms). **D**. The ratio of Type 1/Type 2 events for WT (n = 11 cells from 6 mice) and DS (n = 10 cells from 6 mice) neurons were compared by unpaired t-test (*p = 0.008). **E.** Mean inter-event interval and (**F**) amplitude values for Type 1 and Type 2 mEPSCs were analyzed by two-way ANOVA with posthoc Sidak's tests. Inter-event interval: Genotype $F(1,38) = 1.169$, $p = 0.286$; Interaction $F(1,38) = 5.619$, $p = 0.023$; Type 1 WT vs. DS: $p = 0.600$; Type 2 WT vs. DS: *$p = 0.039$. Amplitude: Genotype $F(1,38) = 0.0699$, $p = 0.795$; Interaction $F(1,38) = 0.388$, $p = 0.538$. See **Supplementary Figure S3** for cumulative distributions of inter-event interval and amplitude data. **G.** Representative 100X images depict VGLUT1 and VGLUT2 staining in WT and DS nRT. Scale bar: 10 µm. **H**. The number and size of VGLUT1 and VGLUT2 puncta (n = 7 mice) were analyzed by two-way ANOVA. Puncta number: Genotype: $F(1,26) = 0.081$, $p = 0.78$; Interaction: $F(1,26) = 0.250$, $p = 0.620$. Puncta size: Genotype: $F(1,26) = 0.031$, $p = 0.86$; Interaction: $F(1,26) = 0.545$, $p = 0.47$. Data points in the bar graphs represent individual neurons (D-F) or mice (H).

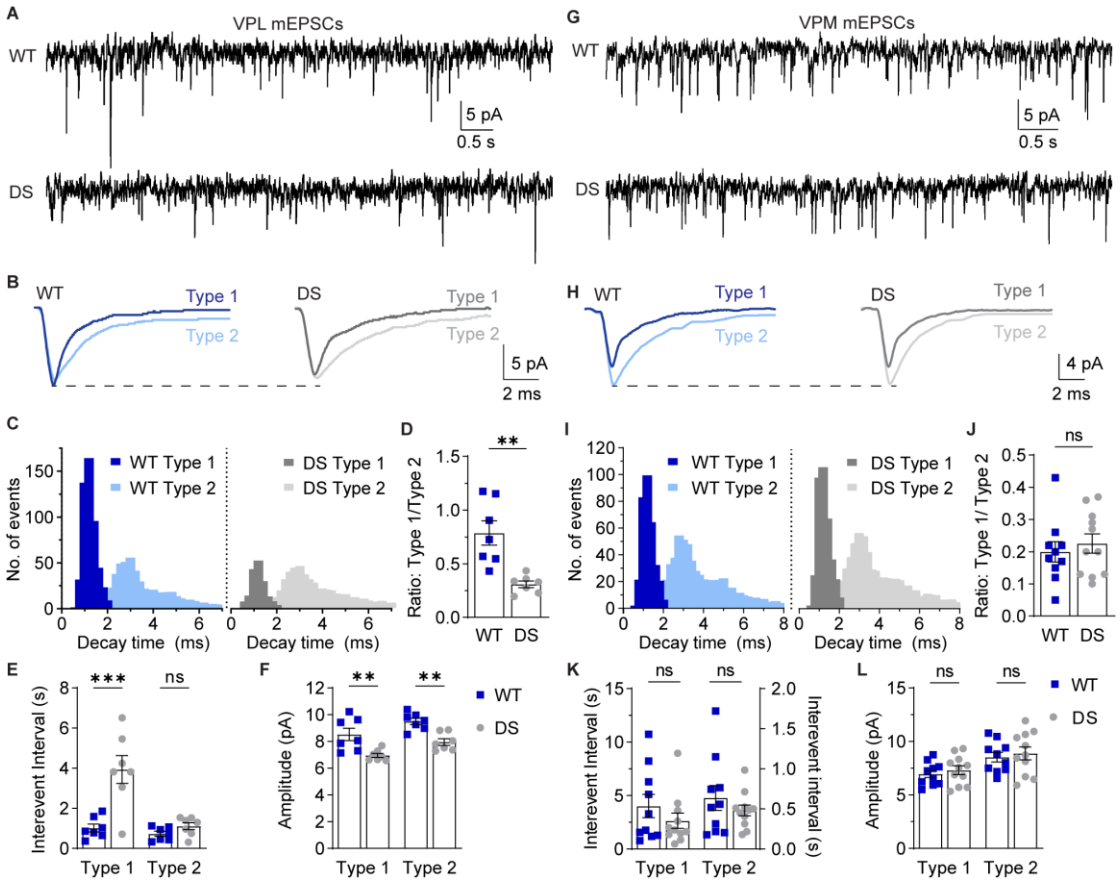

Figure 6. VPL neurons in DS mice exhibit reduced glutamatergic synaptic transmission. **A.** mEPSCs were recorded from VPL neurons in acute brain slices in the presence of 1 μM TTX. **B.** Representative traces show ensemble averages of WT and DS Type 1 and Type 2 VPL mEPSCs as determined by decay times. **C.** The decay time distributions from each cell were averaged for WT and DS groups to generate histograms of the mean number of events per cell (bin size = 0.2 ms). **D.** The ratio of Type 1 to Type 2 events was quantified for each WT (n = 7 cells from 6 mice) and DS neuron (n = 7 cells from 7 mice) and analyzed by unpaired t-test (**p = 0.002). **E.** Inter-event interval and (**F**) amplitude values for Type 1 and Type 2 mEPSCs in VPL neurons were analyzed by two-way ANOVA with posthoc Sidak's tests. Inter-event interval: Genotype $F(1,24) = 19.28$, $p < 0.001$; Interaction $F(1,24) = 11.42$, $p = 0.002$; Type 1 WT vs. DS: ***$p < 0.001$; Type 2 WT vs. DS: $p = 0.73$. Amplitude: Genotype $F(1, 24) = 27.15$, $p < 0.001$; Interaction $F(1,24) = 0.002$, $p = 0.969$. Type 1 WT vs. DS: **$p = 0.002$; Type 2 WT vs. DS: **$p = 0.003$. **G**. mEPSCs were recorded from VPM neurons and (**H)** representative traces show ensemble averages of WT and DS Type 1 and Type 2 mEPSCs. **I.** The decay time distributions from each cell were averaged for WT and DS groups to generate histograms of the mean number of events per cell (bin size = 0.2 ms). **J.** Type 1/Type 2 event ratios for WT (n = 10 cells from 8 mice) and DS (n = 11 cells from 9 mice) VPM neurons were analyzed by unpaired t-test ($p = 0.57$). **K.** Inter-event interval and (**L**) amplitude values for Type 1 and Type 2 mEPSCs in VPM neurons were analyzed by two-way ANOVA with posthoc Sidak's tests. Inter-event interval: Genotype $F(1,38) = 1.407$, $p = 0.243$; Interaction $F(1,38) = 0.893$, $p = 0.351$; Type 1 WT vs. DS: $p = 0.261$; Type 2 WT vs. DS: $p = 0.982$. Amplitude: Genotype $F(1, 38) = 0.573$, $p = 0.454$; Interaction $F(1,38) < 0.001$, $p = 0.993$. Type 1 WT vs. DS: $p = 0.840$; Type 2 WT vs. DS: $p = 0.833$. See **Supplementary Figure S5** for cumulative distribution inter-event interval and amplitude data.

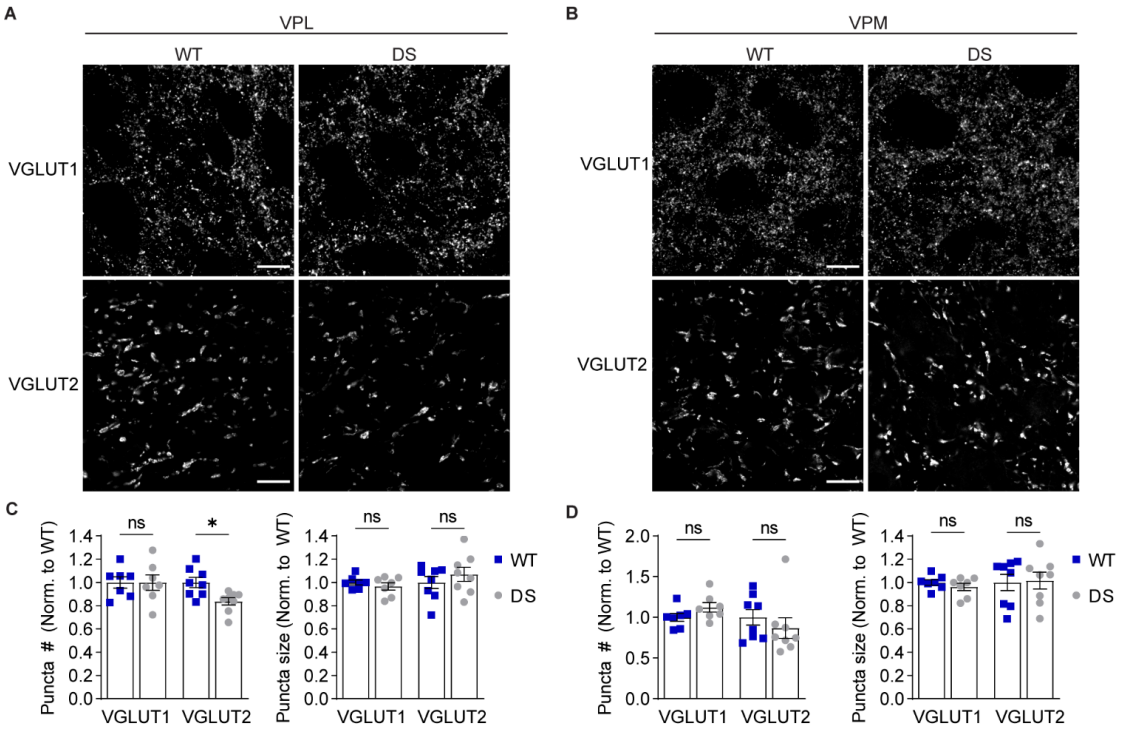

Figure 7. DS mice exhibit reduced ascending sensory input to the VPL. Representative 100X images show VGLUT1 (scale bar: 10 µm) and VGLUT2 (scale bar: 20 µm) immunostaining in the (**A**) VPL and (**B**) VPM. The number and size of VGLUT1 and VGLUT2 puncta were quantified for the (**C**) VPL and (**D**) VPM (n = 7) and analyzed by two-way ANOVA. VPL puncta number: Genotype $F(1,26) = 2.914$, $p = 0.10$; Interaction $F(1,26) = 2.829$, $p = 0.10$; posthoc Sidak's tests: VGLUT1, $p = 0.99$; VGLUT2, $^*p = 0.04$. VPL puncta size: Genotype: $F(1,26) = 0.161$, $p = 0.69$; Interaction: $F(1,26) = 1.262$, $p = 0.27$; posthoc Sidak's tests: VGLUT1, $p = 0.86$; VGLUT2, $p = 0.47$. VPM puncta number: Genotype: $F(1,26) = 0.002$, $p = 0.96$; Interaction: $F(1,26) = 1.9$, $p = 0.18$; posthoc Sidak's tests: VGLUT1, $p = 0.60$; VGLUT2, $p = 0.52$. VPM puncta size: Genotype: $F(1,26) = 0.040$, $p = 0.84$; Interaction: $F(1,26) = 0.221$, $p = 0.64$; posthoc Sidak's tests: VGLUT1, $p = 0.88$; VGLUT2, $p = 0.98$. Data points in all bar graphs represent individual mice.

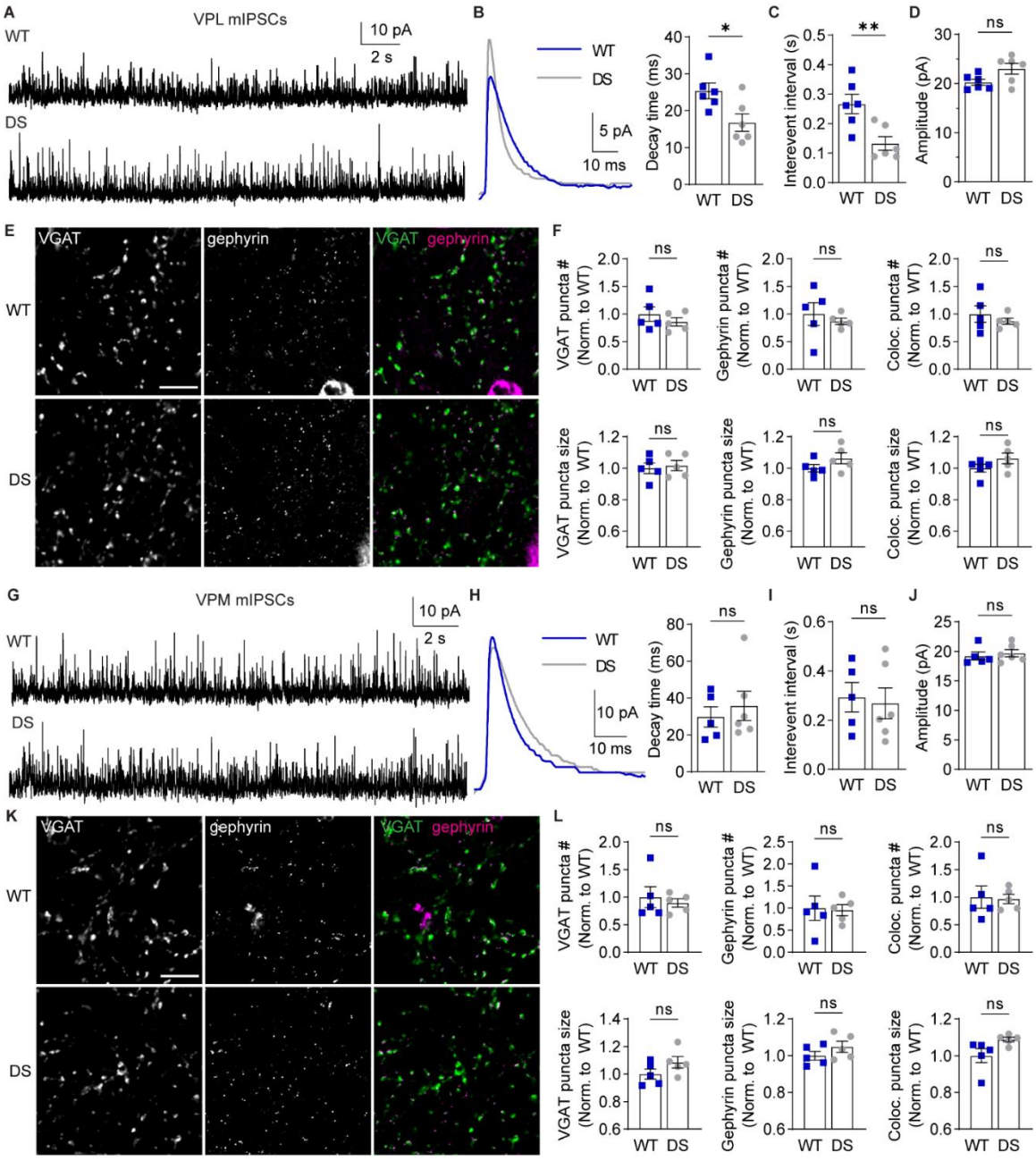

Figure 8. VPL neurons in DS mice exhibit reduced GABAergic synaptic transmission.

Figure 8. VPL neurons in DS mice exhibit reduced GABAergic synaptic transmission. A. mIPSCs were recorded from VPL neurons in acute brain sclies in the presence of 1 μM TTX. **B.** Representative traces show ensemble averages of WT and DS mIPSCs. mIPSC ensemble averages were fitted to determine decay time for WT and DS neurons (n = 6 cells from 5 mice) and compared by unpaired t-test (*p = 0.02). **C.** Inter-event interval and (**D**) amplitude for each WT and DS neuron were quantified and compared by unpaired t-tests. Inter-event interval: **p = 0.008. Amplitude: p = 0.054. **E.** Representative 100X images show VGATand gephyrin immunolabeling in the VPL (scale bar: 10 μm). **F.** The number and size of VGAT, gephyrin, and VGAT-gephryin colocalized puncta in the VPL (n = 5 mice) were compared by unpaired t-tests. VGAT puncta number: p = 0.39, size: p = 0.72; gephyrin puncta number: p = 0.56, size p = 0.17; colocalized puncta number: p = 0.44, size: p = 0.18. **G.** mIPSCs were recorded from VPM neurons, and (**H**) representative traces show ensemble averages of WT and DS mIPSCs. mIPSC ensemble averages were fitted to determine decay time for WT (n = 5 cells from 5 mice) and DS (n = 6 cells from 6 mice) neurons and compared by an unpaired t-test (p = 0.57). **I.** WT and DS inter-event interval and (**J**) amplitude were compared by unpaired t-tests. Inter-event interval: p = 0.785. Amplitude: p = 0.635. **K.** Representative 100X images show VGAT (scale bar: 10 μm) and gephyrin immunolabeling in the VPM. **L.** The number and size of VGAT, gephyrin, and VGAT-gephryin colocalized puncta were quantified in the VPM (n = 5 mice) and compared by unpaired t-tests. VGAT puncta number: p = 0.62, size: p = 0.16; gephyrin puncta number: p = 0.89, size p = 0.24; colocalized puncta number: p = 0.88, size: p = 0.06. The data points in the bar graphs represent individual neurons (B-D, H-J) or mice (F, L).

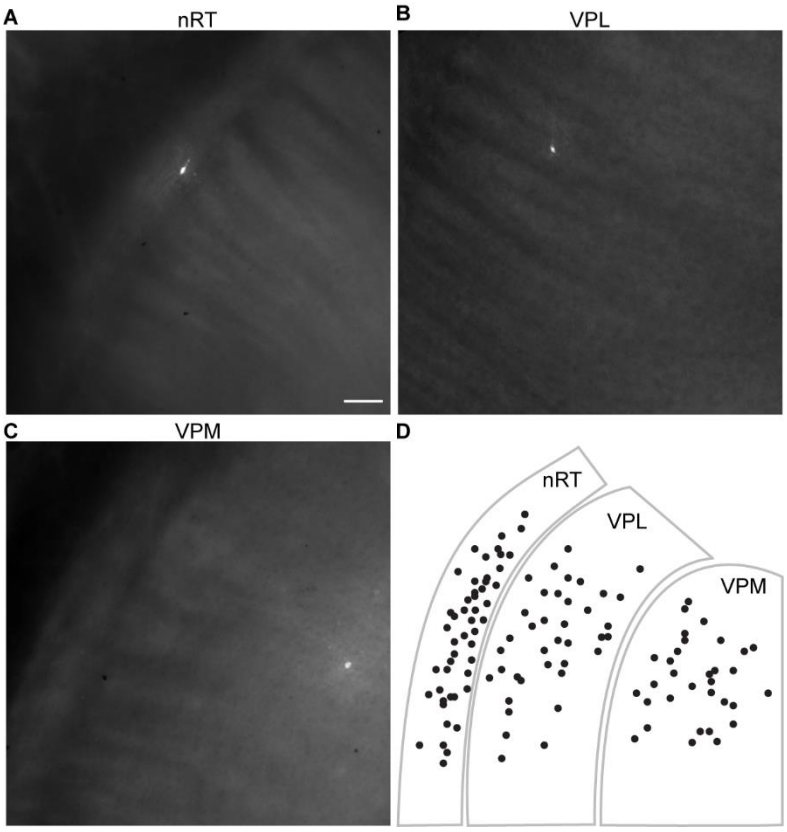

Supplementary Figure S1. Biocytin labeling of recorded neurons. Representative 10X images show biocytin-filled cells labeled with streptavidin-DyLight 594 in acute brain slices following electrophysiological recordings in the (**A**) nRT, (**B**) VPL, and (**C**) VPM. **D**. The black dots illustrate the location of each thalamic neuron recorded in this study, which demonstrates post hoc confirmation that each neuron was located in the appropriate thalamic nucleus.

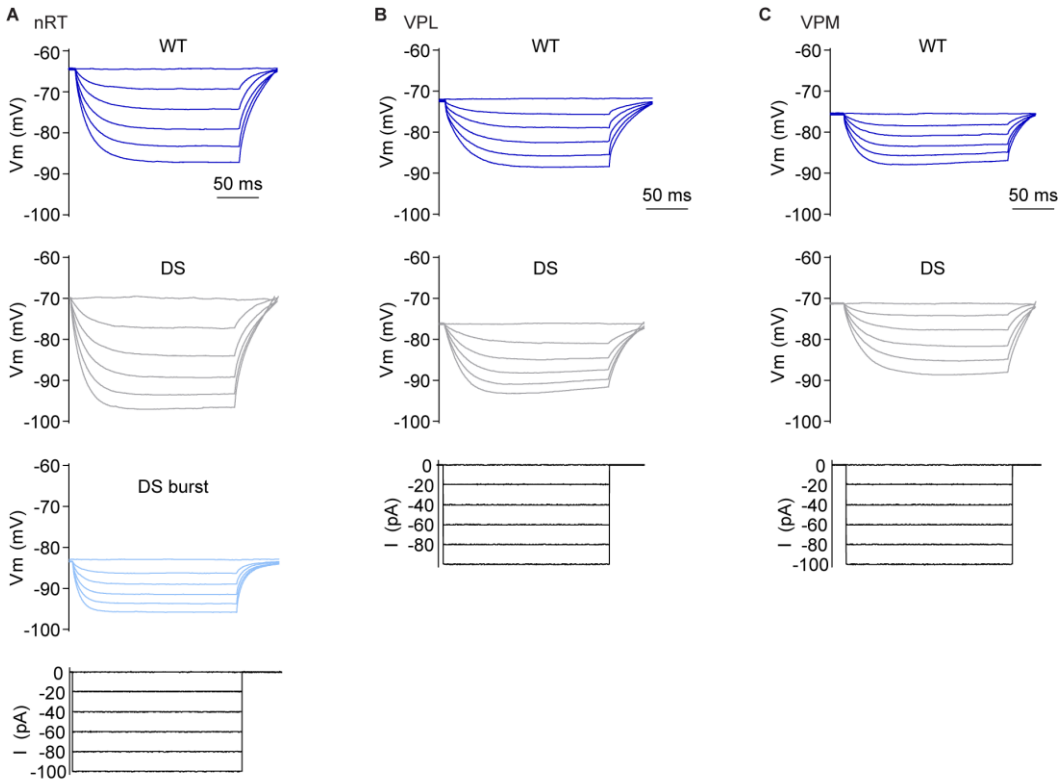

Supplementary Figure S2. Recordings for intrinsic membrane properties of nRT, VPL, and VPM neurons. Representative current-clamp recordings show voltage responses to 200 ms hyperpolarizing current injections for (**A**) nRT, (**B**) VPL, and (**C**) VPM neurons from WT and DS mice. The bottom panels show current injection amplitude.

Table S1. Action Potential Firing Properties of nRT, VPL, and VPM neurons.

	nRT		
	WT	**DS**	**p value**
Amplitude (mV)	40.0 ± 4.3	39.1 ± 1.4	0.70
Half-width (ms)	0.51 ± 0.04	0.51 ± 0.02	0.95
Rise Time (ms) 75% to 10%	0.58 ± 0.28	0.46 ± 0.09	0.69
Decay Time (ms) 10% to 75%	0.34 ± 0.04	0.33 ± 0.02	0.70
After-hyperpolarization Amplitude (mV)	-52.8 ± 0.7	-52.2 ± 1.2	0.69
Threshold (mV)	-50.9 ± 1.2	-50.1 ± 1.7	0.85
N	6 (2)	6 (2)	

	VPL			VPM		
	WT	**DS**	**p value**	**WT**	**DS**	**p value**
Amplitude (mV)	46.8 ± 3.3	52.0 ± 5.1	0.38	48.8 ± 3.4	49.4 ± 3.1	0.90
Half-width (ms)	0.90 ± 0.04	0.83 ± 0.02	0.19	0.81 ± 0.04	0.78 ± 0.04	0.59
Rise Time (ms) 75% to 10%	0.34 ± 0.02	0.32 ± 0.01	0.37	0.29 ± 0.02	0.28 ± 0.02	0.75
Decay Time (ms) 10% to 75%	0.62 ± 0.03	0.53 ± 0.02	0.06	0.58 ± 0.04	0.52 ± 0.02	0.27
After-hyperpolarization Amplitude (mV)	-43.1 ± 1.3	-47.0 ± 2.1	0.16	-43.2 ± 2.2	-47.1 ± 2.2	0.28
Threshold (mV)	-46.7 ± 1.6	-48.0 ± 1.8	0.60	-46.8 ± 1.9	-50.8 ± 2.0	0.17
N	9 (7)	6 (3)		11 (8)	8 (5)	

N values are the number of cells followed by the number of mice in parentheses. WT and DS groups were compared by unpaired t-tests for which the p values are listed.

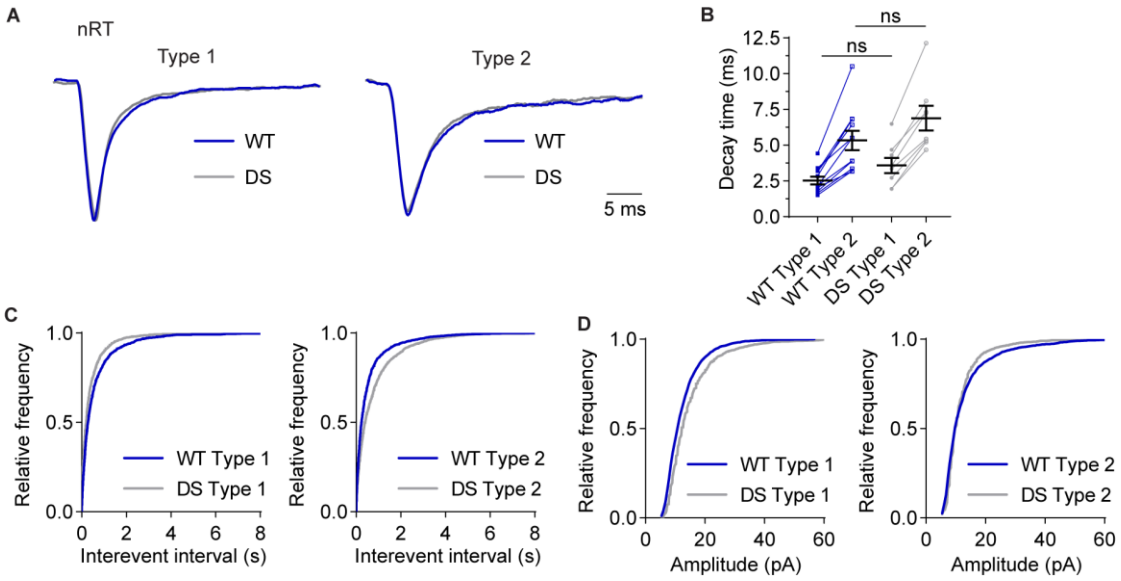

Supplementary Figure S3. nRT mEPSC decay times and cumulative distributions.
A. Traces are ensemble averages of Type 1 and Type 2 mEPSCs from representative WT and DS neurons normalized to the respective WT mEPSC amplitude. **B.** The decay times were measured by fitting ensemble averages of Type 1 and Type 2 mEPSCs for each WT and DS neuron. The plot shows paired data for Type 1 and Type 2 mean decay times from each cell and group data as mean ± s.e.m. Data were analyzed by two-way ANOVA. Genotype: $F(1,34) = 4.615$, $p = 0.038$; mEPSC Type: $F(1,34) = 25.36$, $p < 0.001$; Interaction: $F(1,34) = 0.359$, $p = 0.553$. Cumulative frequency distributions are shown for **(C)** inter-event interval and **(D)** amplitude of Type 1 and Type 2 mEPSCs from all WT (n = 11) and DS (n = 10) neurons.

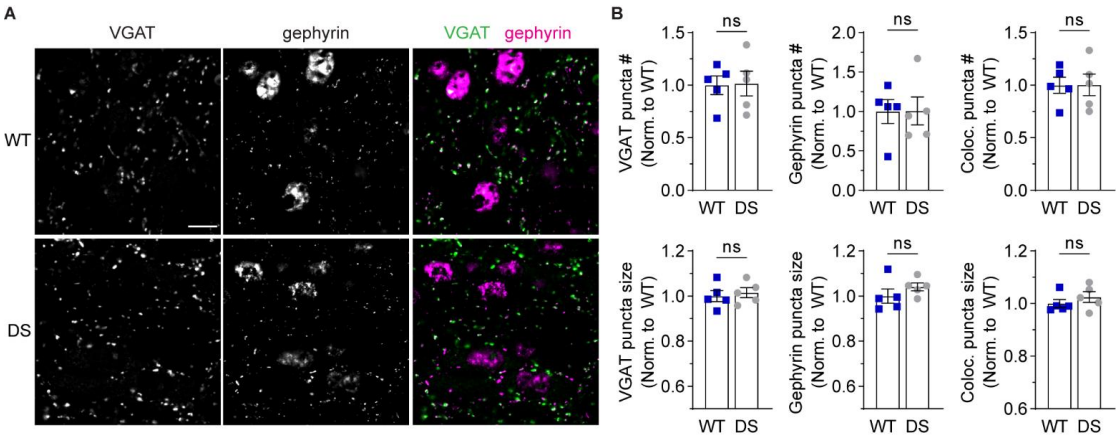

Supplementary Figure S4. GABAergic synapse number and size in the nRT are unchanged in DS mice. A. Representative 100X images show VGAT (scale bar: 10 µm) and gephyrin immunolabeling in the nRT as well as the merged image. **B.** The number and size of VGAT, gephyrin, and colocalized vGat-gephryin puncta were quantified, plotted as group mean ± s.e.m. with data points representing individual mice (n = 5), and compared by unpaired t-tests. VGAT puncta number: p = 0.91, size: p = 0.66; gephyrin puncta number: p = 0.98, size p = 0.29; colocalized puncta number: p = 0.98, size: p = 0.36.

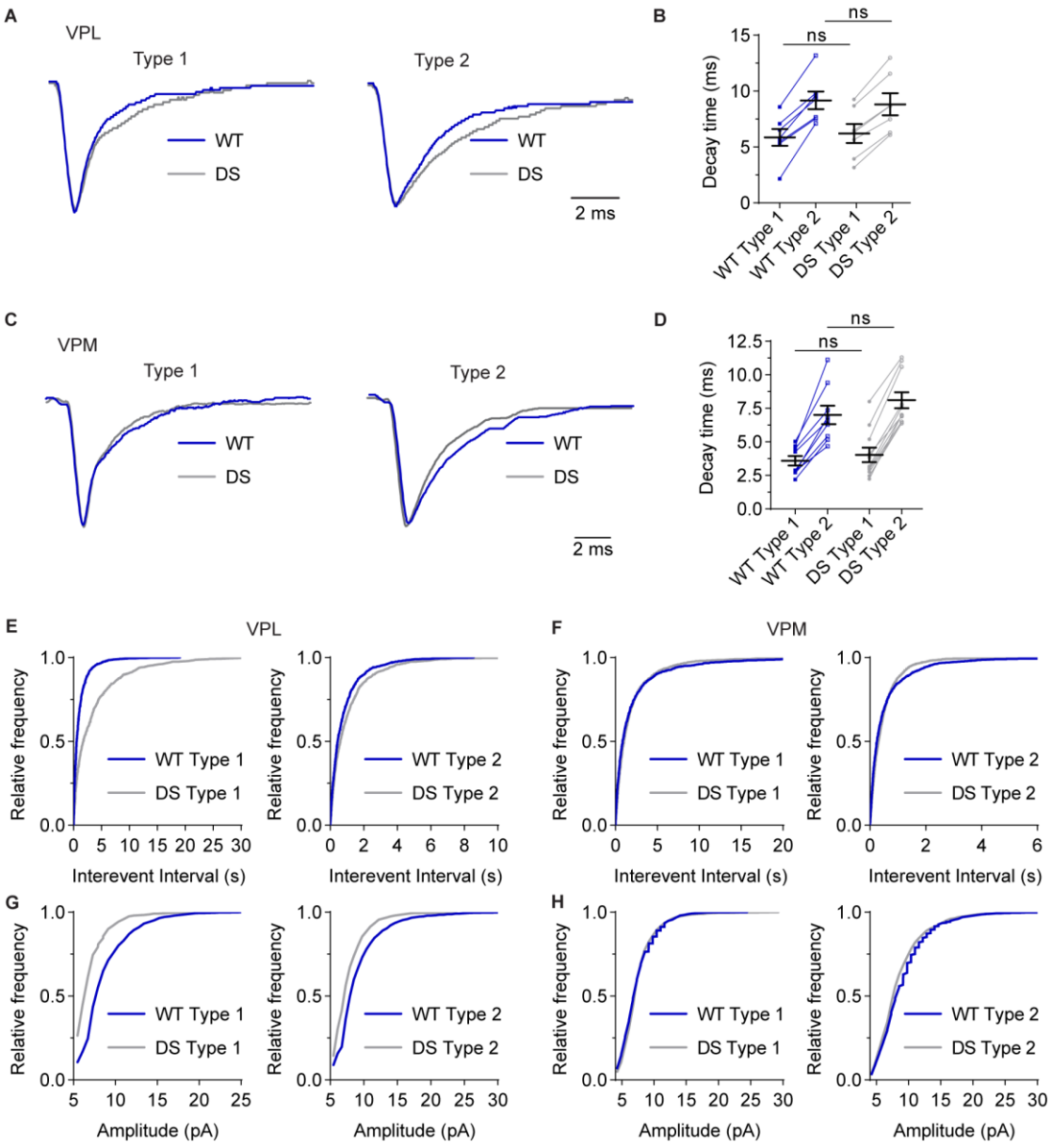

Supplementary Figure S5. VPL and VPM mEPSC decay times and cumulative distributions. Traces are ensemble averages of Type 1 and Type 2 mEPSCs from representative (**A**) VPL and (**C**) VPM neurons normalized to the respective WT mEPSC amplitude. **B,D**. The decay times were measured by fitting ensemble averages of Type 1 and Type 2 mEPSCs for each WT and DS neuron. The plots show paired data for Type 1 and Type 2 mean decay times from each cell and group data as mean ± s.e.m. Data were analyzed by two-way ANOVA. VPL: Genotype, $F(1,24) = 0.001$, $p > 0.99$; mEPSC Type, $F(1,24) = 12.22$, $p = 0.002$; Interaction, $F(1,24) = 0.178$, $p = 0.68$. VPM: Genotype, $F(1,36) = 0.261$, $p = 0.608$; mEPSC Type, $F(1,36) = 43.92$, $p < 0.001$; Interaction, $F(1,36) = 1.826$, $p = 0.185$. Cumulative frequency distributions are shown for **(E,F)** inter-event interval and **(G,H)** amplitude of Type 1 and Type 2 mEPSCs from all WT and DS neurons.

References

Ab Aziz, C.B., and Ahmad, A.H. (2006). The role of the thalamus in modulating pain. Malays J Med Sci *13*, 11-18.

Acker, T.M., Yuan, H., Hansen, K.B., Vance, K.M., Ogden, K.K., Jensen, H.S., Burger, P.B., Mullasseril, P., Snyder, J.P., Liotta, D.C., and Traynelis, S.F. (2011). Mechanism for noncompetitive inhibition by novel GluN2C/D N-methyl-D-aspartate receptor subunit-selective modulators. Mol Pharmacol *80*, 782-795. 10.1124/mol.111.073239.

Almog, Y., Fadila, S., Brusel, M., Mavashov, A., Anderson, K., and Rubinstein, M. (2021). Developmental alterations in firing properties of hippocampal CA1 inhibitory and excitatory neurons in a mouse model of Dravet syndrome. Neurobiol Dis *148*, 105209. 10.1016/j.nbd.2020.105209.

Alshammari, M.A., Alshammari, T.K., and Laezza, F. (2016). Improved Methods for Fluorescence Microscopy Detection of Macromolecules at the Axon Initial Segment. Front Cell Neurosci *10*, 5. 10.3389/fncel.2016.00005.

Azumaya, C.M., Days, E.L., Vinson, P.N., Stauffer, S., Sulikowski, G., Weaver, C.D., and Nakagawa, T. (2017). Screening for AMPA receptor auxiliary subunit specific modulators. PLoS One *12*, e0174742. 10.1371/journal.pone.0174742.

Beenhakker, M.P., and Huguenard, J.R. (2009). Neurons that fire together also conspire together: is normal sleep circuitry hijacked to generate epilepsy? Neuron *62*, 612-632. 10.1016/j.neuron.2009.05.015.

Bender, A.C., Luikart, B.W., and Lenck-Santini, P.P. (2016). Cognitive Deficits Associated with Nav1.1 Alterations: Involvement of Neuronal Firing Dynamics and Oscillations. PLoS One *11*, e0151538. 10.1371/journal.pone.0151538.

Bender, A.C., Natola, H., Ndong, C., Holmes, G.L., Scott, R.C., and Lenck-Santini, P.P. (2013). Focal Scn1a knockdown induces cognitive impairment without seizures. Neurobiol Dis *54*, 297-307. 10.1016/j.nbd.2012.12.021.

Berkvens, J.J., Veugen, I., Veendrick-Meekes, M.J., Snoeijen-Schouwenaars, F.M., Schelhaas, H.J., Willemsen, M.H., Tan, I.Y., and Aldenkamp, A.P. (2015). Autism and behavior in adult patients with Dravet syndrome (DS). Epilepsy Behav *47*, 11-16. 10.1016/j.yebeh.2015.04.057.

Brecht, M., and Sakmann, B. (2002). Whisker maps of neuronal subclasses of the rat ventral posterior medial thalamus, identified by whole-cell voltage recording and morphological reconstruction. J Physiol *538*, 495-515. 10.1113/jphysiol.2001.012334.

Castro-Alamancos, M.A. (2002). Properties of primary sensory (lemniscal) synapses in the ventrobasal thalamus and the relay of high-frequency sensory inputs. J Neurophysiol *87*, 946-953. 10.1152/jn.00426.2001.

Catarino, C.B., Liu, J.Y., Liagkouras, I., Gibbons, V.S., Labrum, R.W., Ellis, R., Woodward, C., Davis, M.B., Smith, S.J., Cross, J.H., et al. (2011). Dravet syndrome as epileptic encephalopathy: evidence from long-term course and neuropathology. Brain *134*, 2982-3010. 10.1093/brain/awr129.

Cheong, E., and Shin, H.S. (2013). T-type Ca2+ channels in normal and abnormal brain functions. Physiol Rev *93*, 961-992. 10.1152/physrev.00010.2012.

Chiron, C. (2011). Current therapeutic procedures in Dravet syndrome. Dev Med Child Neurol *53 Suppl 2*, 16-18. 10.1111/j.1469-8749.2011.03967.x.

Claes, L., Del-Favero, J., Ceulemans, B., Lagae, L., Van Broeckhoven, C., and De Jonghe, P. (2001). De novo mutations in the sodium-channel gene SCN1A cause severe myoclonic epilepsy of infancy. Am J Hum Genet *68*, 1327-1332. 10.1086/320609.

Clemente-Perez, A., Makinson, S.R., Higashikubo, B., Brovarney, S., Cho, F.S., Urry, A., Holden, S.S., Wimer, M., David, C., Fenno, L.E., et al. (2017). Distinct Thalamic Reticular Cell Types Differentially Modulate Normal and Pathological Cortical Rhythms. Cell Rep *19*, 2130-2142. 10.1016/j.celrep.2017.05.044.

Cross, J.H., Caraballo, R.H., Nabbout, R., Vigevano, F., Guerrini, R., and Lagae, L. (2019). Dravet syndrome: Treatment options and management of prolonged seizures. Epilepsia *60 Suppl 3*, S39-S48. 10.1111/epi.16334.

Darra, F., Battaglia, D., Dravet, C., Patrini, M., Offredi, F., Chieffo, D., Piazza, E., Fontana, E., Olivieri, G., Turrini, I., et al. (2019). Dravet syndrome: Early electroclinical findings and long-term outcome in adolescents and adults. Epilepsia *60 Suppl 3*, S49-S58. 10.1111/epi.16297.

Deleuze, C., and Huguenard, J. (2016). Two classes of excitatory synaptic responses in rat thalamic reticular neurons. J Neurophysiol *116*, 995-1011.

Dravet, C. (2011). The core Dravet syndrome phenotype. Epilepsia *52 Suppl 2*, 3-9. 10.1111/j.1528-1167.2011.02994.x.

Favero, M., Sotuyo, N.P., Lopez, E., Kearney, J.A., and Goldberg, E.M. (2018). A Transient Developmental Window of Fast-Spiking Interneuron Dysfunction in a Mouse Model of Dravet Syndrome. J Neurosci *38*, 7912-7927. 10.1523/JNEUROSCI.0193-18.2018.

Fernandez, L.M.J., and Luthi, A. (2020). Sleep Spindles: Mechanisms and Functions. Physiol Rev *100*, 805-868. 10.1152/physrev.00042.2018.

Fogerson, P.M., and Huguenard, J.R. (2016). Tapping the Brakes: Cellular and Synaptic Mechanisms that Regulate Thalamic Oscillations. Neuron *92*, 687-704. 10.1016/j.neuron.2016.10.024.

Gataullina, S., and Dulac, O. (2017). From genotype to phenotype in Dravet disease. Seizure *44*, 58-64. 10.1016/j.seizure.2016.10.014.

Graziano, A., Liu, X.-B., Murray, K.D., and Jones, E.G. (2008). Vesicular Glutamate Transporters Define Two Sets of Glutamatergic Afferents to the Somatosensory Thalamus and Two Thalamocortical Projections in the Mouse. The Journal of Comparative Neurology *507*, 1258-1276.

Hains, B.C., Saab, C.Y., and Waxman, S.G. (2006). Alterations in burst firing of thalamic VPL neurons and reversal by Na(v)1.3 antisense after spinal cord injury. J Neurophysiol *95*, 3343-3352. 10.1152/jn.01009.2005.

Han, S., Tai, C., Westenbroek, R.E., Yu, F.H., Cheah, C.S., Potter, G.B., Rubenstein, J.L., Scheuer, T., de la Iglesia, H.O., and Catterall, W.A. (2012). Autistic-like behaviour in Scn1a+/- mice and rescue by enhanced GABA-mediated neurotransmission. Nature *489*, 385-390. 10.1038/nature11356.

Hansen, K.B., Yi, F., Perszyk, R.E., Furukawa, H., Wollmuth, L.P., Gibb, A.J., and Traynelis, S.F. (2018). Structure, function, and allosteric modulation of NMDA receptors. J Gen Physiol *150*, 1081-1105. 10.1085/jgp.201812032.

Hanson, J.E., Ma, K., Elstrott, J., Weber, M., Saillet, S., Khan, A.S., Simms, J., Liu, B., Kim, T.A., Yu, G.Q., et al. (2020). GluN2A NMDA Receptor Enhancement Improves Brain Oscillations, Synchrony, and Cognitive Functions in Dravet Syndrome and Alzheimer's Disease Models. Cell Rep *30*, 381-396 e384. 10.1016/j.celrep.2019.12.030.

Hedrich, U.B., Liautard, C., Kirschenbaum, D., Pofahl, M., Lavigne, J., Liu, Y., Theiss, S., Slotta, J., Escayg, A., Dihne, M., et al. (2014). Impaired action potential initiation in GABAergic interneurons causes hyperexcitable networks in an epileptic mouse model carrying a human Na(V)1.1 mutation. J Neurosci *34*, 14874-14889. 10.1523/JNEUROSCI.0721-14.2014.

Henderson, L.A., Peck, C.C., Petersen, E.T., Rae, C.D., Youssef, A.M., Reeves, J.M., Wilcox, S.L., Akhter, R., Murray, G.M., and Gustin, S.M. (2013). Chronic pain: lost inhibition? J Neurosci *33*, 7574-7582. 10.1523/JNEUROSCI.0174-13.2013.

Hovelso, N., Sotty, F., Montezinho, L.P., Pinheiro, P.S., Herrik, K.F., and Mork, A. (2012). Therapeutic potential of metabotropic glutamate receptor modulators. Curr Neuropharmacol *10*, 12-48. 10.2174/157015912799362805.

Kadriu, B., Musazzi, L., Johnston, J.N., Kalynchuk, L.E., Caruncho, H.J., Popoli, M., and Zarate, C.A., Jr. (2021). Positive AMPA receptor modulation in the treatment of neuropsychiatric disorders: A long and winding road. Drug Discov Today. 10.1016/j.drudis.2021.07.027.

Kalume, F., Oakley, J.C., Westenbroek, R.E., Gile, J., de la Iglesia, H.O., Scheuer, T., and Catterall, W.A. (2015). Sleep impairment and reduced interneuron excitability in a mouse model of Dravet Syndrome. Neurobiol Dis *77*, 141-154. 10.1016/j.nbd.2015.02.016.

Kalume, F., Yu, F.H., Westenbroek, R.E., Scheuer, T., and Catterall, W.A. (2007). Reduced sodium current in Purkinje neurons from Nav1.1 mutant mice: implications for ataxia in severe myoclonic epilepsy in infancy. J Neurosci *27*, 11065-11074. 10.1523/JNEUROSCI.2162-07.2007.

Khatri, A., Burger, P.B., Swanger, S.A., Hansen, K.B., Zimmerman, S., Karakas, E., Liotta, D.C., Furukawa, H., Snyder, J.P., and Traynelis, S.F. (2014). Structural determinants and mechanism of action of a GluN2C-selective NMDA receptor positive allosteric modulator. Mol Pharmacol *86*, 548-560. 10.1124/mol.114.094516.

Landisman, J.S.H.a.C.E. (2012). State-dependent modulation of gap junction signaling by the persistent sodium current. Frontiers in Cellular Neuroscience *5* (*31*).

Layer, N., Sonnenberg, L., Gonzalez, E.P., Benda, J., Hedrich, U.B.S., Lerche, H., Koch, H., and Wuttke, T.V. (2021). Dravet Variant *SCN1A*^{A1783V} Impairs Interneuron Firing Predominantly by Altered Channel Activation. Frontiers in Cellular Neuroscience *15*.

Lee, J., Kim, D., and Shin, H.S. (2004). Lack of delta waves and sleep disturbances during non-rapid eye movement sleep in mice lacking alpha1G-subunit of T-type calcium channels. Proc Natl Acad Sci U S A *101*, 18195-18199. 10.1073/pnas.0408089101.

Lenz, F.A. (1992). The ventral posterior nucleus of thalamus is involved in the generation of central pain syndromes. APS Journal *1*, 42-51. https://doi.org/10.1016/S1058-9139(06)80011-2.

Li, Y., Lopez-Huerta, V.G., Adiconis, X., Levandowski, K., Choi, S., Simmons, S.K., Arias-Garcia, M.A., Guo, B., Yao, A.Y., Blosser, T.R., et al. (2020). Distinct subnetworks of the thalamic reticular nuclues. Nature *583*, 819-824.

Licheni, S.H., McMahon, J.M., Schneider, A.L., Davey, M.J., and Scheffer, I.E. (2018). Sleep problems in Dravet syndrome: a modifiable comorbidity. Dev Med Child Neurol *60*, 192-198. 10.1111/dmcn.13601.

Liu, J., Shelkar, G.P., Zhao, F., Clausen, R.P., and Dravid, S.M. (2019). Modulation of burst firing of neurons in nucleus reticularis of the thalamus by GluN2C-containing NMDA receptors. Mol Pharmacol. 10.1124/mol.119.116780.

Martinez-Garcia, R.I., Voelcker, B., Zaltsman, J., Patrick, S., Stevens, T., Conners, B., and Cruikshank, S. (2020). Two dynamically distinct circuits driving inhibition in sensory thalamus. bioRxiv.

Mazzitelli, M., Palazzo, E., Maione, S., and Neugebauer, V. (2018). Group II Metabotropic Glutamate Receptors: Role in Pain Mechanisms and Pain Modulation. Front Mol Neurosci *11*, 383. 10.3389/fnmol.2018.00383.

McCafferty, C., David, F., Venzi, M., Lorincz, M.L., Delicata, F., Atherton, Z., Recchia, G., Orban, G., Lambert, R.C., Di Giovanni, G., et al. (2018). Cortical drive and thalamic feed-forward

inhibition control thalamic output synchrony during absence seizures. Nat Neurosci *21*, 744-756. 10.1038/s41593-018-0130-4.

McCormick, D.A., and von Krosigk, M. (1992). Corticothalamic activation modulates thalamic firing through glutamate "metabotropic" receptors. Proc Natl Acad Sci U S A *89*, 2774-2778. 10.1073/pnas.89.7.2774.

Miller, A.R., Hawkins, N.A., McCollom, C.E., and Kearney, J.A. (2014). Mapping genetic modifiers of survival in a mouse model of Dravet syndrome. Genes Brain Behav *13*, 163-172. 10.1111/gbb.12099.

Miyata, M., and Imoto, K. (2006). Different composition of glutamate receptors in corticothalamic and lemniscal synaptic responses and their roles in the firing responses of ventrobasal thalamic neurons in juvenile mice. J Physiol *575*, 161-174. 10.1113/jphysiol.2006.114413.

Moehring, J., von Spiczak, S., Moeller, F., Helbig, I., Wolff, S., Jansen, O., Muhle, H., Boor, R., Stephani, U., and Siniatchkin, M. (2013). Variability of EEG-fMRI findings in patients with SCN1A-positive Dravet syndrome. Epilepsia *54*, 918-926. 10.1111/epi.12119.

Mullasseril, P., Hansen, K.B., Vance, K.M., Ogden, K.K., Yuan, H., Kurtkaya, N.L., Santangelo, R., Orr, A.G., Le, P., Vellano, K.M., et al. (2010). A subunit-selective potentiator of NR2C- and NR2D-containing NMDA receptors. Nat Commun *1*, 90. 10.1038/ncomms1085.

Ogiwara, I., Iwasato, T., Miyamoto, H., Iwata, R., Yamagata, T., Mazaki, E., Yanagawa, Y., Tamamaki, N., Hensch, T.K., Itohara, S., and Yamakawa, K. (2013). Nav1.1 haploinsufficiency in excitatory neurons ameliorates seizure-associated sudden death in a mouse model of Dravet syndrome. Hum Mol Genet *22*, 4784-4804. 10.1093/hmg/ddt331.

Ogiwara, I., Miyamoto, H., Morita, N., Atapour, N., Mazaki, E., Inoue, I., Takeuchi, T., Itohara, S., Yanagawa, Y., Obata, K., et al. (2007). Nav1.1 localizes to axons of parvalbumin-positive inhibitory interneurons: a circuit basis for epileptic seizures in mice carrying an Scn1a gene mutation. J Neurosci *27*, 5903-5914. 10.1523/JNEUROSCI.5270-06.2007.

Papale, L.A., Makinson, C.D., Christopher Ehlen, J., Tufik, S., Decker, M.J., Paul, K.N., and Escayg, A. (2013). Altered sleep regulation in a mouse model of SCN1A-derived genetic epilepsy with febrile seizures plus (GEFS+). Epilepsia *54*, 625-634. 10.1111/epi.12060.

Parri, R.H., and Crunelli, V. (1998). Sodium current in rat and cat thalamocortical neurons: role of a non-inactivating component in tonic and burst firing. J Neuroscience *18*.

Ragona, F. (2011). Cognitive development in children with Dravet syndrome. Epilepsia *52 Suppl 2*, 39-43. 10.1111/j.1528-1167.2011.03000.x.

Ritter-Makinson, S., Clemente-Perez, A., Higashikubo, B., Cho, F.S., Holden, S.S., Bennett, E., Chkhaidze, A., Eelkman Rooda, O.H.J., Cornet, M.C., Hoebeek, F.E., et al. (2019). Augmented

Reticular Thalamic Bursting and Seizures in Scn1a-Dravet Syndrome. Cell Rep *26*, 54-64 e56. 10.1016/j.celrep.2018.12.018.

Rodda, J.M., Scheffer, I.E., McMahon, J.M., Berkovic, S.F., and Graham, H.K. (2012). Progressive gait deterioration in adolescents with Dravet syndrome. Arch Neurol *69*, 873-878. 10.1001/archneurol.2011.3275.

Rubinstein, M., Han, S., Tai, C., Westenbroek, R.E., Hunker, A., Scheuer, T., and Catterall, W.A. (2015a). Dissecting the phenotypes of Dravet syndrome by gene deletion. Brain *138*, 2219-2233. 10.1093/brain/awv142.

Rubinstein, M., Westenbroek, R.E., Yu, F.H., Jones, C.J., Scheuer, T., and Catterall, W.A. (2015b). Genetic background modulates impaired excitability of inhibitory neurons in a mouse model of Dravet syndrome. Neurobiol Dis *73*, 106-117. 10.1016/j.nbd.2014.09.017.

Shane R. Crandall, S.C., Barry Connors (2015). A Corticothalamic Switch: Controlling the Thalamus with Dynamic Switches. Neuron *86*, 768-782.

Sherman, S.M. (2001). Tonic and burst firing: dual modes of thalamocortical relay. Trends Neurosci *24*, 122-126. 10.1016/s0166-2236(00)01714-8.

Stafstrom, C.E. (2007). Persistent Sodium Current and Its Role in Epilepsy. Current Review in Basic Science *7*, 15-22.

Steriade, M., and Llinas, R.R. (1988). The functional states of the thalamus and the associated neuronal interplay. Physiol Rev *68*, 649-742. 10.1152/physrev.1988.68.3.649.

Swanger, S.A., Vance, K.M., Acker, T.M., Zimmerman, S.S., DiRaddo, J.O., Myers, S.J., Bundgaard, C., Mosley, C.A., Summer, S.L., Menaldino, D.S., et al. (2018). A Novel Negative Allosteric Modulator Selective for GluN2C/2D-Containing NMDA Receptors Inhibits Synaptic Transmission in Hippocampal Interneurons. ACS Chem Neurosci *9*, 306-319. 10.1021/acschemneuro.7b00329.

Tai, C., Abe, Y., Westenbroek, R.E., Scheuer, T., and Catterall, W.A. (2014). Impaired excitability of somatostatin- and parvalbumin-expressing cortical interneurons in a mouse model of Dravet syndrome. Proc Natl Acad Sci U S A *111*, E3139-3148. 10.1073/pnas.1411131111.

Takayama, R., Fujiwara, T., Shigematsu, H., Imai, K., Takahashi, Y., Yamakawa, K., and Inoue, Y. (2014). Long-term course of Dravet syndrome: a study from an epilepsy center in Japan. Epilepsia *55*, 528-538. 10.1111/epi.12532.

Temereanca S, S.D. (2004). Functional topography of corticothalamic feedback enhances thalamic spatial response tuning in the somatosensory whisker/barrel system. Neuron *41*, 639-651.

Villas, N., Meskis, M.A., and Goodliffe, S. (2017). Dravet syndrome: Characteristics, comorbidities, and caregiver concerns. Epilepsy Behav *74*, 81-86. 10.1016/j.yebeh.2017.06.031.

Wolff, M., and Vann, S.D. (2019). The Cognitive Thalamus as a Gateway to Mental Representations. J Neurosci *39*, 3-14. 10.1523/JNEUROSCI.0479-18.2018.

Yi, F., Rouzbeh, N., Hansen, K.B., Xu, Y., Fanger, C.M., Gordon, E., Paschetto, K., Menniti, F.S., and Volkmann, R.A. (2020). PTC-174, a positive allosteric modulator of NMDA receptors containing GluN2C or GluN2D subunits. Neuropharmacology *173*, 107971. 10.1016/j.neuropharm.2020.107971.

Zhao, P., Waxman, S.G., and Hains, B.C. (2006). Sodium channel expression in the ventral posterolateral nucleus of the thalamus after peripheral nerve injury. Mol Pain *2*, 27. 10.1186/1744-8069-2-27.

Zikopoulos, B., and Barbas, H. (2006). Prefrontal projections to the thalamic reticular nucleus form a unique circuit for attentional mechanisms. J Neurosci *26*, 7348-7361. 10.1523/JNEUROSCI.5511-05.2006.

Chapter 3

Ventral posterolateral and Ventral posteromedial Thalamic Nuclei Exhibit Distinct Cellular Excitability

Carleigh Studtmann[ab], Mackenzie A. Topolski[a], and Sharon A. Swanger[acd]

[a]Center for Neurobiology Research, Fralin Biomedical Research Institute at VTC, Virginia Tech, Roanoke, VA, USA.

[b]Graduate Program in Translational Biology, Medicine, and Health, Virginia Tech, Blacksburg, VA, USA.

[c]Department of Biomedical Sciences and Pathobiology, Virginia-Maryland College of Veterinary Medicine, Virginia Tech, Blacksburg, VA, USA.

[d]Department of Internal Medicine, Virginia Tech Carilion School of Medicine, Roanoke, VA, USA.

Corresponding Author:

Sharon A. Swanger

Fralin Biomedical Research Institute at VTC

Virginia Tech

2 Riverside Circle

Roanoke, VA 24016

Abstract

The somatosensory corticothalamic circuit is responsible for propagating somatosensory signals through the ventrobasal (VB) thalamus, which is comprised of two distinct nuclei- the ventral posterolateral (VPL) and ventral posteromedial (VPM) thalamic nuclei. The VPL and VPM receive ascending sensory signals from the body and head, respectively, and also receive distinct cell-type-specific input from the adjacent reticular nucleus of the thalamus (nRT). Though there is evidence for cell-type-specific function between the two nuclei, they have largely been studied as one VB complex in both healthy and diseased circuit models. Here, we used C57Bl6J mice of both sexes aged P25-P31 to directly compare the cellular excitability of VPL and VPM neurons. We revealed that VPL neurons exhibit enhanced depolarization-induced firing compared to VPM neurons including elevated number of spikes and reduced rheobase and latency to fire. In addition, VPL neurons exhibited enhanced spike frequency adaptation compared to VPM neurons. However, no distinctions were identified in the strength of hyperpolarization-induced rebound bursting in the two thalamic nuclei. These data introduce the first direct comparison of VPL and VPM neuronal excitability and provide evidence that these populations may process somatosensory information differently, and thus make distinct contributions to circuit-wide function and dysfunction.

Keywords

Somatosensory thalamus, corticothalamic, ventrobasal, ventral posterolateral nucleus, ventral posteromedial nucleus, excitability

Abbreviations

CT: corticothalamic; VPL: ventral posterolateral; VPM: ventral posteromedial; nRT: reticular nucleus of the thalamus; PV: parvalbumin; SOM: somatostatin; RMP: resting membrane potential; aCSF: artificial cerebral spinal fluid; CACC: calcium-activated chloride channel; ANO2: anoctamin-2; HCN: hyperpolarization-activated cation channels

Introduction

The corticothalamic (CT) network of the brain is a broad series of reciprocal loops, bidirectionally connecting the cortex and thalamus, and is essential for sensory, motor, emotional, and cognitive processing. The somatosensory CT circuit is responsible for propagating somatic information from the periphery to the cortex through the ventrobasal (VB) thalamus. Aside from processing somatosensory information, this circuit is involved in attention, sleep cycles, and nociception (Beenhakker and Huguenard, 2009; Fanselow and Nicolelis, 1999; Wolff and Vann, 2019). The VB thalamus participates in the generation of intra-thalamic oscillations, termed sleep spindles, which are necessary for certain stages of NREM sleep (Fernandez and Luthi, 2020). Moreover, pathological function within the somatosensory CT circuit is implicated in a variety of neurological and psychiatric diseases such as Alzheimer's disease, schizophrenia, epilepsy, and autism (Baran et al., 2019; Beenhakker and Huguenard, 2009; Hazra et al., 2016; Khan et al., 2016). Thus, elucidating the complete mechanisms underlying this circuit's function is important for understanding both health and disease states.

The VB thalamus is composed of two distinct thalamic nuclei, the ventral posterolateral (VPL) and ventral posteromedial (VPM) nuclei, which receive ascending somatic information from the body and head, respectively. These two glutamatergic nuclei propagate somatosensory information to the primary somatosensory cortex (S1), which returns reciprocal glutamatergic feedback to the VPL and VPM (Aziz and Ahmad, 2006; Brecht and Sakmann, 2002; Lenz, 1992). The S1 cortex and VPL/VPM send collaterals to the reticular nucleus of the thalamus (nRT), a sheet of GABAergic neurons that provide the primary inhibitory input to the VPL and VPM (**Figure 1A**). Both nRT and VPL/VPM

neurons exhibit two distinct firing modes that regulate overall circuit output (Sherman, 2001; Steriade and Llinas, 1988). At depolarized membrane potentials, thalamic cells respond to further depolarization in a tonic firing mode that underlies general somatosensory informational processing. However, at sufficiently hyperpolarized membrane potentials, they respond in a rebound burst mode, which is critical for generating intra-thalamic oscillations (Llinas and Steriade, 2006). Proper output from excitatory VPL and VPM neurons, as well as inhibitory nRT neurons, is required for both somatosensory information processing and circuit-wide rhythmogenesis. Though the core components of the somatosensory CT circuit are well understood, further investigations into cell-type-specific functions within the circuit have just begun.

The VPL and VPM comprise distinct nuclei with unique synaptic connectivity, but they have historically been studied largely as one VB complex (Abbas et al., 2006; Astori et al., 2011; Cheong et al., 2011; Ha et al., 2016; Huguenard and Prince, 1994; Jacobsen et al., 2001; Talley et al., 1999; Warren et al., 1994; Zobeiri et al., 2019). The two nuclei receive distinct synaptic input, both from ascending sensory input and from the nRT. The VPL nucleus receives ascending somatosensory information from the body via the medial lemniscus and spinothalamic pathways, while the VPM receives ascending information from the head via the trigeminothalamic pathway (O'Reilly et al., 2021). In addition, recent evidence revealed that the two nuclei receive distinct cell-type-specific input from the nRT. The VPL reportedly receives input from both somatostatin (SOM)- and parvalbumin (PV)-expressing nRT neurons, while the VPM recieves input from only PV-expressing nRT neurons (Clemente Perez et al., 2017). It is postulated that the distinct connectivity of the two nuclei may underlie potential unique contributions to circuit-wide function.

In addition to their unique inputs, there is evidence that the VPL and VPM may be differentially dysregulated in disease states. For example, VPL and VPM neurons exhibited hypo- and hyperexcitable depolarization-induced firing, respectively, in a mouse model of Dravet Syndrome, an infantile epileptic encephalopathy (Studtmann et al., 2021). Spike frequency adaptation and hyperpolarization-induced rebound bursting in the VPL, but not the VPM, was also altered in diseased animals (Studtmann *et al.*, 2021). In addition, the intrinsic membrane properties of the two populations were differentially affected in this model, with VPL DS neurons exhibiting a reduced resting membrane potential (RMP) and VPM DS neurons exhibiting enhanced input resistance (Studtmann *et al.*, 2021). In a spinal cord injury mouse model, VPL neurons, but not VPM neurons, exhibited a compensatory upregulation in the voltage-gated sodium channel, $Na_V1.3$ (Peng Zhao, 2006). Thus, there is evidence to suggest that the VPL and VPM thalamic nuclei may contribute to pathological disease states differently. However, most studies investigating CT circuit dysfunction in disease models assess the VB as one thalamic complex, without distinguishing the VPL and VPM nuclei (David et al., 2018; Hall and Lifshiftz, 2010; Hazra *et al.*, 2016; Jeanne T. Paz, 2013; Paz et al., 2011; Princivalle et al., 2003; Stefanie Ritter-Makinson, 2019; Ulrike B.S. Hedrich, 2014). This lack of distinction may obscure cell-type-specific alterations in disease states and contributions to pathological circuit-wide function. From a therapeutic perspective, if specific cell types underlie circuit dysfunction, effective pharmacological tools will target those particular cell types and not the entire circuit. Thus, studying the VPL and VPM as one nucleus hinders therapeutic development.

While the intrinsic properties of VPL and VPM neurons have been assessed individually, there has been no systematic and direct comparison of the excitability and

membrane properties of the two populations (Chiaia et al., 1991; Landisman and Connors, 2007). A thorough understanding of the cellular properties of VPL and VPM neurons is essential to elucidate how they may be uniquely processing information and contributing to circuit function. Because these two populations receive unique inputs and respond differentially in some disease states, we hypothesized that VPL and VPM neurons contribute to somatosensory CT circuit function distinctly through unique cellular excitability. Herein, we report enhanced depolarization-induced firing and spike frequency adaptation in VPL neurons compared to VPM neurons, without distinctions in hyperpolarization-induced rebound bursts. These findings broaden our understanding of cell-type-specific function within the CT circuit and provide further evidence that the VPL and VPM may play distinct roles in regulating CT circuit output.

Materials and Methods

Slice Preparation

Mouse studies were performed according to protocols approved by the Institutional Animal Care and Use Committee at Virginia Polytechnic Institute and State University and in accordance with the National Institutes of Health guidelines. C57Bl6J mice of both sexes aged P25-P31 were used for all experiments. Mice were housed in a 12 hour light/dark cycle with *ad libitum* access to food and water. Mice were deeply anesthetized with an overdose of inhaled isoflurane and transcardially perfused with ice-cold sucrose-based artificial cerebrospinal fluid (aCSF) containing (in mM) 230 sucrose, 24 $NaHCO_3$, 10 glucose, 3 KCl, 10 $MgSO_4$, 1.25 NaH_2PO_4, and 0.5 $CaCl_2$ saturated with 95% O_2 / 5% CO_2. The brain was removed and glued to a vibratome stage (Leica VT1200S), and horizontal 300 μm slices were cut in an ice-cold sucrose-aCSF bath. Slices were incubated in a NaCl-

based aCSF containing (in mM) 130 NaCl, 24 $NaHCO_3$, 10 glucose, 3 KCl, 4 $MgSO_4$, 1.25 NaH_2PO_4, and 1 $CaCl_2$ saturated with 95% O_2 / 5% CO_2 at 32°C for 30 min. The slices were then equilibrated to room temperature (RT) for 30 minutes and maintained at room temperature until used for recordings up to 8 hr later. One cell was recorded per slice, and no more than three cells in any dataset are from the same mouse.

Electrophysiology

Recordings were made using a Multiclamp 700B amplifier (Molecular Devices), sampled at 20 kHz (Digidata 1550B, Molecular Devices), and low-pass filtered at 10 kHz using Axon pClamp 11 software (Molecular Devices). The VPL and VPM were identified by the arcuate lamina, which separates them (**Figure 1B**). The extracellular recording solution contained (in mM) 130 NaCl, 24 $NaHCO_3$, 10 glucose, 3 KCl, 1 $MgSO_4$, 1.25 NaH_2PO_4, and 2 $CaCl_2$ saturated with 95% O_2 / 5% CO_2, and was maintained at 32°C for all recordings. Synaptic blockers APV (100 μM), NBQX (10 μM), and gabazine (10 μM) were washed into extracellular solution immediately upon breakthrough and applied for at least five minutes prior to current injection experiments. For whole-cell current-clamp recordings, borosilicate glass recording electrodes (4-6 MΩ) were filled with either (in mM) 135 K-gluconate, 13 KCl, 1.7 NaCl, 10 HEPES, 0.2 EGTA, 4 ATP-Mg, 0.3 GTP-Tris, 5 phosphocreatine-K, and 0.1% biocytin, pH 7.3 or 119 mM potassium gluconate, 15 mM KCl, 3.75 mM $MgCl_2$, 5 mM HEPES, 4 mM K-ATP, 14 mM phosphocreatine, 0.3 mM Tris-GTP, and 50 U/mL creatine phosphokinase, pH 7.2. Pipette capacitance neutralization and bridge balance were enabled during current-clamp recordings for capacitance and series resistance compensation. Membrane potential values were corrected for the liquid junction potential after the recording (15 mV). To analyze intrinsic membrane

properties, voltage responses were elicited by 200 ms hyperpolarizing current injections between 20 – 100 pA (20 pA steps). Depolarization-induced spike firing was elicited by 500 ms depolarizing current injections between 10 – 400 pA (either 10 or 20 pA steps used). Hyperpolarization-induced rebound bursting was elicited by 500 ms hyperpolarizing current injections between 50 – 200 pA (50 pA steps). All current-clamp experiments were conducted from the natural resting membrane potential (RMP) of the cell, and three trials were completed for each current injection experiment.

Biocytin labeling in acute brain slices

The cell location in either the VPL or VPM was confirmed after electrophysiology recordings by biocytin labeling. Briefly, brain slices were fixed with 4% PFA in 1X PBS, pH 7.4, overnight at 4°C, washed in 1X PBS, and then stored at -20°C in cryoprotectant solution containing 0.87 M sucrose, 5.37 M ethylene glycol, and 10 g/L polyvinyl-pyrrolidone-40 in 0.1 M phosphate buffer, pH 7.4. For biocytin labeling, slices were blocked with 10% NDS in 1X PBS with 0.25% Triton X-100, and then incubated with 1.0 µg/ml DyLight 594-conjugated streptavidin (Jackson Immunoresearch) in blocking solution overnight at RT. Slices were placed on a glass slide with a coverslip and DABCO mounting media (Sigma Aldrich). 10X images were acquired on an Olympus IX83 microscope with a Hamamatsu Orca Flash 4.0 camera, X-Cite Xylis LED, and DAPI and TRITC filter sets using CellSens software.

Electrophysiology Data Analysis

Recordings were assigned numerical identifiers and analysis was performed blind to cell location. All current-clamp recordings were analyzed in Clampfit 11 (Molecular Devices). RMP was measured from current-clamp recordings following five-minute

synaptic blocker application and after RMP stabilization. Input resistance (R_{in}) was determined from the amplitude of voltage responses to 200 ms hyperpolarizing current injections, the time constant (τ_m) was determined by a mono-exponential fit of the voltage response, and cell capacitance was calculated by $C_m = \tau_m/R_{in}$. The Clampfit 11 threshold detection module was used to quantify the number of spikes, spike frequency, and latency to the first spike in response to 500 ms depolarizing current injections or upon removal of 500 ms hyperpolarizing current injections. Rheobase was defined as the smallest depolarizing current injection that elicited an action potential. Values were averaged across three runs for all current injection experiments.

The shape of single action potentials was analyzed using the Action Potential Search module in ClampFit 11. The baseline was manually set, and single action potentials at or near rheobase were analyzed for amplitude, half width, rise and decay time, after hyperpolarization amplitude, and threshold.

Spike frequency adaptation was evaluated by measuring spike frequency across depolarizing current injections. The frequency of the first two spikes and last two spikes were averaged across multiple runs in the same cell. The spike frequency ratio is defined as the frequency of the last two spikes/frequency of the first two spikes.

Statistical analysis

A priori power analyses were performed in GPower 3.1 to estimate required samples sizes given appropriate statistical tests with $\alpha = 0.05$, power $(1 - \beta) = 0.8$, and a moderate effect size or effect sizes based on pilot data. Statistical analyses were performed in GraphPad. All parameters measured in response to multiple current injections were compared by fitting data with a linear or nonlinear regression accompanied by a sum of

squares F test. Resulting data is plotted as regression lines accompanied by 95% confidence interval bands. The specific tests used and associated test statistics are reported in the respective figure legend or table. All other group data are plotted as mean ± s.e.m. in the figures, and numerical data reported in the text are mean ± s.e.m., unless otherwise stated.

Results

Enhanced depolarization-induced firing in VPL compared to VPM neurons

Depolarization-induced firing in both VPL and VPM neurons is critical for reliable propagation of somatosensory information to the cortex. Further, there is evidence that the depolarization-induced firing of the two populations is differentially altered in disease states (Studtmann et al., 2021). However, the depolarization-induced firing properties of the VPL and VPM have not been directly compared. Therefore, we directly compared VPL and VPM firing properties including the number of spikes, latency to first spike, and rheobase in response to depolarizing current injections.

Across all current injections, VPL neurons fired significantly more spikes than VPM neurons (**Figure 2A**). VPL neurons also exhibited an overall reduction in latency to first spike across current injections compared to VPM neurons (**Figure 2B**). Qualitatively, this effect seems to be enhanced at lower current injections (**Figure 2B**). The rheobase of VPL neurons was also significantly lower than VPM neurons (VPL: 51 ± 7.9, VPM: 141 ± 21.1 ; **Figure 2C**).

Differences in action potential shape across cell-types often indicate the presence of distinct voltage-dependent conductances. Therefore, we analyzed the shape of individual action potentials at or near rheobase of VPL and VPM neurons in order to reveal further changes in firing properties. However, no significant changes were identified in action

potential amplitude, half width, rise or decay time, after-hyperpolarization amplitude, or threshold in VPL compared to VPM neurons (**Table 1**). Together, these results indicate enhanced depolarization-induced firing in VPL neurons compared to VPM neurons, without alterations in the composition of individual action potentials.

Intrinsic membrane properties are unaltered in VPL compared to VPM neurons

Distinct intrinsic membrane properties in the VPL and VPM may underlie the observed differences in depolarization-induced firing. Thus, we directly compared the membrane properties to reveal existing differences in the two populations. No significant changes were identified in the RMP, cell capacitance (C_m), input resistance (R_{in}), or time constant (τ) of VPL and VPM neurons (**Table 2; Supplementary Figure S1**). We wanted to determine if spontaneous synaptic transmission contributed to the RMP of VPL and VPM neurons differently, potentially contributing to their distinct excitabilities. Thus, RMP here was assessed across the application of glutamatergic (APV and NBQX) and GABAergic (gabazine) synaptic blockers. No significant changes were detected in the RMP over the time course of drug application in either VPL or VPM neuron populations (**Supplementary Figure S2**). These results indicate that there are no detectable differences in membrane properties between VPL and VPM neuron populations. Further, these results suggest that combined spontaneous glutamatergic and GABAergic synaptic input do not contribute significantly to the RMP of either VPL or VPM neurons.

Enhanced spike frequency adaptation in VPL compared to VPM neurons

Spike frequency adaptation is a reduction in the action potential frequency of a neuron over a sustained period of depolarization. Though it has been established that VB neurons exhibit activity-dependent spike frequency adaptation, this phenomenon has not

been characterized or compared in the VPL and VPM (Cheong *et al.*, 2011; Ha *et al.*, 2016; Landisman and Connors, 2007). Physiologically, spike frequency adaptation in VB neurons has been proposed as a self-inhibiting mechanism, limiting the propagation of information during excessive activation (Ha *et al.*, 2016). Thus, it is important to elucidate whether there are distinctions in the spike frequency adaptation of VPL and VPM neurons, which would suggest that the two nuclei likely affect thalamocortical function differently.

We first assessed whether the frequency of the initial two spikes and the last two spikes across current injections differed between VPL and VPM neurons. To do so, we plotted spike frequency across current injections from 200-400 pA and compared the linear regressions for VPL and VPM groups. The frequency of the first two spikes was significantly enhanced in VPL neurons compared to VPM neurons over all current injections (VPL: 196 ± 21 Hz; VPM: 110 ± 31 Hz; **Figure 3A**). The frequency of the last two spikes was also significantly increased over all current injections in VPL neurons compared to VPM (VPL: 83 ± 10 Hz; VPM: 61 ± 12 Hz; **Figure 3B**). The spike frequency adaptation ratio is defined as the frequency of the last two spikes/frequency of the first two spikes. This ratio was significantly increased in VPM neurons compared to VPL neurons across all current injections (VPL: 0.46 ± 0.09; VPM: 0.75 ± 0.13, **Figure 3C**).

These findings indicate that VPL neurons exhibit enhanced spike frequency adaptation compared to VPM neurons, which suggests the two populations may utilize unique activity-dependent adaptation properties or mechanisms.

Unchanged hyperpolarization-induced rebound firing in VPL and VPM neurons

Hyperpolarization-induced rebound bursting is an essential firing mode of both VPL and VPM neurons which underlies intra-thalamic oscillations. Feedforward nRT-VPL/VPM inhibition leads to a hyperpolarized membrane potential in VPL and VPM

neurons, which respond to subsequent depolarization with a low-threshold calcium spike, accompanied by a high-frequency rebound burst of action potentials. Recurrent rebound bursts between the nRT and the VB thalamus generate oscillations which underlie important physiological processes, such as sleep spindles. Recent evidence revealed distinct, cell-type-specific connectivity between the VPL and VPM and the nRT, indicating the two thalamic nuclei may contribute to circuit-wide oscillations distinctly. However, the rebound burst properties of VPL and VPM neurons have not yet been directly compared. Thus, here we directly compared properties of hyperpolarization-induced rebound bursting in the two populations including the number of spikes per burst and latency to first spike.

VPL and VPM neurons exhibited no significant change in the number of spikes fired per burst in response to increasing hyperpolarizing currents (**Figure 4B**). VPL neurons exhibit a trend towards a reduced latency to first spike compared to VPM neurons, particularly at lower currents, though this result is not statistically significant (**Figure 4C**). Together, these results suggest there are no detectable differences in the hyperpolarization-induced rebound bursting of VPL and VPM neurons.

Discussion

The systematic comparison of VPL and VPM neuronal excitability presented here provides novel evidence of distinct firing properties in the two neuron populations. The depolarization-induced firing of VPL neurons was enhanced compared to VPM neurons, including increased number of spikes, reduced latency, and reduced rheobase. Further, spike frequency adaptation was enhanced in VPL neurons compared to VPM. Interestingly, no accompanying significant changes in hyperpolarization-induced rebound bursting were identified in the two populations. Together, these results indicate that the VPL and VPM

may process information and contribute to circuit function differently due to distinct cellular excitability.

The expression and function of membrane channels underlying tonic firing in VPL and VPM neurons have not been compared. Thus, our understanding of the potential mechanisms underlying distinct depolarization-induced firing in the two populations is limited at this point. The enhanced spike frequency adaptation during tonic firing of VPL neurons suggests that a unique activity-dependent mechanism is contributing to VPL firing across sustained depolarization. It is established that the anoctamin-2 (ANO2), a calcium-activated chloride channel (CACC), mediates spike frequency adaptation in the VB thalamus generally (Ha and Cheong, 2017; Ha *et al.*, 2016). The model developed from this evidence posits that sustained depolarization leads to elevated increases of intracellular calcium over time through voltage-gated calcium channels, thereby activating ANO2 channels (Ha and Cheong, 2017). The resulting influx of chloride ions into the cell hyperpolarizes the membrane potential of the neuron, thereby reducing the propensity to spike (Ha and Cheong, 2017). However, the study establishing ANO2 as the mediating channel in this model studied the VB thalamus as one complex, without differentiating the VPL and VPM (Ha *et al.*, 2016). Thus, it is possible that ANO2 has greater expression or function in the VPL than the VPM, thereby contributing to the observed enhanced spike frequency adaptation. It also remains possible that an unidentified activity-dependent mechanism preferentially impacts VPL firing.

The enhancement in VPL firing immediately upon depolarization and reduced latency to first spike compared to the VPM suggests an additional, non-activity-dependent mechanism may be contributing to spike firing in the VPL. However, no significant

changes were identified in the shape of individual action potentials or the intrinsic membrane properties of VPL and VPM neurons. Though the input resistance was not significantly different, there may be a trend towards a higher input resistance in VPL neurons compared to VPM. This would be consistent with more closed membrane channels and enhanced excitability in VPL neurons. Thus, it remains possible that alterations in the expression or function of membrane channels such as voltage-gated sodium or potassium channels may contribute to distinct depolarization-induced firing in the VPL and VPM. Indeed, evidence from a disease model suggests that voltage-gated sodium channels may have differential expression or function in the two populations (Studtmann *et al.*, 2021). Haploinsufficiency of $Na_V1.1$ in a Dravet Syndrome mouse model leads to opposing changes in VPL and VPM cellular excitability, indicating that $Na_V1.1$ or other voltage-gated sodium channel isoforms may play differential roles in the cell populations (Studtmann *et al.*, 2021). Further, changes in the density, localization, or function of Na_V channels could result in the distinct latencies in VPL and VPM spike firing. However, understanding the precise mechanisms underlying distinctions in VPL and VPM depolarization-induced firing will require a systematic investigation of the precise membrane channels contributing to cell excitability in each population.

An interesting finding of this study is the lack of significant changes in the hyperpolarization-induced rebound bursting in the VPL and VPM. It has been postulated that the nRT-VPM loop is the primary pacemaker in oscillation generation within the broader circuit (Clemente Perez *et al.*, 2017). The idea is supported by the unique innervation of the VPL and VPM by nRT subpopulations. The VPL receives input from both PV- and SOM-expressing nRT neurons, while the VPM is innervated by only PV-

expressing nRT neurons (Clemente Perez *et al.*, 2017). PV-expressing nRT neurons exhibit stronger rebound burst properties than SOM-expressing cells and make stronger contributions to circuit-wide rhythmogenesis (Clemente Perez *et al.*, 2017). Thus, it is hypothesized that the nRT-VPM loop may be more important in intra-thalamic oscillation generation and maintenance than the nRT-VPL loop. Therefore, we anticipated that VPM neurons may exhibit stronger rebound burst properties than VPL neurons. There may be a trend towards an increase in the number of spikes per burst in VPM neurons, though the difference was not statistically significant due to high variability in this study. Indeed, qualitatively, there were multiple VPL neurons that fired no bursts at any hyperpolarized current, while all VPM neurons fired at most current injections. There was also a trend towards a reduced latency to first spike upon relief from hyperpolarization in the VPL group compared to the VPM. Thus, it is possible that there is a difference in rebound burst strength between the two populations that was undetected here.

Potential differences in latency to first spike or the number of spikes per burst would likely be due to distinctions in the expression or function of T-type calcium channels or hyperpolarization-activated cyclic nucleotide-gated (HCN) channels. T-type calcium channels are expressed in nRT, VPL, and VPM neurons and are the primary mechanism underlying rebound bursts (Llinas and Steriade, 2006). T-type calcium channels are de-inactivated at hyperpolarized membrane potentials, and subsequent depolarizing input results in their activation and a resulting low-threshold spike (Llinas and Steriade, 2006). This spike depolarizes the neuron sufficiently to activate canonical action potential machinery, resulting in a high-frequency burst of action potentials on top of the low-threshold spike (Llinas and Steriade, 2006). Thus, distinctions in T-type calcium channel

function could alter the kinetics or amplitude of the low-threshold spike, affecting both latency to first spike and the number of spikes per burst. It is established that nRT and VB neurons express different T-type calcium channel isoforms with nRT neurons expressing $Ca_V3.2$ and $Ca_V3.3$, while VB neurons express predominantly $Ca_V3.1$ (Astori *et al.*, 2011; Talley *et al.*, 1999). However, Ca_V channel expression has not been studied in VPL and VPM populations individually. In addition to T-type calcium channels, both VB and nRT neurons express HCN channels that are activated at hyperpolarized potentials and further contribute to rebound bursting (Abbas *et al.*, 2006; Zobeiri *et al.*, 2019). Yet, HCN channel function has not been investigated in the VPL and VPM individually. Fully elucidating potential distinctions in burst firing of the two nuclei will require systematic investigation into the expression and function of such channels in both the VPL and VPM.

From a functional perspective, the differences in depolarization-induced firing indicate that the VPL and VPM may process ascending somatosensory information distinctly. There is likely an evolutionary advantage to processing somatosensory information from the body and head through distinct circuits, though at this time we can only speculate what that advantage might be. Both the number and frequency of spike trains encode critical information that is propagated from the VPL and VPM to the somatosensory cortex (Kenshalo et al., 1980; Martin et al., 1996). Specifically, VPL neurons have been shown to increase their frequency of output in response to increasingly noxious stimuli, as opposed to innocuous sensory input (Kenshalo *et al.*, 1980; Martin *et al.*, 1996). Thus, it is possible that VPL neurons have a different sensitivity to incoming signals from noxious stimuli compared to VPM neurons, as reflected in their increased firing frequency. The enhanced spike frequency adaptation in the VPL may indicate they are more likely to slow

their response to repeated incoming sensory signals than their VPM counterparts. At this time, it is difficult to interpret how these changes in excitability impact overall sensory processing because the properties of cells upstream of the VPL and VPM have not been well characterized. It is possible that neurons within the ascending somatosensory tracts to the VPL and VPM have unique cellular properties and excitability. The VPL and VPM could therefore receive ascending input with distinct patterns or strengths that shape how they process and relay sensory signals. Thus, it is crucial to understand the nature of ascending input to both nuclei in order to interpret how their unique excitability contributes to overall sensory processing. Future studies will seek to reveal the strength and nature of input from the brainstem to the VPL and VPM.

The evidence presented here provides strong indications that the VPL and VPM process somatosensory information differently and may contribute to somatosensory circuit-wide function distinctly. This information is not only important for better understanding of a healthy circuit, but also in determining how disease models are studied. Investigations into pathological function within the somatosensory CT circuit have historically treated the VB thalamus as a uniform complex, potentially obscuring cell-type-specific effects in the VPL and VPM. This is therapeutically important, as identifying cell-type-specific dysfunction within the two nuclei may provide novel, pathway-specific therapeutic targets by which to correct circuit function. Somatosensory circuit dysfunction is implicated in a broad range of diseases, and revisiting disease models to investigate cell-specific changes in the VPL and VPM may reveal previously unidentified therapeutic opportunities (David *et al.*, 2018; Hall and Lifshiftz, 2010; Hazra *et al.*, 2016; Jeanne T. Paz, 2013; Paz *et al.*, 2011; Princivalle *et al.*, 2003; Stefanie Ritter-Makinson, 2019; Ulrike

B.S. Hedrich, 2014). The data presented here, as well as recent evidence regarding distinct inputs to the VPL and VPM, strongly suggest that the VPL and VPM form two distinct microcircuits within the broader somatosensory circuit (Clemente Perez *et al.*, 2017). Further investigation is required to uncover how these microcircuits function to process sensory signals and generate circuit-wide rhythmogenesis, and how they may be uniquely suited for therapeutic targeting.

Funding

This work was supported by the National Institutes of Health [NS105804], CURE Epilepsy, the Dravet Syndrome Foundation, and Brain Research Foundation.

Declaration of interests

None

Author contributions

Carleigh Studtmann: Validation, Formal analysis, Investigation, Writing – original draft, Visualization.

Mackenzie A. Topolski: Validation, Investigation, Writing – review & editing.

Sharon A. Swanger: Conceptualization, Methodology, Validation, Formal analysis, Investigation, Resources, Writing – original draft, Visualization, Supervision, Project administration, Funding acquisition.

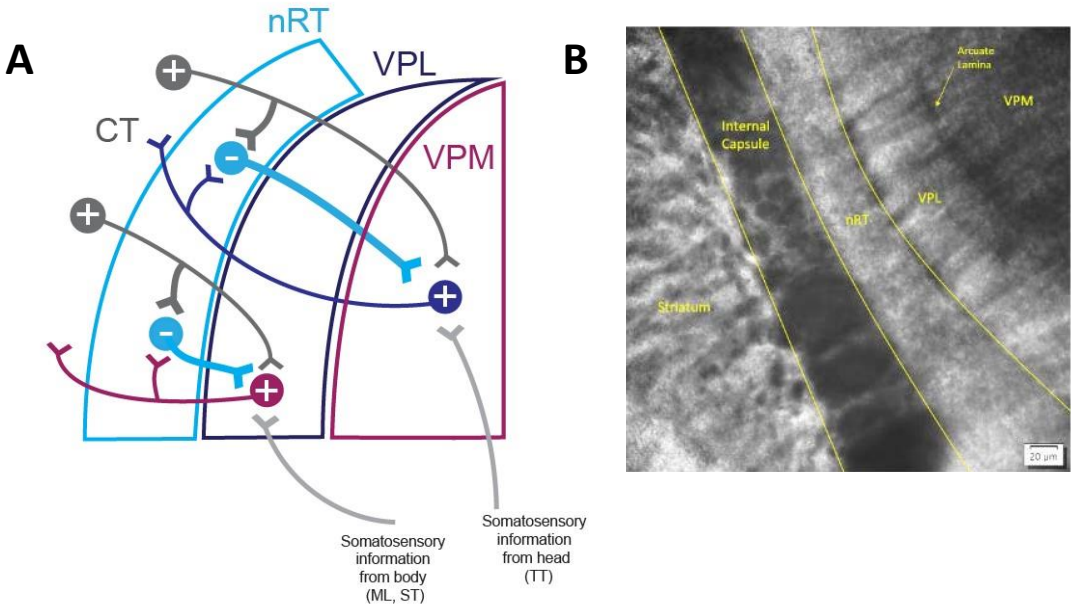

Figure 1. Somatosensory corticothalamic circuit including VPL and VPM thalamic nuclei. **A.** The core somatosensory CT circuit includes the primary somatosensory cortex, the nRT, and the VPL and VPM thalamic nuclei. The VPL and VPM recieve somatosensory input from the body and head, respectively via the medial lemniscus (ML), spinothalamic (ST), and trigeminothalamic (TT) tracts. **B.** Representative infrared image of horizontal acute brain slice showing VPL and VPM thalamic nuclei separated by the arcuate lamina.

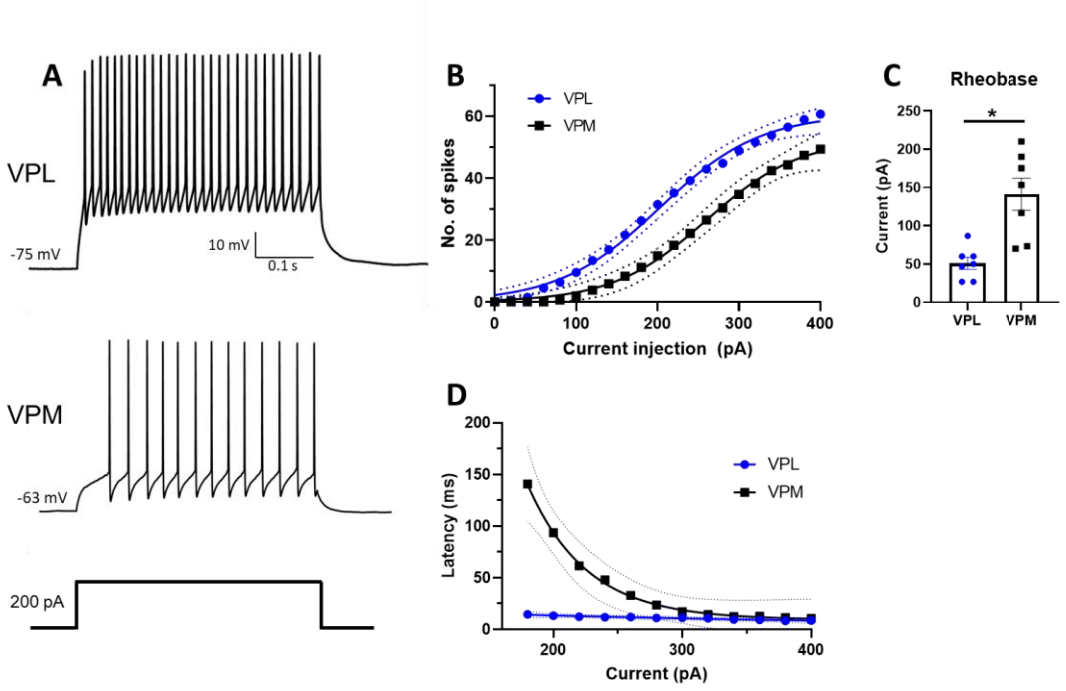

Figure 2. Enhanced depolarization-induced firing in VPL neurons. A. Representative traces show VPL and VPM neuron spike firing in response to depolarizing current injections from RMP. **B.** The number of spikes at each current injection for VPL (n = 6 cells from 3 mice) and VPM (n = 7 cells from 4 mice) neurons are plotted. A nonlinear regression yielded the plotted lines with 95% confidence interval bands, and resulting fits were compared using a sum of squares F test: $F(3, 267)= 26.35$; *$p<0.0001$. **C**. Latency to the first spike was quantified for each cell in panel **B** and nonlinear regression fit yielded the plotted lines with 95% confidence interval bands. Resulting fits were compared using a sum of squares F test: $F(3, 162)= 22.88$, *$p<0.0001$. **D.** Rheobase was quantified for VPL (n = 7 cells from 4 mice) and VPM (n = 7 cells from 4 mice) and analyzed by unpaired t-test (*$p=0.002$).

Table 1. Action Potential Firing Properties of VPL and VPM neurons

	VPL	VPM	P-value
Amplitude (mV)	53.6 ± 5.3	51.2 ± 4.2	0.70
Half duration (ms)	0.92 ± 0.1	0.82 ± 0.07	0.41
Rise Time (ms) 75% to 10% of peak	0.33 ± 0.05	0.30 ± 0.04	0.53
Decay Time (ms) 10% to 75% of peak	0.61 ± 0.07	0.56 ± 0.05	0.54
After-hyperpolarization Amplitude (mV)	-48.2 ± 1.8	-47.5 ± 2.6	0.86
Threshold (mV)	-48.7 ± 2.1	-51.7 ± 2.9	0.49
N	6 (4)	9 (4)	

Table 1. VPL and VPM parameters were compared using unpaired t-tests. N values represent number of cells followed by number of mice in parentheses.

Table 2. Membrane properties of VPL and VPM neurons

	VPL	VPM	P-value
RMP (mV)	-76.6 ± 2.8	-72.9 ± 3.8	0.45
C_m (pF)	169 ± 23	204 ± 36	0.42
R_{in} (MΩ)	160 ± 13	135 ± 12	0.20
Tau (ms)	26.8 ± 4.0	28.1 ± 5.5	0.85
N	8 (4)	8 (4)	

Table 2. VPL and VPM parameters were compared using unpaired t-tests. N values represent number of cells followed by number of mice in parentheses.

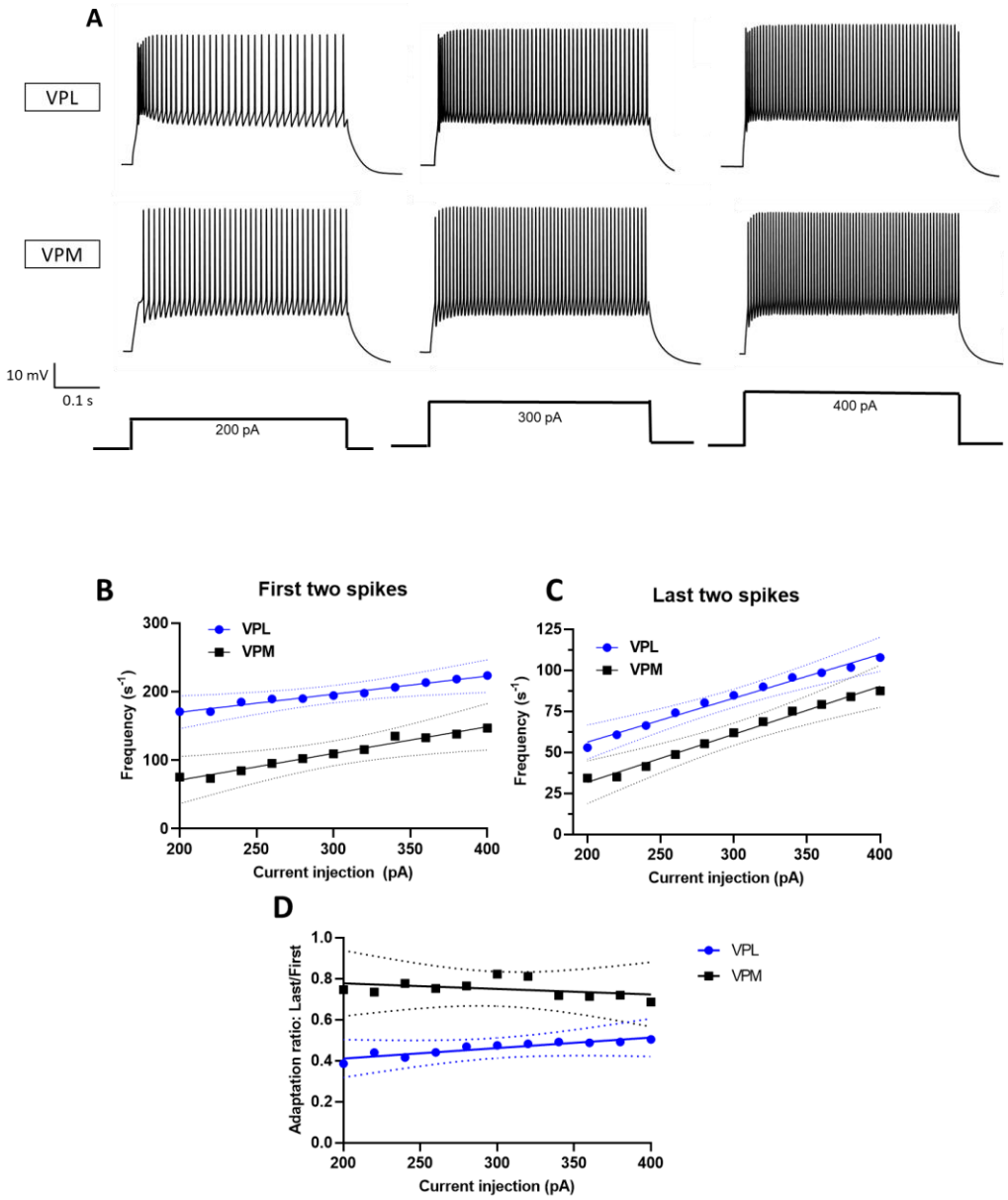

Figure 3. Enhanced spike frequency adaptation in VPL neurons. A. Representative traces of VPL and VPM spike firing demonstrating spike frequency adaptation in response to 200 pA, 300 pA, and 400 pA current injections. **B.** The average frequency of the first two spikes are plotted for VPL (n= 6 cells from 3 mice) and VPM (n=7 cells from 4 mice) across current injections. Nonlinear regression of frequency data yielded plot with 95% confidence interval bands and were compared using a sum of squares F test: $F(2, 138)= 28.79$, $p<0.0001$. **C.** The average frequency of the last two spikes are plotted for VPL (n= 6 cells from 3 mice) and VPM (n=7 cells from 4 mice) across current injections. Nonlinear regression of frequency data yielded plot with 95% confidence interval bands and were compared using a sum of squares F test: $F(2, 138)= 11.93$, $p<0.0001$. **D**. Frequency adaptation ratios (last 2 spikes/first two spikes) were averaged for all cells at each current injection. Nonlinear regression yielded plot with 95% confidence interval band and were compared using a sum of squares F test: $F(2, 138)= 16.41$, $p<0.0001$.

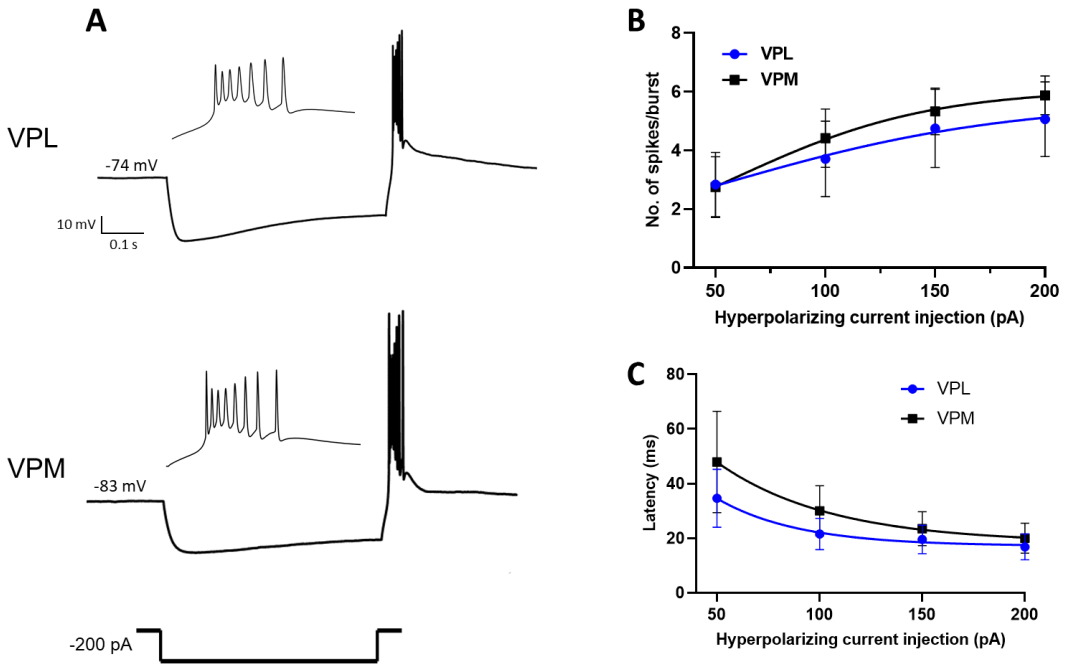

Figure 4. Unaltered rebound bursting in VPL and VPM neurons. A. Representative traces show VPL and VPM neuron rebound bursting in response to hyperpolarizing current injections from RMP. **B.** The number of spikes per burst at each current injection for VPL (n = 8 cells from 4 mice) and VPM (n = 8 cells from 4 mice) neurons are plotted. A nonlinear regression yielded the plotted lines. Points are mean ± s.e.m. Resulting fits were compared using a sum of squares F test: $F(3, 58)= 0.2106$; $p=0.89$. **C**. Latency to the first spike was quantified for VPL (n=7 cells from 4 mice) and VPM (n= 8 cells from 4 mice) and nonlinear regression fit yielded the plotted lines. One VPL outlier was identified for burst latency using Grubb's test and was excluded from data analysis. Points are mean ± s.e.m. Resulting fits were compared using a sum of squares F test: $F(3, 41)= 2.758$, $p<0.0544$.

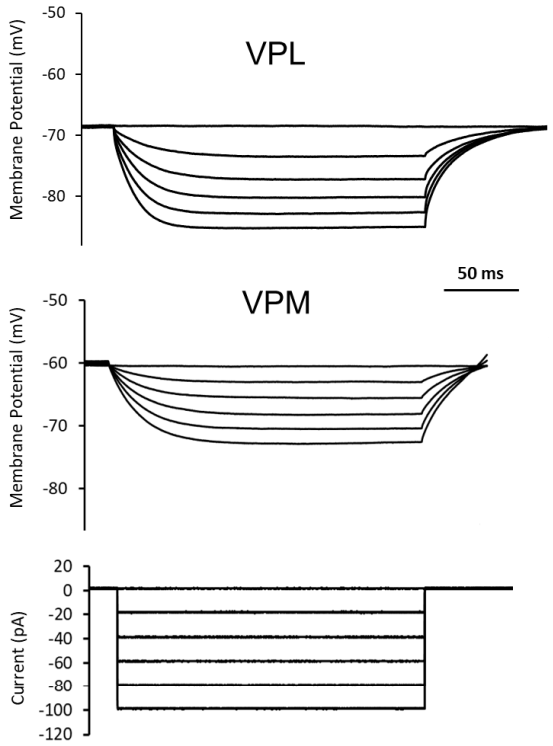

Supplementary Figure S1. Intrinsic membrane properties recordings. Representative traces showing voltage response to 200 ms hyperpolarizing current injections in VPL and VPM neurons used to calculate intrinsic membrane properties. Bottom panel shows current injection amplitudes.

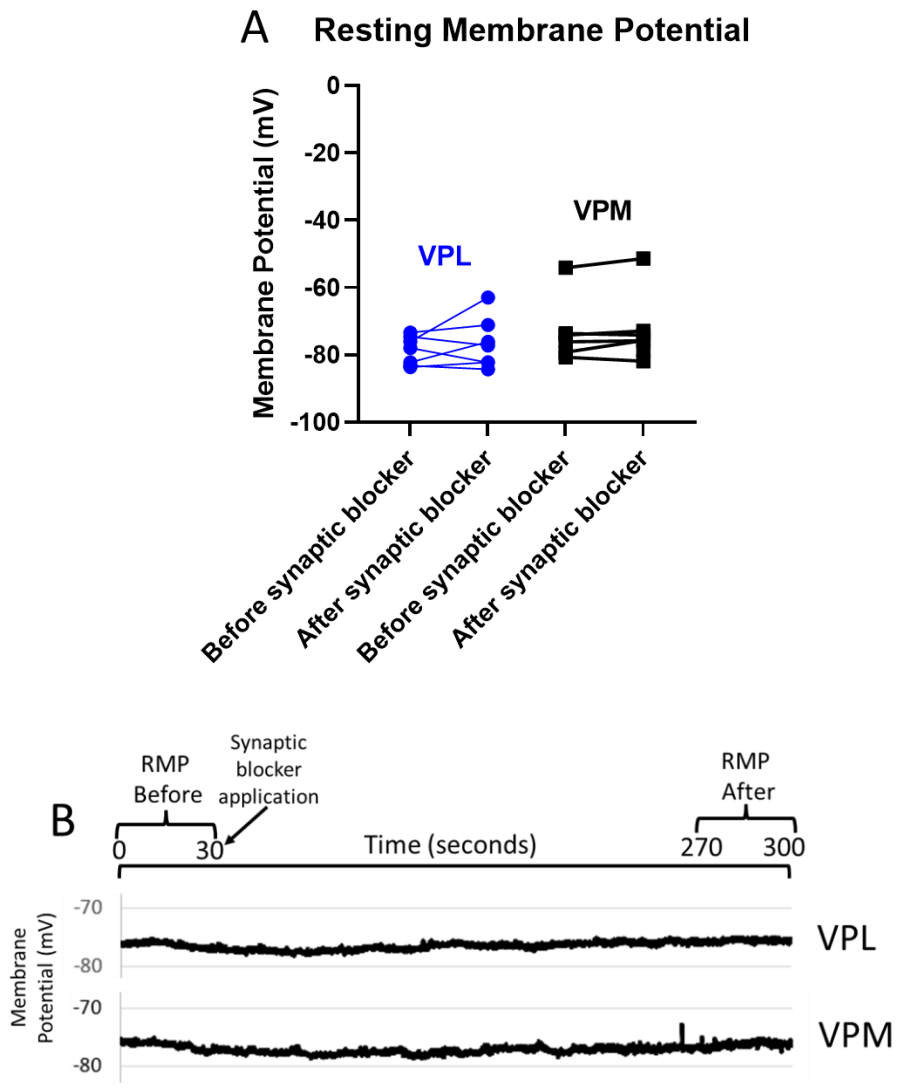

Supplementary Figure S2. Resting membrane potential before and after synaptic blocker application. A. Resting membrane potential in VPL (n= 7 cells from 4 mice) and VPM neurons (n= 7 cells from 4 mice) measured before and after application of synaptic blockers APV, NBQX, and gabazine. RMP averaged in 30 second bins and reported values are before and after five-minute drug application. RMP values within VPL and VPM groups were analyzed with paired t-test (VPL, p=0.38; VPM, p=0.23). RMP values between VPL and VPM groups were analyzed using unpaired t-tests for groups before (p=0.18) and after (p=.45) drug application. **B.** Representative traces from VPL and VPM neurons showing RMP across synaptic blocker application.

References

Abbas, S.Y., Ying, S.-W., and Goldstein, P.A. (2006). Compartmental distribution of hyperpoarization-activated cyclic-nucleotide-gated channel 2 and hyperpolarization-activated-activated cyclic-nucleotide-gated channel 4 in thalamic reticular and thalamocortical relay neurons. Neuroscience *141*, 1811-1825.

Astori, S., Wmmer, R.D., Prosser, H.M., Corti, C., Corsi, M., Liaudet, N., Volterra, A., Franken, P., Adelman, J.P., and Luthi, A. (2011). The Cav3.3 calcium channel is the major sleep spindle pacemaker in thalamus. PNAS *108*, 13823-13828.

Aziz, C.B.A., and Ahmad, A.H. (2006). The Role of the Thalamus in Modulating Pain. Malaysian Journal of Medical Sciences *13*, 11-18.

Baran, B., Karahanoglu, F.I., Myloas, D., Demanuele, C., Vangel, M., Stickgold, R., Anticevic, A., and Manoach, D.S. (2019). Increased Thalamocortical Connectivity in Schizophrenia Correlates with Sleep Spindle Deficits: Evidence for a Common Pathophysiology. Biology Psychiatry: Cognitve Neuroscience and Neuroimaging *4*, 706-714.

Beenhakker, M.P., and Huguenard, J.R. (2009). Neurons that fire together also conspire together: is normal sleep circuitry hijacked to generate epilepsy? Neuron *62*, 612-632.

Brecht, M., and Sakmann, B. (2002). Whisker maps of neuronal subclasses of the rat ventral posterior medial thalamus, identified by whole-cell voltage recording and morphological reconstruction. Journal of Physiology *538*, 495-515.

Cheong, E., Kim, C., Choi, B.J., Sun, M., and Shin, H.-S. (2011). Thalamic ryanodine receptors are involved in controlling the tonic firing of thalamocortical neurons and inflammatory pain signal processing. Journal of Neuroscience *31*, 1213-1218.

Chiaia, N.L., Rhoades, R.W., Fish, S.E., and Killackey, H.P. (1991). Thalamic Processing of Vibrissal Information in the Rat: II. Morphological and Functional Properties of Medial Ventral Posterior Nucleus and Posterior Nucleus Neurons. The Journal of Comparative Neurology *314*, 217-236.

Clemente Perez, A., Ritter-Makinson, S., Higashikubo, B., Brovarney, S., Cho, F.S., Urry, A., Holden, S.S., Wimer, M., Dávid, C., Fenno, L.E., et al. (2017). Distinct thalamic reticular cell types differentially modulate normal and pathological cortical rhythms. Cell Reports *19*, 2130-2142.

David, F., C¸arc¸ak, N., Furdan, S., Onat, F., Gould, T., Me´sza´ros, A.d.m., Giovanni, G.D., Hernandez, V.M., Chan, C.S., Lo˝rincz, M.L., and Crunelli, V. (2018). Suppression of Hyperpolarization-Activated Cyclic Nucleotide-Gated Channel Function in Thalamocortical Neurons Prevents Genetically Determined and Pharmacologically Induced Absence Seizures. Journal of Neuroscience *38*, 6615-6627.

Fanselow, E.E., and Nicolelis, M.A.L. (1999). Behavioral Modulation of Tactile Responses in the Rat Somatosensory System. Journal of Neuroscience *19*, 7603-7616.

Fernandez, L.M.J., and Luthi, A. (2020). Sleep Spindles: Mechanisms and Functions. Physiological Reviews *100*, 805-868.

Ha, G.E., and Cheong, E. (2017). Spike Frequency Adaptation in Neurons of the Central Nervous System. Exp Neurobiol *26*, 179-185.

Ha, G.E., Lee, J., Kwak, H., Song, K., Kwon, J., Jung, S.-Y., Hong, J., Chang, G.-E., Hwang, E.M., Shin, H.-S., et al. (2016). The Ca^{2+}-activated chloride channel anoctamin-2 mediates spike-frequency adaptation and regulates sensory transmission in thalamocortical neurons. Nature Communications *7*.

Hall, K.D., and Lifshiftz, J. (2010). Diffuse traumatic brain injury initially attenuates and later expands activation of the rat somatosensory whisker circuit concomitant with neuroplastic responses. Brain Research *1323*, 161-173.

Hazra, A., Corbett, B.F., You, J.C., Aschmies, S., Zhao, L., Li, K., Lepore, A.C., Marsh, E.D., and Chin, J. (2016). Corticothalamic network dysfucntion and behavioral deficits in a mouse model of Alzheimer's disease. Neurobiology of Aging *44*, 96-107.

Huguenard, J., and Prince, D. (1994). Intrathalamic rhythmicity studied in vitro: nominal T-current modulation causes robust antioscillatory effects. Journal of Neuroscience *14*, 5485-5502.

Jacobsen, R.B., Ulrich, D., and Huguenard, J.R. (2001). GABAb and NMDA Receptors Contribute to Spindle-Like Oscillations in Rat Thalamus In Vitro. Journal of Neurophysiology *86*.

Jeanne T. Paz, T.J.D., Eric S. Frechette, Bruno Delord, Isabel Parada, Kathy Peng, Karl Deisseroth, John R. Huguenard (2013). Closed-loop optogenetic control of thalamus as a new tool to interrupt seizures after cortical injury. Nat Neurosci *16*, 64-70.

Kenshalo, D.R., Jr, Jr, G.J.G., Leonard, R.B., and Willis, W.D. (1980). Responses of neurons in primate ventral posterior lateral nucleus to noxious stimuli. Journal of Neurophysiology *43*, 1594-1614.

Khan, S., Hashmi, J.A., Mamashli, F., Bharadwaj, F., Bharadwaj, H.M., Ganesan, S., Michmizos, K.P., Kitzbichler, M.G., Zatino, M., Garel, K.-L.A., et al. (2016). Altered Onset Response Dynamics in Somatosensory Processing in Autism Spectrum Disorder. Frontiers in Neuroscience *10*.

Landisman, C.E., and Connors, B.W. (2007). VPM and PoM Nuclei of the Rat Somatosensory Thalamus: Intrinsic Neuronal Properties and Corticothalamic Feedback. Cerebral Cortex *17*, 2853-2865.

Lenz, F.A. (1992). The Ventral Posterior Nucleus of Thalamus is Involved in the Generation of Central Pain Syndromes. APS Journal *1*, 42-51.

Llinas, R.R., and Steriade, M. (2006). Bursting of thalamic neurons and states of vigilance. Journal of Neurophysiology *95*, 3297-3308.

Martin, W.J., Hohmann, A.G., and Walker, J.M. (1996). Suppression of Noxious Stimulus-Evoked Activity in the Ventral Posterolateral Nucleus of the Thalamus by a Cannabinoid Agonist: Correlation between Electrophysiological and Antinociceptive Effects. Journal of Neuroscience *16*, 6601-6611.

O'Reilly, C., Iavarone, E., Yi, J., and Hill, S.L. (2021). Rodent somatosensory thalamocortical circuitry: Neurons, synapses, and connectivity. Neuroscience & Behavioral Reviews *126*, 213-235.

Paz, J.T., Bryant, A.S., Peng, K., Fenno, L., Yizhar, O., Franklel, W.N., Deisseroth, K., and Huguenard, J.R. (2011). A new mode of corticothalamic transmission revealed in the Gria4-/- model of absence epilepsy. Nat Neurosci *14*, 1167-1173.

Peng Zhao, S.G.W., Bryan C Hains (2006). Sodium channel expression in the ventral posterolateral nucleus of the thalamus after peripheral nerve injury. Mol Pain *2*.

Princivalle, A.P., Richards, D.A., Duncan, J.S., Spreafico, R., and Bowery, N.G. (2003). Modification of $GABA_{B1}$ and $GABA_{B2}$ receptor subunits in the somatosensory cerebral cortex and thalamus of rats with absence seizures (GAERS). Epilepsy Research *55*, 39-51.

Sherman, S.M. (2001). Tonic and burst firing: dual modes of thalamocortical relay. Trends in Neuroscience *24*, 122-126.

Stefanie Ritter-Makinson, A.C.-P., Bryan Higashikubo, Frances Cho, Stephanie Holden, Ereic Bennett, Ana Chkaidze, Oscar Eelkman Rooda, Marie-Coralie Cornet, Freek Hoebeek, Kazuhiro Yamakawa, Maria Roberta Cilio, Bruno Delord, Jeanne Paz (2019). Augmented Reticular Thalamic Bursting and Seizures in Scn1a-Dravet Syndrome. Cell Reports *26*, 54-64.

Steriade, M., and Llinas, R.R. (1988). The Functional States of the Thalamus and the Associated Neuronal Interplay. Physiological Reviews *68*, 649-742.

Studtmann, C., Ladislav, M., Topolski, M.A., Safari, M., and Swanger, S.A. (2021). Synaptic and intrinsic mechanisms impair reticular thalamus and thalamocortical neuron function in a Dravet syndrome mouse model. bioRxiv. https://doi.org/10.1101/2021.09.03.458635.

Talley, E.M., Cribbs, L.L., Lee, J.H., Daud, A., Perez-Reyes, E., and Bayliss, D.A. (1999). Differential distribution of three members of a gene family encoding low voltage-activated (T-type) calcium currents. J Neuroscience *19*, 1895-1911.

Ulrike B.S. Hedrich, C.L., Daniel Kirschenbaum, Martin Pofahl, Jennifer Lavigne, Yuanyuan Liu, Stephan Theiss, Johannes Slotta, Andrew Escayg, Marcel Dihne, Heinz Beck, Massimo

Mantegazza, Holger Lerche (2014). Impaired Action Potential Initiation in GABAergic Interneurons Caused Hyperexcitable Networks in an Epileptic Mouse Model Carrying a Human Nav1.1 Mutation. Journal of Neuroscience *34*, 14874-14889.

Warren, R.A., Agmon, A., and Jones, E.G. (1994). Oscillatory synaptic interactions between ventroposterior and reticular neurons in mouse thalamus in vitro. Journal of Neurophysiology *72*.

Wolff, M., and Vann, S.D. (2019). The Cognitive Thalamus as a Gateway to Mental Representations. The Journal of Neurosciencw *39*, 3-14.

Zobeiri, M., Chaudhary, R., Blaich, A., Rottmann, M., Herrmann, S., Meuth, P., Bista, P., Kanyshkova, T., Lüttjohann, A., Narayanan, V., et al. (2019). The Hyperpolarization-Activated HCN4 Channel is Important for Proper Maintenance of Oscillatory Activity in the Thalamocortical System. Cerebral Cortex *29*, 2291-2304.

Chapter 4

General Discussion and Future Perspectives

Dravet syndrome remains amongst the most debilitating infantile epilepsies, resulting in severe lifelong symptoms with few available treatments. Attention in the research community remains focused on revealing the underlying disease mechanisms and predicting effective therapeutic strategies to lower seizure burden and alleviate symptoms associated with developmental delay. The developmental nature of the disease, as well as its broad phenotypic profile, complicate the identification of disease mechanisms and effective therapeutics. A key remaining question in the field is whether epileptic activity leads to further phenotypes through long-term, downstream changes in circuit structure and function. Alternatively, mutations or haploinsufficiency of $Na_V1.1$ could be sufficient itself to produce both seizures and the other progressive phenotypes of the disease (Valassina et al., 2022). Another key question to the field is whether DS is a disease of only inhibitory neurons that affects all brain circuits similarly (Catterall, 2016). Alternatively, there is recent evidence that some excitatory populations are affected in the disease and that disease mechanisms may be circuit-specific (Yael Almog, 2021). Answering these questions is critical for developing rational therapeutic strategies and a timeline of intervention that will effectively treat both seizures and further progressive symptoms.

4.1 Therapeutic Potential of Synaptic Modulators in Dravet Syndrome

Here, we have provided evidence which is consistent with our hypothesis that haploinsufficiency of $Na_V1.1$ leads to somatosensory thalamic circuit dysfunction through synaptic-level alterations. This discovery is among the first reported synaptic changes in the disease and supports the theory that haploinsufficiency of $Na_V1.1$ may result in

secondary phenotypes through activity-dependent synaptic alterations. From a therapeutic perspective, altered synapse function in the thalamus opens the door to correcting circuit-wide function through synaptic modulators. Yet, there remain unanswered questions which must be addressed in order to fully evaluate the potential effectiveness of such modulators.

Firstly, investigating the timeline of precisely when synaptic-level deficits arise relative to changes in intrinsic excitability is essential to identify potential windows of therapeutic intervention. There are reports of transient changes in the intrinsic excitability of some cortical and hippocampal neuronal populations (Morgana Favero, 2018; Yael Almog, 2021). However, no longitudinal studies have assessed changes in the intrinsic excitability of thalamic neurons across disease progression. If there is a transient period of altered excitability in thalamic neurons during development, it is likely that synaptic-level alterations are responsible for long-term circuit dysfunction and the associated persistent phenotypes. In this case, rescuing $Na_V1.1$ expression may not be sufficient to correct circuit function after the transient window of altered excitability has closed, while synaptic modulation may be an effective therapeutic strategy. Even if there is no window of altered intrinsic excitability in thalamic neurons, understanding when synaptic alterations arise and whether they persist across disease progression will provide a therapeutic window to intervene with synaptic modulators.

Secondly, it is essential to determine the extent to which cell-type-specific alterations in intrinsic excitability and synaptic connectivity are contributing to circuit-level thalamic dysfunction. A variety of cell-type-specific changes were identified in the excitability and synaptic connectivity of nRT, VPL, and VPM neurons (Studtmann et al., 2021). Yet, how these cell-specific excitability and synaptic alterations come together to

result in altered circuit function remains unclear. It is possible that the observed reduction in glutamatergic synaptic input to the nRT and VPL is contributing to their reduced excitability through hyperpolarizing their RMP. This can be elucidated through assessing intrinsic excitability absent of changes in RMP and synaptic input. This scenario offers an interesting therapeutic opportunity, as correcting synaptic-level deficits in these populations could correct their RMP and at least partially rescue cell excitability and output. In addition, driving the cortical and ascending inputs to the nRT, VPL, and VPM using optogenetics will offer an assessment of how cell-specific synaptic and intrinsic changes together result in altered cell and circuit output. To dissect how intrinsic and synaptic changes individually contribute to altered thalamic function, a recent conditional *Scn1a* knock-in model could be utilized to re-activate *Scn1a* after critical periods of development and presumably altered synaptic-level changes are established (Valassina *et al.*, 2022). Assessing circuit-wide function after rescuing $Na_V1.1$ levels in the thalamus in adulthood would provide direct evidence of the role synapse alterations play in persistent circuit dysfunction. Likewise, utilizing a conditional *Scn1a* knock-out to reduce $Na_V1.1$ levels after critical periods of circuit development have occurred would indicate how altered excitability, absent of changes in synaptic connectivity, contribute to circuit dysfunction. Parsing apart the relative contribution of intrinsic and synaptic-level deficits to overall circuit dysfunction will provide insight into the therapeutic potential of synaptic modulators compared to genetic approaches to rescue $Na_V1.1$ function.

Thirdly, the therapeutic potential of available synaptic modulators must be evaluated. As previously discussed, there are a diversity of synaptic receptors expressed in the thalamus, and the development of an increasing number of pharmacological tools

provides flexibility in modulating synaptic transmission in the region. Subunit-selective pharmacological tools for AMPA receptors, NMDA receptors, and metabotropic glutamate receptors offer the ability to positively and negatively modulate glutamatergic synaptic transmission (Bashkim Kadriu, 2021; Caleigh M. Azumaya, 2017; Kasper Hansen, 2018; Mariacristina Mazzitelli, 2018; N Hovelso, 2012). However, the cell-type-specific roles that these receptor subtypes play in thalamic synaptic transmission have not been fully elucidated. Thus, it remains challenging to predict how particular modulators will impact synaptic transmission and overall cell output in a diseased circuit. Identifying the potentially unique roles of receptors in specific thalamic neuron populations could also provide cell-type-specific therapeutic options to correct circuit-function.

4.2 Glutamatergic Neuron Dysfunction in Dravet Syndrome

Dravet syndrome has canonically been understood as a disease of inhibitory neurons, impacting a variety of inhibitory populations across the brain (Catterall, 2016). Indeed, reduced excitability in inhibitory neurons of the cortex, hippocampus, cerebellum, and reticular nucleus of the thalamus is exhibited in DS models (Chao Tai, 2014; Franck Kalume, 2007; Franck Kalume, 2015; Ikuo Ogiwara, 2007; Mistry et al., 2014; Ritter-Makinson et al., 2019; Ulrike B.S. Hedrich, 2014; Yael Almog, 2021). If indeed only inhibitory neuron populations exhibited reduced excitability throughout the brain, global augmentation of inhibition should effectively correct brain excitability and reduce seizure burden. However, attempting to modulate global levels of inhibition has historically failed to ameliorate the variety of seizures experienced by DS patients (Catterall, 2016; J. Helen Cross, 2019; Rumiko Takayama, 2014). Accumulating evidence indicates that the effects of $Na_V1.1$ haploinsufficiency are circuit-specific, affecting particular glutamatergic

neurons in addition to many GABAergic populations (Studtmann *et al.*, 2021; Yael Almog, 2021).

The work presented here revealed altered excitability in two distinct thalamic glutamatergic populations- VPL and VPM neurons (Studtmann *et al.*, 2021). This is amongst the first reports of altered excitability in a glutamatergic neuron population in DS (Yael Almog, 2021). However, the opposing changes in the excitability of VPL and VPM neurons presented here likely have profound impacts on both somatosensory processing and intra-thalamic oscillations. Thus, augmenting global inhibition through traditional anti-epileptic drugs would be ineffective in correcting somatosensory circuit dysfunction. The application of these findings is critically important for translational approaches to DS research. If $Na_V1.1$ haploinsufficiency differentially impacts the excitability of glutamatergic and GABAergic neurons in a circuit-specific manner, effective therapeutic approaches likely need to also be circuit-specific. For example, the therapeutic intervention which corrects hippocampal circuit function may not be effective in rescuing thalamic circuit function due to distinct cell-type-specific effects.

Translational approaches to DS research are further complicated by the high degree of strain-dependent phenotype and molecular variability exhibited in mouse models of the disease (Alison Miller, 2014; Moran Rubinstein, 2015). It is also possible that contradictory reports of altered excitability in specific neuron populations is the result of the specific $Na_V1.1$ mutations at play (Franck Kalume, 2015; Ritter-Makinson *et al.*, 2019; Studtmann *et al.*, 2021; Ulrike B.S. Hedrich, 2014). Together, these findings suggest that DS disease mechanisms may be mutation- and circuit-specific and modulated by genetic

modifiers. Therapeutically, this indicates effective treatments may need to be highly specific to the patient and aimed at correcting particular phenotypes.

4.3 Somatosensory Thalamic Neuron Diversity

The distinct excitability of VPL and VPM neurons identified in both a healthy and diseased circuit is another important discovery reported here. As previously discussed, the VB thalamus containing both the VPL and VPM has canonically been studied as one thalamic nucleus in both health and disease (Abbas et al., 2006; Astori et al., 2011; Cheong et al., 2011; David et al., 2018; Ha et al., 2016; Hall and Lifshiftz, 2010; Hazra et al., 2016; Huguenard and Prince, 1994; Jacobsen et al., 2001; Jeanne T. Paz, 2013; Paz et al., 2011; Princivalle et al., 2003; Ritter-Makinson *et al.*, 2019; Talley et al., 1999; Ulrike B.S. Hedrich, 2014; Warren et al., 1994; Zobeiri et al., 2019). Here, we reported evidence that VPL and VPM neurons exhibit distinct excitability including depolarization-induced firing. This finding contributes not only to our understanding of somatosensory processing but adds to our accumulating appreciation of cellular diversity in the brain. As increasing genetic and molecular tools are developed, our understanding of cellular diversity in circuits that have traditionally been studied uniformly has continued to grow. Knowledge of the existing cellular diversity in the brain gives us a more complete understanding of the complex mechanisms underlying circuit function and it provides more specific therapeutic targets in disease. Though we now have evidence for functional variation in the VPL and VPM, the genetic and molecular distinctions underlying such function remain unknown. It will be critical to elucidate such molecular distinctions, as they may provide novel means to target the two populations in a cell-type-specific manner.

Beyond Dravet syndrome, distinct functional properties of VPL and VPM neurons have important implications for many other disease states. The somatosensory thalamus has been implicated in a variety of diseases including Alzheimer's disease, schizophrenia, epilepsy, autism, and chronic pain (Baran et al., 2019; Beenhakker and Huguenard, 2009; Fanselow and Nicolelis, 1999; Hains and Waxman, 2007; Wolff and Vann, 2019). Some of these disease states involve dysfunctional somatosensory processing, and the identification of unique molecular targets could allow for specific targeting of ascending somatosensory information from the body and head. Other disease states such as absence seizures involve pathological oscillations within the somatosensory thalamus (Huguenard, 2019). However, intra-thalamic oscillations have primarily been studied in the VB as one nucleus, and distinct roles of VPL and VPM neurons in oscillation generation and maintenance are only beginning to be uncovered. Thus, it is possible that modulating the two populations individually could differentially affect circuit oscillations, thereby providing more effective therapeutic targets by which to correct circuit function. The diversity in VPL and VPM function presented here lays the groundwork for re-exploration of the somatosensory thalamus as two microcircuits that may contribute distinctly to healthy and diseased circuit function.

4.4 Conclusions

The data presented here establish precisely how haploinsufficiency of $Na_V1.1$ alters the excitability of nRT, VPL, and VPM neurons in a cell-type-specific manner. Further, we report novel evidence of altered glutamatergic and GABAergic synaptic connectivity within the somatosensory thalamus of a DS mouse model. These findings expand current models of thalamic dysregulation in DS to include both glutamatergic neuron and synaptic

dysfunction. In addition, we have revealed that VPL and VPM neurons exhibit distinct firing properties in a healthy circuit, which lays the foundation to investigate how they may differentially contribute to circuit function in both health and disease.

References

Abbas, S.Y., Ying, S.-W., and Goldstein, P.A. (2006). Compartmental distribution of hyperpoarization-activated cyclic-nucleotide-gated channel 2 and hyperpolarization-activated-activated cyclic-nucleotide-gated channel 4 in thalamic reticular and thalamocortical relay neurons. Neuroscience *141*, 1811-1825.

Alison Miller, N.H., Clint McCollom, Jennifer Kearney (2014). Mapping genetic modifiers of survival in a mouse model of Dravet syndrome. Genes Brain Behav. *13*, 163-172.

Astori, S., Wmmer, R.D., Prosser, H.M., Corti, C., Corsi, M., Liaudet, N., Volterra, A., Franken, P., Adelman, J.P., and Luthi, A. (2011). The Cav3.3 calcium channel is the major sleep spindle pacemaker in thalamus. PNAS *108*, 13823-13828.

Baran, B., Karahanoglu, F.I., Myloas, D., Demanuele, C., Vangel, M., Stickgold, R., Anticevic, A., and Manoach, D.S. (2019). Increased Thalamocortical Connectivity in Schizophrenia Correlates with Sleep Spindle Deficits: Evidence for a Common Pathophysiology. Biology Psychiatry: Cognitve Neuroscience and Neuroimaging *4*, 706-714.

Bashkim Kadriu, L.M., Jenessa N. Johnston, Lisa E. Kalynchuk, Hector J. Caruncho, Maurizio Popoli, Carlos A. Zarate Jr. (2021). Positive AMPA receptor modulation in the treatment of neuropsychiatric disorders: A long and winding road. Drug Discovery Today.

Beenhakker, M.P., and Huguenard, J.R. (2009). Neurons that fire together also conspire together: is normal sleep circuitry hijacked to generate epilepsy? Neuron *62*, 612-632.

Caleigh M. Azumaya, E.L.D., Paige N. Vinson, Shaun Stauffer, Gary Sulikowski, C. David Weaver, Terunaga Nakagawa (2017). Screening for AMPA receptor auxiliary subunit specific modulators. PLOS One.

Catterall, W.A. (2016). Dravet Syndrome: A Sodium Channel Interneuronopathy. In Ion Channels in Health and Disease, G.S. Pitt, ed. (Academic Press).

Chao Tai, Y.A., Ruth Westenbroek, Todd Scheuer, William Catterall (2014). Impaired excitability of somatostatin- and parvalbumin-expressing cortical interneurons in a mouse model of Dravet syndrome. PNAS, E3139-E3148.

Cheong, E., Kim, C., Choi, B.J., Sun, M., and Shin, H.-S. (2011). Thalamic ryanodine receptors are involved in controlling the tonic firing of thalamocortical neurons and inflammatory pain signal processing. Journal of Neuroscience *31*, 1213-1218.

David, F., C¸arc¸ak, N., Furdan, S., Onat, F., Gould, T., Me´sza´ros, A.d.m., Giovanni, G.D., Hernandez, V.M., Chan, C.S., Lo″rincz, M.L., and Crunelli, V. (2018). Suppression of Hyperpolarization-Activated Cyclic Nucleotide-Gated Channel Function in Thalamocortical Neurons Prevents Genetically Determined and Pharmacologically Induced Absence Seizures. Journal of Neuroscience *38*, 6615-6627.

Fanselow, E.E., and Nicolelis, M.A.L. (1999). Behavioral Modulation of Tactile Responses in the Rat Somatosensory System. Journal of Neuroscience *19*, 7603-7616.

Franck Kalume, F.H.Y., Ruth E. Westenbroek, Todd Scheuer, William Catterall (2007). Reduced Sodium Current in Purkinje Neurons from Nav1.1 Mutant Mice: Implications for Ataxia in Severe Myoclonic Epilepsy in Infancy. Neurobiology of Disease *27*, 11065-11074.

Franck Kalume, J.C.O., Ruth E. Westenbroek, Jennifer Gile, Horacio O. de la Iglesia, Todd Scheuer, William A. Catterall (2015). Sleep Impairment and Reduced Interneuron Excitability in a Mouse Model of Dravet Syndrome. Neurobiology of Disease *77*, 141-154.

Ha, G.E., Lee, J., Kwak, H., Song, K., Kwon, J., Jung, S.-Y., Hong, J., Chang, G.-E., Hwang, E.M., Shin, H.-S., et al. (2016). The Ca^{2+}-activated chloride channel anoctamin-2 mediates spike-frequency adaptation and regulates sensory transmission in thalamocortical neurons. Nature Communications *7*.

Hains, B.C., and Waxman, S.G. (2007). Sodium channel expression and the molecular pathophysiology of pain after SCI. Progress in Brain Research *161*, 195-203.

Hall, K.D., and Lifshiftz, J. (2010). Diffuse traumatic brain injury initially attenuates and later expands activation of the rat somatosensory whisker circuit concomitant with neuroplastic responses. Brain Research *1323*, 161-173.

Hazra, A., Corbett, B.F., You, J.C., Aschmies, S., Zhao, L., Li, K., Lepore, A.C., Marsh, E.D., and Chin, J. (2016). Corticothalamic network dysfucntion and behavioral deficits in a mouse model of Alzheimer's disease. Neurobiology of Aging *44*, 96-107.

Huguenard, J. (2019). Current Controversy: Spikes, Bursts, and Synchrony in Generalized Absence Epilepsy: Unresolved Questions Regarding Thalamocortical Synchrony in Absence Epilepsy. Epilepsy Currents *19*.

Huguenard, J., and Prince, D. (1994). Intrathalamic rhythmicity studied in vitro: nominal T-current modulation causes robust antioscillatory effects. Journal of Neuroscience *14*, 5485-5502.

Ikuo Ogiwara, H.M., Noriyuki Morita, Emi Mazaki, Ikuyo Inoue, Tamaki Takeuchi, Shigeyoshi Itohara, Yuchio Yanagawa, Kunihiko Obata, Teiichi Furuichi, Takao K. Hensch, Kazuhiro Yamakawa (2007). Nav1.1 Localizes to Axons of Parvalbumin-Positive Inhibitory Interneurons: A Circuit Basis for Epileptic Seizures in Mice Carrying an Scn1a Gene Mutation. Neurobiology of Disease *27*, 5903-5914.

J. Helen Cross, R.H.C., Rima Nabbout, Federico Vigevano, Renzo Guerrini, Lieven Lagae (2019). Dravet syndrome: Treatment options and management of prolonged seizures. Epilepsia *60*, S39-S48.

Jacobsen, R.B., Ulrich, D., and Huguenard, J.R. (2001). GABAb and NMDA Receptors Contribute to Spindle-Like Oscillations in Rat Thalamus In Vitro. Journal of Neurophysiology *86*.

Jeanne T. Paz, T.J.D., Eric S. Frechette, Bruno Delord, Isabel Parada, Kathy Peng, Karl Deisseroth, John R. Huguenard (2013). Closed-loop optogenetic control of thalamus as a new tool to interrupt seizures after cortical injury. Nat Neurosci *16*, 64-70.

Kasper Hansen, F.Y., Riley Perszyk, Hiro Furukawa, Lonnie Wollmuth, Alasdair Gibb, Stephen Traynelis (2018). Structure, function, and allosteric modulation of NMDA receptors. J. Gen. Physiology *150*, 1081- 1105.

Mariacristina Mazzitelli, E.P., Sabatino Maione, and Volker Neugebauer (2018). Group II Metabotropic Glutamate Receptors: Role in Pain Mechanisms and Pain Modulation. Frontiers in Molecular Neuroscience *11*.

Mistry, A.M., Thompson, C.H., Miller, A.R., Vanoye, C.G., George Jr, A.L., and Kearney, J.A. (2014). Strain- and age- dependent hippocampal neuron sodium currents correlate with epilepsy severity in Dravet syndrome mice. Neurobiology of Disease *65*, 1-11.

Moran Rubinstein, R.E.W., Frank H. Yu, Christina J. Jones, Todd Scheuer, William A. Catterall (2015). Genetic background modulates impaired excitability of inhibitory neurons in a mouse model of Dravet syndrome. Neurobiology of Disease *73*, 106-117.

Morgana Favero, N.P.S., Emily Lopez, Jennifer A. Kearney, Ethan M. Goldberg (2018). A Transient Developmental Window of Fast-Spiking Interneuron Dysfunction in a Mouse Model of Dravet Syndrome. Neurobiology of Disease *38*, 7912-7927.

N Hovelso, F.S., L. P. Montezinho, P. S. Pinheiro, K. F. Herrik, and A. Mork (2012). Therapeutic Potential of Metabotropic Glutamate Receptor Modulators. Curr Neuropharmacol *10*, 12-48.

Paz, J.T., Bryant, A.S., Peng, K., Fenno, L., Yizhar, O., Franklel, W.N., Deisseroth, K., and Huguenard, J.R. (2011). A new mode of corticothalamic transmission revealed in the Gria4-/- model of absence epilepsy. Nat Neurosci *14*, 1167-1173.

Princivalle, A.P., Richards, D.A., Duncan, J.S., Spreafico, R., and Bowery, N.G. (2003). Modification of $GABA_{B1}$ and $GABA_{B2}$ receptor subunits in the somatosensory cerebral cortex and thalamus of rats with absence seizures (GAERS). Epilepsy Research *55*, 39-51.

Ritter-Makinson, S., Clemente-Perez, A., Higashikubo, B., Cho, F., Holden, S., Bennett, E., Chkaidze, A., Rooda, O.E., Cornet, M.-C., Hoebeek, F., et al. (2019). Augmented Reticular Thalamic Bursting and Seizures in Scn1a-Dravet Syndrome. Cell Reports *26*, 54-64.

Rumiko Takayama, T.F., Hideo Shigematsu, Katsumi Imai, Yukitoshi Takahashi, Kazuhiro Yamakawa, Yushi Inoue (2014). Long-term course of Dravet syndrome: A study from an epilepsy center in Japan. Epilepsia *55*, 528-538.

Studtmann, C., Ladislav, M., Topolski, M.A., Safari, M., and Swanger, S.A. (2021). Synaptic and intrinsic mechanisms impair reticular thalamus and thalamocortical neuron function in a Dravet syndrome mouse model. bioRxiv. https://doi.org/10.1101/2021.09.03.458635.

Talley, E.M., Cribbs, L.L., Lee, J.H., Daud, A., Perez-Reyes, E., and Bayliss, D.A. (1999). Differential distribution of three members of a gene family encoding low voltage-activated (T-type) calcium currents. J Neuroscience *19*, 1895-1911.

Ulrike B.S. Hedrich, C.L., Daniel Kirschenbaum, Martin Pofahl, Jennifer Lavigne, Yuanyuan Liu, Stephan Theiss, Johannes Slotta, Andrew Escayg, Marcel Dihne, Heinz Beck, Massimo Mantegazza, Holger Lerche (2014). Impaired Action Potential Initiation in GABAergic Interneurons Caused Hyperexcitable Networks in an Epileptic Mouse Model Carrying a Human Nav1.1 Mutation. Journal of Neuroscience *34*, 14874-14889.

Valassina, N., Brusco, S., Salamone, A., Serra, L., Luoni, M., Giannelli, S., Bido, S., Massimino, L., Ungaro, F., Mazzara, P.G., et al. (2022). Scn1a gene reactivation after symptom onset rescues pathological phenotypes in a mouse model of Dravet syndrome. Nature Communications *13*.

Warren, R.A., Agmon, A., and Jones, E.G. (1994). Oscillatory synaptic interactions between ventroposterior and reticular neurons in mouse thalamus in vitro. Journal of Neurophysiology *72*.

Wolff, M., and Vann, S.D. (2019). The Cognitive Thalamus as a Gateway to Mental Representations. The Journal of Neurosciencw *39*, 3-14.

Yael Almog, S.F., Marina Brusel, Anat Mavashov, Karen Anderson, Moran Rubinstein (2021). Developmental alterations in firing properties of hippocampal CA1 inhibitory and excitatory neurons in a mouse model of Dravet syndrome. Neurobiology of Disease *148*.

Zobeiri, M., Chaudhary, R., Blaich, A., Rottmann, M., Herrmann, S., Meuth, P., Bista, P., Kanyshkova, T., Lüttjohann, A., Narayanan, V., et al. (2019). The Hyperpolarization-Activated HCN4 Channel is Important for Proper Maintenance of Oscillatory Activity in the Thalamocortical System. Cerebral Cortex *29*, 2291-2304.